UCLouvain

École polytechnique de Louvain

Stochastic Geometry-based Modelling of Wireless Communication Networks

UAV-based Networks

Author: **François De Saint Moulin**
Supervisors: **Prof. Claude Oestges, Prof. Luc Vandendorpe**
Readers: **Prof. Jérôme Louveaux, Charles Wiame**
Academic year 2019–2020
Master [120] in Electrical Engineering

Acknowledgments

The design and writing of this master's thesis was ultimately carried out thanks to many people that I would like to thank.

Thank you in particular to my supervisors: Prof. Claude Oestges, Prof. Luc Vandendorpe, and Charles Wiame. Their availability and the continuous help and precious advice they provided me throughout this academic year,allowed me to achieve my last year of engineering with success. They knew how to answer my questions, guide me in my research, and help me to solve the problems that faced me.

Then I would like to thank Prof. Jérôme Louveaux for agreeing to take his time to read this document.

Finally, thank you my loved ones who supported me throughout this year, and especially my parents who also helped to improve the English of this master's thesis.

Abstract

The objective of this master thesis is to evaluate the new possibilities brought by the introduction of Unmanned Aerial Vehicles (UAV) in wireless communication networks using stochastic geometry, with a particular focus on the achievable performance for UAV-based relay networks. For this purpose, a summary of the different models and performance metrics which are generally used in the literature is proposed. Based on that, the coverage probability, the average SE and the average exposure for a UAV-based relay network are analysed using stochastic geometry. All the links are either in line-of-sight or non line-of-sight, and are subject to path-loss, shadowing and small-scale fading. First, the UAVs are supposed to hover at fixed positions. Then, they are allowed to move following two different mobility schemes. The achievable performance for a given network configuration is evaluated with the developed framework.

Contents

List of Abbreviations

AF	Amplify-and-Forward
A2G	Air-to-Ground
BPP	Binomial Point Process
BS	Base Station
CCDF	Complementary Cumulative Distribution Function
CDF	Cumulative Distribution Function
CP	Coverage Probability
DF	Decode-and-Forward
DSCN	Drone empowered Small Cellular Network
DU	Downlink User
D2D	Device-to-Device
EE	Energy Efficiency
G2G	Ground-to-Ground
HAP	High Altitude Platform
HCPP	Hard-Core Point Process
HPPP	Homogeneous Poisson Point Process
IHPPP	Inhomogeneous Poisson Point Process
LAP	Low Altitude Platform
LoS	Line-of-Sight
LT	Laplace Transform
MC	Monte-Carlo
MCP	Matérn Cluster Process
MHCPP	Matérn Hard-Core Point Process
MMSE	Minimum Mean Square Error
NLoS	Non Line-of-Sight
NOMA	Non Orthogonal Multiple Access
NYU	New-York University

OP	Outage Probability
PGFL	Probability Generating Functional
PP	Point Process
PCP	Poisson Cluster Process
PDF	Probability Density Function
PLE	Path-Loss Exponent
PPP	Poisson Point Process
QoS	Quality of Service
RD	Relay-to-Destination
RN	Relay Node
RV	Random Variable
RW	Random Walk
RWPM	Random Waypoint
SD	Source-to-Destination
SE	Spectral Efficiency
SG	Stochastic Geometry
SIR	Signal-to-Interference Ratio
SINR	Signal-to-Interference-plus-Noise Ratio
SNR	Signal-to-Noise Ratio
SR	Source-to-Relay
SRD	Source-through-Relay-to-Destination
TBS	Terrestrial Base Station
TCP	Thomas Cluster Process
UAV	Unmanned Aerial Vehicle
UE	User Equipment
UMa	Urban Macro-cellular
3GPP	3nd Generation Partnership Project
5G	Fifth Generation

Chapter 1

Introduction

Unmanned Aerial Vehicles (UAV) designates any aircraft without a human pilot on board. These vehicles gave rise to a growing interest in the area of wireless network researches over the past few years because of their mobility, their cost, and the higher probability to have Line-of-Sight (LoS) links owing to their altitude. Commonly known as drones, they can be categorised based on either their altitude or their structure.

First, they are separated according to altitude into **High Altitude Platforms** (HAP) or **Low Altitude Platforms** (LAP). Generally, HAPs fly at altitudes between seventeen and twenty-two kilometers and they are usually quasi-stationary. They are designed for long term operations (up to few months), in order to provide a wide coverage for large geographic areas. Thanks to their high altitude, the probability to have LoS links is higher than for Terrestrial Base Stations (TBS). Therefore, TBSs may be replaced by HAPs providing less costs linked to their deployment and maintenance [1]. Figure 1.1 gives a comparison between typical parameters of broadband terrestrial, HAP and satellite service.

	Terrestrial (e.g. B-FWA)	HAP	LEO satellite (e.g. Teledesic[31])	GEO satellite
Station coverage (typical diameter)	<1 km	up to 200 km	>500 km	up to global
Cell size (diameter)	0·1–1 km	1–10 km	c. 50 km	400 km minimum
Total service area	spot service	national/regional	global	quasi-global
Maximum transmission rate per user	155 Mbit/s	25–155 Mbit/s	<2 Mbit/s up 64 Mbit/s down	155 Mbit/s
System deployment	several base stations before use	flexible	many satellites before use	flexible, but long lead time
Estimated cost of infrastructure	varies	$50 million upwards?	c. $9 billion	>$200 million
In-service date	2000	2003–2008?	2005	1998

Figure 1.1: Comparison of broadband terrestrial, HAP and satellite services: typical parameters (Source: [1]).

In contrast, LAPs fly at altitudes of dozens meters up to few kilometers and they are usually mobile. They are preferred for limited-duration missions when a swift deployment or high mobility is needed, for example in emergency situations or for data collection from ground sensors. Their mobility can also be used for a dynamic adjustment of the LAPs'

positions and speeds in order to enhance the performance of the network depending on the environment or the quality of the different links. Compared to HAPs, they have a smaller endurance, but they can be recharged or replaced easily, and they are less costly. Additionally, thanks to their altitude, the probability to have LoS links is also higher for LAPs than for TBSs, and the short-distance links which can be obtained enables lower path-loss than for HAPs [2].

Second, according to structure, UAVs are distinguished as **fixed** or **rotary wing** models. The first ones are composed of a simple structure with rigid wings. It flies thanks to a forward thrust which generates a lift. The second ones use multiple rotor blades which generate a lift even if the drone is hovering. Fixed wing models are generally heavier, have a longer endurance, can reach higher speeds, and are maintained or repaired easily thanks to the simplicity of their structure. In contrast rotary wing models can hover and remain stationary over a given area [3]. Figure 1.2 summarises the different distinctions which can be made for UAVs and their pros and cons.

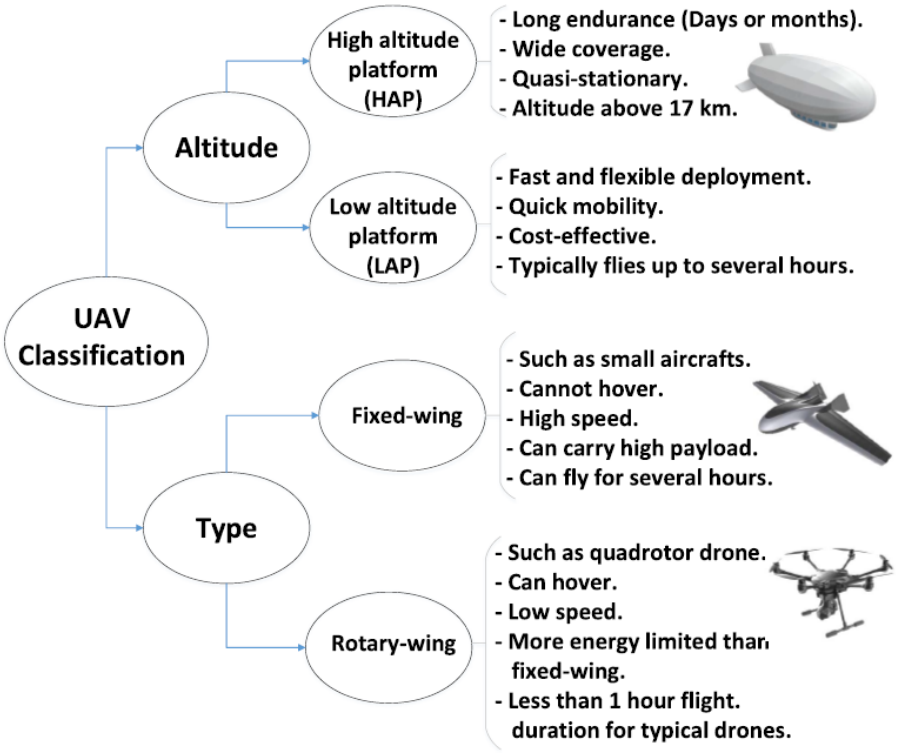

Figure 1.2: Summary of the UAV classification and their different pros and cons (Source: [3]).

In this thesis, the use of Unmanned Aerial Vehicles (UAV) in wireless networks is analysed in different scenarios, with a particular focus on fixed and mobile UAV-based relay networks, for which new models have been developed. The average performance of the network is evaluated using Stochastic Geometry (SG) and Monte-Carlo (MC) simulations.

Stochastic Geometry is a branch of mathematics which provides mathematical models and appropriate statistical methods to study and analyse random spatial patterns based on Point Process (PP) or random shape theory [4]. This tool is well suited for

the analysis of large scale wireless networks since they can be viewed as a collection of nodes, located randomly in space. These nodes represent transmitters or receivers of different types depending on the considered network topology, as User Equipments (UE) or TBSs [5]. It enables estimation of the average performance (coverage probability, average spectral efficiency, average exposure, ...) for wireless networks through closed-form (or quasi closed-form) analytical expressions.

Monte-Carlo simulations are the most common alternative to obtain some insight about the network performance without any restrictive assumptions. However, it can be very time consuming or computationally expensive. Moreover, closed-form expressions obtained with SG enable to extract analytically the impact of some parameters in order to optimise the network, while this is not possible with MC simulations [6].

SG has also some drawbacks. First, SG only evaluates the average performance of the network, while MC simulations can provide an estimation of the complete network statistics. Second, the model of the network can lead to results which are mathematically intractable with SG, or the obtained expressions can be so complex that numerical operations (integration, derivation, ...) are needed. In these conditions, optimisation of the network based on the analytical expressions becomes mostly impossible, and the study of the impact of some parameters becomes difficult. The use of additional assumptions can help to simplify the expressions, but the model will not reflect precisely the reality anymore. Therefore, the relevance of SG must also be analysed in comparison to MC simulations in terms of complexity.

This thesis is structured as following: first, the SG's concepts and other theorems useful for the understanding of the mathematical developments presented in this study are described in Chapter 2.

Next, the state of the art is detailed: models which are generally used to model wireless networks and performance metrics are detailed in Chapter 3. Additionally, existing studies involving UAVs in wireless networks with SG in various scenarios are described.

Then, in Chapter 4, a general framework to evaluate the average performance of a simple UAV-based wireless relay network with fixed TBSs and hovering UAV Relay Nodes (RN) is developed using SG. This model is extended in Chapter 5 by allowing the UAV to move following specific mobility schemes.

Finally, using the framework developed in Chapter 4 and 5, the achievable performance of a UAV-based relay network with direct links neglected or taken into account is evaluated for a given network configuration. Moreover, the computational complexity of SG and MC simulations is compared.

Chapter 2

Mathematical Background: Stochastic Geometry and Other Useful Theorems

As described in Chapter 1, SG (and more particularly the PP theory) is useful to model the topology of the network. Therefore, in this chapter, all the SG's mathematical concepts essential for the understanding of the mathematical developments presented in this thesis are detailed. More precisely, the PP theory and the Palm theory are briefly presented. Some useful PPs for wireless networks are also described. The Poisson Point Process (PPP) is especially developed, and some helpful theorems and properties of this PP are listed. Finally, others theorems not related to SG, which are used to develop the results presented in this study are detailed.

2.1 Point Process Theory

2.1.1 Definition

A **Point Process** (PP) $\mathbf{\Phi}$ is a countable random collection of points that reside in some measurable space (typically in $\mathbb{R}^n$) [4]. It is usually used to model the positions of network nodes, as UEs or BSs. It can be defined as a set of Random Variables (RV) $\boldsymbol{X}_i \in \mathbb{R}^n$ describing the coordinates of the nodes of the PP, or through its **random counting measure** $\Psi_{\mathbf{\Phi}}$, a function which returns the number of points of $\mathbf{\Phi}$ in any subset $A \subset \mathbb{R}^n$:

$$\mathbf{\Phi} = \{\boldsymbol{X}_i, i \in \mathbb{N}\} \quad \leftrightarrow \quad \Psi_{\mathbf{\Phi}} : A \subset \mathbb{R}^n \to \mathbb{N} : A \to \sum_{\boldsymbol{X}_i \in A} \mathbb{1}\left(\boldsymbol{X}_i \in A\right). \tag{2.1}$$

Some important statistical measures of a PP can be defined:

Intensity measure: Also known as **expectation measure** or **mean measure**, the intensity measure of a PP $\mathbf{\Phi}$ on a subset A is the mean of the random counting measure:

$$\Lambda_{\mathbf{\Phi}} : A \subset \mathbb{R}^n \to \mathbb{R} : A \to \mathbb{E}_{\Psi_{\mathbf{\Phi}}}\left[\Psi_{\mathbf{\Phi}}(A)\right]. \tag{2.2}$$

Void Probability: The void probability of a PP $\mathbf{\Phi}$ on a subset A is defined as

$$V_{\mathbf{\Phi}} : A \subset \mathbb{R}^n \to \mathbb{R} : A \to \mathbb{P}_{\Psi_{\mathbf{\Phi}}}\left(\Psi_{\mathbf{\Phi}}(A) = 0\right). \tag{2.3}$$

Two simple PPs are determined by their void probability, and they are equivalent if they have the same void probability for all bounded sets [4].

Probability generating functional: Let us consider a function space F containing all the functions defined as $f : \mathbb{R}^n \to \mathbb{R}^+$. The Probability Generating FunctionaL (PGFL) of a PP with respect to f is the mean of the product of the function's values at each point of the PP:

$$\Pi_{\boldsymbol{\Phi}} : F \to \mathbb{R} : f \to \mathbb{E}_{\boldsymbol{\Phi}} \left[\prod_{\boldsymbol{X}_i \in \boldsymbol{\Phi}} f(\boldsymbol{X}_i) \right]. \tag{2.4}$$

It is especially useful to compute the **Laplace Transform** (LT) of a RV Z which can be expressed as $Z = \sum_{\boldsymbol{X}_i \in \boldsymbol{\Phi}} f(\boldsymbol{X}_i)$:

$$\mathcal{L}_Z(s) = \mathbb{E}_{\boldsymbol{\Phi}} \left[\exp\left(-s \sum_{\boldsymbol{X}_i \in \boldsymbol{\Phi}} f(\boldsymbol{X}_i) \right) \right] = \mathbb{E}_{\boldsymbol{\Phi}} \left[\prod_{\boldsymbol{X}_i \in \boldsymbol{\Phi}} \exp\left(-sf(\boldsymbol{X}_i)\right) \right] = \Pi_{\boldsymbol{\Phi}} \left(\exp\left(-sf\right)\right). \tag{2.5}$$

2.1.2 Useful Point Processes

In the context of wireless networks, some particular PPs are especially useful to model the topology of the network. These PPs are detailed in this section.

Binomial Point Process

A **Binomial Point Process** (BPP) on a bounded set $A \subset \mathbb{R}^n$ is a PP such that a fixed number N of points are distributed uniformly in A. Consequently, the number of points comprised in any bounded subset $B \subset A$ follows a Binomial distribution:

$$\mathbb{P}_\Psi \left(\Psi(B) = k\right) = \binom{N}{k} \left(\frac{|B|}{|A|}\right)^k \left(1 - \frac{|B|}{|A|}\right)^{N-k}, \tag{2.6}$$

where $|A|$ denotes the Lebesgue measure of A.

Poisson Point Process

A **Poisson Point Process** (PPP) $\boldsymbol{\Phi}$ in $\mathbb{R}^n$ with intensity measure Λ is a PP such that

- the numbers of points in any disjoint sets $A_i \subset \mathbb{R}^n$ are independent;
- for any subset $A \subset \mathbb{R}^n$, the number of points in A follows a Poisson distribution:

$$\mathbb{P}_\Psi \left(\Psi(A) = k\right) = \frac{\left(\Lambda(A)\right)^k}{k!} \exp\left(-\Lambda(A)\right). \tag{2.7}$$

A PPP is completely characterised by its intensity measure Λ. However, it can also be characterised using its **density** (or **intensity function**) $\lambda : \mathbb{R}^n \to \mathbb{R}$. The density of a

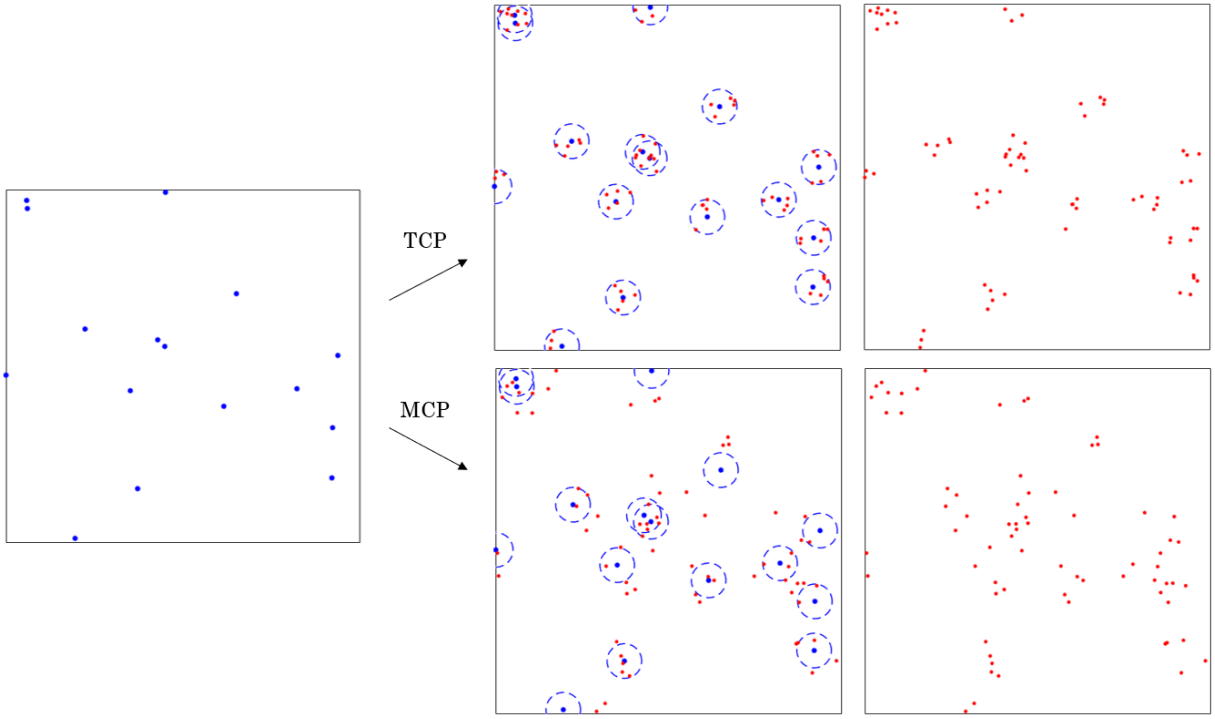

Figure 2.1: Generation of a MCP and a TCP in $\mathbb{R}^2$. The blue points are the parent points (HPPP), while the red points are the clusters generated around their locations. The dashed circles show the radius of generation for the TCP, and the standard deviation of the normal distribution for the MCP.

PPP is defined as the intensity measure of this PPP for an infinitesimal volume $\mathrm{d}\boldsymbol{x} \subset \mathbb{R}^n$ located at $\boldsymbol{x} \in \mathbb{R}^n$:

$$\Lambda(\mathrm{d}\boldsymbol{x}) = \lambda(\boldsymbol{x})\mathrm{d}\boldsymbol{x} \quad \leftrightarrow \quad \Lambda(A) = \int_A \lambda(\boldsymbol{x})\mathrm{d}\boldsymbol{x}. \tag{2.8}$$

The product $\lambda(\boldsymbol{x})\mathrm{d}\boldsymbol{x}$ can be interpreted as the infinitesimal probability that there is a point of the PPP in an infinitesimal area $\mathrm{d}\boldsymbol{x}$ located at $\boldsymbol{x} \in \mathbb{R}^n$.

An **Homogeneous** Poisson Point Process (HPPP) is a PPP with a uniform density λ, such that the intensity measure of the PPP can be expressed as $\Lambda(A) = \lambda|A|$ for any subset $A \subset \mathbb{R}^n$. Therefore, for an HPPP, the density λ can be defined as the mean number of points of the PP in a given subset $A \subset \mathbb{R}^n$. In the other case, the PPP is often called **InHomogeneous** Poisson Point Process (IHPPP).

The PPP is the most commonly used to model wireless networks since the distribution of the points in space is quite realistic compared to many real networks, and because it has a lot of useful properties (described in Section 2.2) which lead to tractable results.

Poisson Cluster Process

The **Poisson Cluster Process** (PCP) is a PP composed of clusters of points, centered at positions given by a HPPP. This is useful to model scenarios where points are susceptible to be grouped in limited volumes. For example, in a wireless network, the locations of UEs can be grouped in a limited area if there is a particular event at this location.

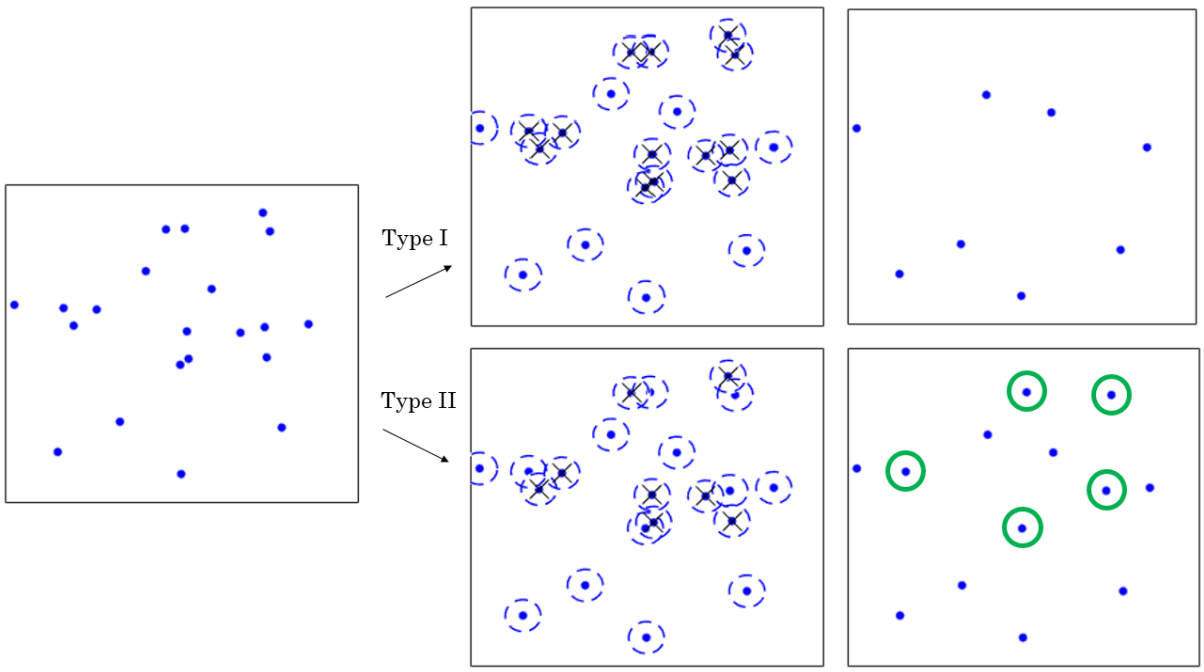

Figure 2.2: Generation of MHCPPs of type I and II in $\mathbb{R}^2$. The dashed circles show the repulsive distance around each point of the initial HPPP, while the crosses show which points are suppressed for both types (resp. at top and bottom). The green circles shows the points which has been kept in the MHCPP of type II, but killed for the MHCPP of type I.

In $\mathbb{R}^2$, two particular PCP are the **Matérn Cluster Process** (MCP) and the **Thomas Cluster Process** (TCP) [7]. For the first one, a fixed or random number of points is uniformly distributed in circular areas located around each parent point. For the second one, a fixed or random number of points is normally distributed around each parent point. Theses PPs are illustrated in Figure 2.1.

Hard-Core Point Process

A **Hard-Core Point Process** (HCPP) with **repulsive distance** $d \in \mathbb{R}^n$ is a PP for which all the points are mutually separated by a distance higher than d. It enables to avoid unrealistic scenarios where two points are really close to each other. For example, in a wireless network, this is unlikely for the location of the BSs. Unfortunately, the mathematical developments are often intractable since their PGFL does not exist.

Two particular HCPP are the **Matérn Hard-Core Point Process** (MHCPP) of type I and II [8]. Both are generated starting from an HPPP:

- To generate an MHCPP of type I with repulsive distance d, the point of the parent HPPP must be kept if and only if they are mutually located at a distance higher than d;
- To generate an MHCPP of type II with repulsive distance d, a random mark is associated with each point of the parent HPPP, and a point is deleted if there exists another point at a distance closer than d with a smaller mark.

These PPs are illustrated in Figure 2.2.

2.1.3 Palm Theory

The **Palm theory** formalises the notion of conditional distribution for PPs given it has some point at an arbitrary location. Two particular distributions of this theory are the Palm distribution and the reduced Palm distribution:

- The **Palm distribution** of a PP is the conditional distribution of a PP given that a point is located at an arbitrary location;
- The **reduced Palm distribution** of a PP is the conditional distribution of a PP given that a point is located at an arbitrary location, and assuming that this point is not included in the distribution.

A useful theorem based on Palm theory is the Slivnyak-Mecke's theorem, presented in Section 2.2.6.

For wireless networks, it is also necessary to define the notion of **typical node**: the performance of the network is studied in the point of view of one node called the typical node, and the performance experienced by this node should be the same for every other node of the same kind in the network. Each node should have the same chance of being selected to be considered typical: it cannot be chosen arbitrarily, otherwise the observed performance could be biased compared to the performance experienced by the others.

2.2 Poisson Point Process: Useful Theorems and Properties

As explained in Section 2.1.2, one of the reason that makes PPP to be the most commonly used PP to model wireless networks is its mathematical tractability. This is a consequence of useful theorems and properties which are detailed in this section.

2.2.1 Campbell's Theorem

Campbell's Theorem [4] Let us consider a function space F containing all the functions defined as $f : \mathbb{R}^n \to \mathbb{R}^+$ and a PPP $\mathbf{\Phi}$ with intensity measure Λ. The expectation of a RV Z which can be expressed as $Z = \sum_{\boldsymbol{X}_i \in \mathbf{\Phi}} f(\boldsymbol{X}_i)$ is given by

$$\mathbb{E}_Z [Z] = \int_{\mathbb{R}^n} f(\boldsymbol{x}) \Lambda(\mathrm{d}\boldsymbol{x}). \tag{2.9}$$

For the particular case of an HPPP with density λ, this can be further simplified:

$$\mathbb{E}_Z [Z] = \lambda \int_{\mathbb{R}^n} f(\boldsymbol{x}) \mathrm{d}\boldsymbol{x}. \tag{2.10}$$

Let us consider another particular case in polar coordinates: an IHPPP $\mathbf{\Phi}$ in $\mathbb{R}^2$ with intensity measure $\Lambda(r\mathrm{d}r\mathrm{d}\theta) = \lambda(r)\, r\mathrm{d}r\mathrm{d}\theta$. Thanks to the Campbell's theorem, the expectation of a RV Z which can be expressed as $Z = \sum_{\boldsymbol{X}_i \in \mathbf{\Phi}} f(\|\boldsymbol{X}_i\|)$ is given by

$$\mathbb{E}_Z\left[Z\right] = \int_{\mathbb{R}^2} f(\|\boldsymbol{x}\|)\Lambda(\mathrm{d}\boldsymbol{x}) = \int_0^{2\pi}\int_0^{\infty} f(r)\lambda(r) r\mathrm{d}r\mathrm{d}\theta = 2\pi\int_0^{\infty} f(r)\lambda(r) r\mathrm{d}r. \tag{2.11}$$

2.2.2 Probability Generating Functional

Let us consider a function space F containing all the functions defined as $f : \mathbb{R}^n \to [0,1]$. The PGFL of a PPP $\mathbf{\Phi}$ in $\mathbb{R}^n$ with intensity measure Λ is given by

$$\Pi_{\mathbf{\Phi}}(f) = \exp\left(-\int_{\mathbb{R}^n}\left(1 - f(\boldsymbol{x})\right)\Lambda(\mathrm{d}\boldsymbol{x})\right). \tag{2.12}$$

For the particular case of an HPPP with density λ, this can be further simplified:

$$\Pi_{\mathbf{\Phi}}(f) = \exp\left(-\lambda\int_{\mathbb{R}^n}\left(1 - f(\boldsymbol{x})\right)\mathrm{d}\boldsymbol{x}\right). \tag{2.13}$$

Therefore, if $\mathbf{\Phi}$ is a PPP, following Equation (2.5), the LT of a RV Z which can be expressed as $Z = \sum_{\boldsymbol{X}_i \in \mathbf{\Phi}} f(\boldsymbol{X}_i)$ is given by

$$\mathcal{L}_Z(s) = \Pi_{\mathbf{\Phi}}\left(\exp\left(-sf\right)\right) = \exp\left(-\int_{\mathbb{R}^n}\left(1 - \exp\left(-sf(\boldsymbol{x})\right)\right)\Lambda(\mathrm{d}\boldsymbol{x})\right), \tag{2.14}$$

and for an HPPP with density λ:

$$\mathcal{L}_Z(s) = \Pi_{\mathbf{\Phi}}\left(\exp\left(-sf\right)\right) = \exp\left(-\lambda\int_{\mathbb{R}^n}\left(1 - \exp\left(-sf(\boldsymbol{x})\right)\right)\mathrm{d}\boldsymbol{x}\right). \tag{2.15}$$

Let us consider another particular case in polar coordinates: an IHPPP $\mathbf{\Phi}$ in $\mathbb{R}^2$ with intensity measure $\Lambda(r\mathrm{d}r\mathrm{d}\theta) = \lambda(r)\, r\mathrm{d}r\mathrm{d}\theta$. Thanks to the PGFL, the LT of a RV Z which can be expressed as $Z = \sum_{\boldsymbol{X}_i \in \mathbf{\Phi}} f(\|\boldsymbol{X}_i\|)$ is given by

$$\begin{aligned}
\mathcal{L}_Z(s) &= \exp\left(-\int_{\mathbb{R}^2}\left(1 - \exp\left(-sf(\|\boldsymbol{x}\|)\right)\right)\Lambda(\mathrm{d}\boldsymbol{x})\right) \\
&= \exp\left(-\int_0^{2\pi}\int_0^{\infty}\left(1 - \exp\left(-sf(r)\right)\right)\lambda(r)\, r\mathrm{d}r\mathrm{d}\theta\right) \\
&= \exp\left(-2\pi\int_0^{\infty}\left(1 - \exp\left(-sf(r)\right)\right)\lambda(r)\, r\mathrm{d}r\right).
\end{aligned} \tag{2.16}$$

2.2.3 Displacement Theorem

Displacement Theorem [4,5] The transformation of a PPP $\mathbf{\Phi}$ in $\mathbb{R}^n$ with intensity measure Λ by a probability kernel $p : \mathbb{R}^n \times A \subset \mathbb{R}^{n'} \to [0,1]$ is a PPP $\mathbf{\Phi}'$ in $\mathbb{R}^{n'}$ with intensity measure Λ' given by

$$\Lambda'(A) = \int_{\mathbb{R}^n} p(\boldsymbol{x}, A)\Lambda(\mathrm{d}\boldsymbol{x}), \qquad A \subset \mathbb{R}^{n'} \tag{2.17}$$

For the particular case of an HPPP with density λ, this can be further simplified:

$$\Lambda'(A) = \lambda \int_{\mathbb{R}^n} p(\boldsymbol{x}, A) \mathrm{d}\boldsymbol{x}, \qquad A \subset \mathbb{R}^{n'}. \tag{2.18}$$

The displacement theorem can also be expressed in terms of density instead of intensity measure: let us consider the Probability Density Function (PDF) of the displacement vector from $\boldsymbol{x} \in \mathbb{R}^n$ to $\boldsymbol{x}' \in \mathbb{R}^{n'}$ $f_{\boldsymbol{x}'|\boldsymbol{x}} : \mathbb{R}^{n'} \times \mathbb{R}^n \to [0, 1]$. In cartesian coordinates, the density λ' of the generated PPP $\boldsymbol{\Phi}'$ is given by

$$\lambda'(\boldsymbol{x}') = \int_{\mathbb{R}^n} f_{\boldsymbol{x}'|\boldsymbol{x}}(\boldsymbol{x}') \lambda(\boldsymbol{x}) \mathrm{d}\boldsymbol{x}. \tag{2.19}$$

In $\mathbb{R}^2$, it can also be expressed in polar coordinates: if $\boldsymbol{x} = (r\cos\theta, r\sin\theta)$ and $\boldsymbol{x}' = (r'\cos\theta', r'\sin\theta')$ the density λ' of the generated PPP $\boldsymbol{\Phi}'$ is given by

$$\lambda'(r', \theta') = \int_0^{2\pi} \int_0^{\infty} \frac{f_{r',\theta'|r,\theta}(r', \theta')}{r'} \lambda(r, \theta)\, r \mathrm{d}r\mathrm{d}\theta. \tag{2.20}$$

If we define a deterministic transformation (**mapping**) by a bijection $g : \mathbb{R}^n \to \mathbb{R}^{n'}$, it is a particular case of the displacement theorem where a point $\boldsymbol{x} \in \mathbb{R}^n$ in $\boldsymbol{\Phi}$ is transformed into $\boldsymbol{x}' = g(\boldsymbol{x}) \in \mathbb{R}^{n'}$ with probability 1. In that case, the resulting PP is a PPP $\boldsymbol{\Phi}'$ in $\mathbb{R}^{n'}$ with intensity measure Λ' given by [5]

$$\Lambda'(A) = \Lambda(g^{-1}(A)), \qquad A \subset \mathbb{R}^n. \tag{2.21}$$

Thanks to the displacement theorem, it can be shown that any HPPP is **stationary** and **isotropic**, namely that any translation or rotation of an HPPP results on a HPPP with the same distribution.

2.2.4 Thinning

Let us consider a thinning probability $p : \mathbb{R}^n \to [0, 1]$. The **thinning** operation of a PPP $\boldsymbol{\Phi}$ in $\mathbb{R}^n$ with intensity measure Λ, where each point $\boldsymbol{X}_i \in \boldsymbol{\Phi}$ is kept with probability $p(\boldsymbol{X}_i)$, independently of the thinning of the other points, generates a PPP $\boldsymbol{\Phi}_p$ in $\mathbb{R}^n$ with intensity measure Λ_p given by

$$\Lambda_p(A) = \int_A p(\boldsymbol{x}) \Lambda(\mathrm{d}\boldsymbol{x}), \qquad A \subset \mathbb{R}^n. \tag{2.22}$$

Furthermore, the PP $\boldsymbol{\Phi}_{1-p}$ in $\mathbb{R}^n$ composed of the points $\boldsymbol{X}_i \in \boldsymbol{\Phi}$ which has been independently removed from $\boldsymbol{\Phi}$ with probability $1 - p(\boldsymbol{X}_i)$ is also a PPP, independent with $\boldsymbol{\Phi}_p$, and with intensity measure Λ_{1-p} given by

$$\Lambda_{1-p}(A) = \int_A (1 - p(\boldsymbol{x})) \Lambda(\mathrm{d}\boldsymbol{x}), \qquad A \subset \mathbb{R}^n. \tag{2.23}$$

Note that the thinning theorem can be seen as a consequence of the Displacement theorem, in which the points $\boldsymbol{X}_i \in \boldsymbol{\Phi}$, defined in an hyperplane $\mathbb{R}^n$, are displaced independently out of the hyperplane in $\mathbb{R}^{n+1}$ with probability $1 - p(\boldsymbol{X}_i)$. The generated PPP $\boldsymbol{\Phi}_p$ is composed of the points which are still in the hyperplane.

2.2.5 Superposition

Let us consider k PPPs $\boldsymbol{\Phi}_i, i = 1, ..., k$ in $\mathbb{R}^n$, with intensity measures $\Lambda_i, i = 1, ..., k$. The **superposition** of the k PPPs generates a new PPP $\boldsymbol{\Phi}$ in $\mathbb{R}^n$ with intensity measure $\Lambda = \sum_{i=1}^{k} \Lambda_k$ if the latter is a locally finite measure. The superposition of multiple PPPs is also denoted using the union symbol $\cup$: $\boldsymbol{\Phi} = \bigcup_{i=1}^{k} \boldsymbol{\Phi}_i$.

2.2.6 Slivnyak-Mecke's Theorem

Slivnyak-Mecke's Theorem [4, 5] Let consider a PPP $\boldsymbol{\Phi}$ in $\mathbb{R}^n$. The reduced Palm distribution of $\boldsymbol{\Phi}$ is equal to its original distribution.

This means that a PPP keeps the same distribution, even if one of its points is removed. It is a consequence of the independence between the number of points of $\boldsymbol{\Phi}$ in any disjoint set: removing a point $\boldsymbol{X}_i \in \boldsymbol{\Phi}$ is equivalent to suppress an infinitesimally small ball around it $\mathcal{B}(\boldsymbol{X}_i, \epsilon), \epsilon \to 0$, and therefore it will not affect the distribution of the points in $\mathbb{R}^n \setminus \mathcal{B}(\boldsymbol{X}_i, \epsilon), \epsilon \to 0$ [9].

2.3 Other Useful Theorems

Three other theorems are helpful to develop the mathematical expressions of this study: the Gil-Pelaez theorem, the Leibniz integral rule and the binomial theorem.

First, the Gil-Pelaez Theorem enables to compute the Complementary Cumulative Distribution Function (CCDF) of a RV based on its characteristic function.

Gil-Pelaez Theorem If X is an univariate random variable with characteristic function $\phi_X(t)$, the CCDF of X is given by

$$\mathbb{P}(X \geq a) = \frac{1}{2} + \frac{1}{\pi} \int_0^\infty \frac{\mathrm{Im}\left[\phi_X(\tau) \exp(-j\tau a)\right]}{\tau} \mathrm{d}\tau. \tag{2.24}$$

Then, the Leibniz integral rule enables to evaluate the derivative of the integral of a function with a varying integration domain.

Leibniz Integral Rule Let us consider an integral of the form

$$I(x) = \int_{a(x)}^{b(x)} f(x,t)\mathrm{d}t,$$

with $-\infty < a(x)$ and $b(x) < \infty$, the derivative of this integral is given by

$$\frac{\mathrm{d}}{\mathrm{d}x}I(x) = f(x,b(x))\frac{\mathrm{d}}{\mathrm{d}x}b(x) - f(x,a(x))\frac{\mathrm{d}}{\mathrm{d}x}a(x) + \int_{a(x)}^{b(x)} \frac{\partial}{\partial x}f(x,t)\mathrm{d}t. \tag{2.25}$$

Finally, the binomial theorem is helpful to expand polynomials into a sum of products.

Binomial theorem Any polynomial in the form $(x+y)^n$ with $n \in \mathbb{N}^+$ can be developed as

$$(x+y)^n = \sum_{k=0}^{n} \binom{n}{k} x^k y^{n-k} = \sum_{k=0}^{n} \binom{n}{k} x^{n-k} y^k. \tag{2.26}$$

Chapter 3

Modelisation of UAV-based Wireless Networks and Applications

In order to evaluate precisely the performance of a wireless network, different models must be adopted to represent the topology of the network and the propagation conditions. Additionally, depending on the scenario, the evaluation of the performance is based on different metrics. In this chapter, typical metrics and models which are commonly used in SG (and more particularly in scenarios involving UAVs) are described. Moreover, existing studies involving UAV-based wireless networks with SG are presented.

3.1 Network Modelling

Depending on the scenario which is studied, the models used for the network topology vary a lot, but the main tools to represent the randomness of the number of nodes and their locations are PPs.

In UAV-based wireless networks, three kinds of nodes are generally involved: TBSs, UAVs, and UEs. Some studies consider multiple kinds of TBSs for heterogeneous networks [10, 11], while the others use different types of UEs in the model, as Device-to-Device (D2D) communicating UEs [12–14], or UEs served by UAVs separated from those served by TBSs [15].

In downlink scenarios, a typical UE is selected arbitrarily among the UEs and the performance of the link between the typical UE and the serving UAV or TBS is evaluated. The node is considered typical in the sense of the Palm theory: the performance observed for this node is representative of the performance which would be observed for any other node of the same type. In these scenarios, PPs are commonly used to model the distribution of TBSs and/or UAVs, since a subset of these nodes will interfere with the typical link.

In uplink scenarios, a typical TBS or UAV is selected arbitrarily, and the link between the typical node and the UEs is evaluated. In the latter cases, PPs are usually used to model the distribution of UEs.

Note that, even if it is not always required, the UEs are sometimes also modelled using PPs in downlink, and the TBSs or UAVs in uplink, when it helps to model the distance between the typical node and the others, as in [7].

When there is no specific constraint about the distribution of these nodes, PPPs are generally used. As explained in Chapter 2, the distribution of the points in space with this process is quite realistic compared to real networks, and it leads to tractable results.

MHCPPs would be more suitable since TBSs are commonly never close to each other. However, these PPs lead to intractable mathematics. An indirect way to take it into account is proposed by [16]: instead of a PPP of density λ to model the RNs, they use a PPP with density

$$\tilde{\lambda} = \frac{1 - \exp\left(-\lambda \pi d^2\right)}{\pi d^2}, \tag{3.1}$$

where d denotes the hard-core distance of the HCPP. This choice is motivated by the fact that PPPs are good approximations of MHCPPs of type II for nodes which are further away from the hard-core distance.

When the number of nodes in the area of interest is fixed, BPPs are well suited [17].

Finally PCPs are particularly interesting in post-disaster or hotspot scenarios, as described in Section 3.7.

3.2 Beamforming Modelling

The TBSs and UAVs can be equipped with antenna arrays to improve the capacity, the coverage, or benefit from diversity. In the context of UAV-based wireless networks, it can be taken into account by introducing small-scale fading and beamforming matrices, as in [18], where specific beamforming or transmission techniques are used. However, a simpler model called the **sectored antenna model** is also proposed in [16, 19, 20]:

$$G(\phi, \theta) = \begin{cases} G_M & \text{if} |\phi| \leq \frac{\phi_{bw}}{2} \text{ and } |\theta| \leq \frac{\theta_{bw}}{2} \\ G_m & \text{otherwise} \end{cases}, \tag{3.2}$$

where G_M is the maximum beamforming gain obtained when the elevation and azimuth angles are respectively within the half elevation and azimuth power beamwidth θ_{bw} and ϕ_{bw}, and G_m is the minimum beamforming gain obtained in the other cases. This model is illustrated in Figure 3.1. Note that it can also be extended for more complex patterns.

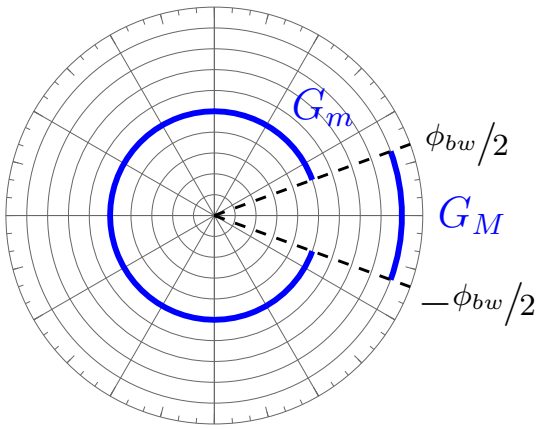

Figure 3.1: Sectored antenna model.

The sectored antenna model is helpful when beamforming is dedicated to generate directional beams, in order to increase the Signal-to-Interference-plus-Noise Ratio (SINR) at the receiver for the same transmitted power. Moreover, receivers which are not aligned with the beam are less sensitive to the interferences generated by the node. It is often used in mmWave scenarios, where the beamforming gain compensates the high path-loss experienced at these frequencies.

3.3 Channel Modelling

Various propagation models are described in the literature. Either some phenomena are not present in specific scenarios, or they are omitted for simplification purposes. In this study, the propagation model is separated in four parts:

- the **path-loss**, which models the attenuation of the link as a function of the distance of transmission;
- the **large-scale fading** (or **shadowing**), which models the random fluctuations of the link due to obstacles;
- the **small-scale fading** (or **fast fading**), which models the rapid variations experienced by the link owing to the movements of the nodes or close scatterers;
- the **LoS probability** model, which defines the probability for the links to be in LoS depending on the topology of the network.

3.3.1 Path-Loss

Accurate Air-to-Ground (A2G) and Ground-to-Ground (G2G) propagation channel models for both UAVs and TBSs communication links are presented in [21, 22]. Usually, path-loss are taken into account using linear or dual-slope models when power attenuations are expressed in decibels, with fixed or floating intercept. Additionally, the parameters can vary depending on if the link is LoS or Non Line-of-Sight (NLoS). Therefore, a general formulation of linear path-loss models is given by

$$L_{PL,n}(r)\ [dB] = \beta_n + 10\alpha_n \log_{10}\left(\frac{r}{r_0}\right), \tag{3.3}$$

where $n = \{L, N\}$ indicates whether LoS or NLoS links are considered. The parameters β_n and α_n are fitting parameters for LoS or NLoS links, at which we will respectively refer as path-loss coefficients and Path-Loss Exponents (PLE).

The path-loss coefficients can also be interpreted as the path-loss at a distance r_0 in free space for a LoS or NLoS link:

$$\beta_n = 10\log_{10} A_n = 20\log_{10}\left(\frac{4\pi r_0 f}{c}\eta_n\right). \tag{3.4}$$

Following this physical interpretation, the parameter η_L is set to one, while the parameter η_N is a penalty factor for the NLoS case.

3.3.2 Large-scale Fading (Shadowing)

The shadowing is induced by the presence of obstacles. In a general case, it is introduced by a RV S_n which model the variations observed in regards to the linear path-loss model, in NLoS and in LoS, as described in [21].

Given its physical interpretation [6], the PDF of S_n is commonly log-normally distributed:

$$f_{S_n}(x;\mu_{S_n},\sigma^2_{S_n}) = \frac{10}{x\ln 10\sqrt{2\pi\sigma^2_{S_n}}}\exp\left(-\frac{1}{2}\frac{(10\log_{10}x-\mu_{S_n})^2}{\sigma^2_{S_n}}\right)u(x), \tag{3.5}$$

where u denotes the Heaviside step function. The parameters μ_{S_n} are usually set to zero, while the parameters σ_{S_n} are scaled depending on the deviation of the measurements around the path-loss models.

3.3.3 Small-scale Fading (Fast Fading)

The small-scale fading is induced by the movements of the emitter, receiver or scatterers. In mmWave scenarios, it is sometimes neglected since the scattered components of the signal are more attenuated compared to systems working at lower frequencies [16]. Otherwise, even if it can be modelled in several ways, the most widely adopted models are **Rayleigh**, **Rice** and **Nakagami-m** fading.

Rayleigh Fading

Rayleigh fading is well suited when there is a lot of multipath components with no dominant path in the link. In that case, the amplitude of the channel gain is modelled with a RV following a Rayleigh distribution, and its phase is modelled with a uniformly distributed RV. Therefore, the PDF of the amplitude of the channel gains are given by

$$f_{|h_n|}(x;\sigma^2_{h_n}) = \frac{x}{\sigma^2_{h_n}}\exp\left(-\frac{1}{2}\frac{x^2}{\sigma^2_{h_n}}\right)u(x). \tag{3.6}$$

Since the variances of these RVs are given by $\mathbb{E}\left[|h_n|^2\right] = 2\sigma^2_n$, the parameters σ^2_n are usually set to $1/2$ for normalisation. Therefore, the PDF of the channel power gain follows an exponential distribution of mean 1:

$$f_{|h_n|^2}(x) = \exp(-x)\,u(x). \tag{3.7}$$

As in [10, 11, 15], this model is often used thanks to its simplicity and tractability, even if it is not suited for LoS links.

Rician Fading

Rician fading is applied when there is one dominant component in the link. In that case, the amplitude of the channel gains follows a Rice distribution, and their PDF is given by

$$f_{|h_n|}(x;K_n,\Omega_n) = \frac{2(K_n+1)x}{\Omega_n}\exp\left(-K_n-\frac{K_n+1}{\Omega_n}x^2\right)I_0\left(2\sqrt{\frac{K_n(K_n+1)}{\Omega_n}}x\right)u(x), \tag{3.8}$$

where K_n are the K-factors, ratios between the powers of the dominant path ν_n and the powers of the other scattered paths $2\sigma_n^2$, $\Omega_n = \nu_n^2 + 2\sigma_n^2$ are the total powers from all the paths, and I_0 is the $0^{th}-$order modified Bessel function of the first kind. The power of the direct and scattered paths are expressed in terms of K_n and Ω_n as

$$\nu_n^2 = \frac{K_n}{K_n + 1}\Omega_n \qquad \text{and} \qquad 2\sigma_n^2 = \frac{1}{K_n + 1}\Omega_n. \tag{3.9}$$

Furthermore, since the variances of the channel gains are given by $\mathbb{E}\left[|h_n|^2\right] = \Omega_n$, the parameters Ω_n are usually set to 1 for normalisation. Therefore, the PDFs of the channel power gains are given by

$$f_{|h_n|^2}(x; K_n, 1) = (K_n + 1)\exp\left(-K_n - (K_n + 1)x\right) I_0\left(2\sqrt{K_n(K_n + 1)x}\right) u(x). \tag{3.10}$$

Note that, when the parameters K_n are set to zero, Equation (3.8) becomes identical to Equation (3.6).

Even if Rician fading is a better model for LoS and NLoS propagation compared to Rayleigh fading, it is barely used, and studies which does not apply Rayleigh fading rather choose Nakagami-m fading.

Nakagami-m Fading

Nakagami-m fading is a refined model for channels with large delay spreads and different clusters of reflected waves [23]. With this model, the amplitude of the channel gains is given by

$$f_{|h_n|}(x; m_n, \Omega) = \frac{2m_n^{m_n}}{\Gamma(m_n)\Omega_n^{m_n}} x^{2m_n - 1} \exp\left(-\frac{m_n}{\Omega_n}x^2\right) u(x). \tag{3.11}$$

The parameters m_n are shape parameters, Ω_n are spread parameters, and Γ is the Gamma function.

Since the variances of the channel gains are given by $\mathbb{E}\left[|h_n|^2\right] = \Omega_n$, the parameters Ω_n are usually set to 1 for normalisation. Therefore, the PDFs of the channel power gains follow a Gamma distribution with shape parameters m_n and scale parameters $1/m_n$:

$$f_{|h_n|^2}\left(x; m_n\right) = \frac{m_n^{m_n}}{\Gamma(m_n)} x^{m_n - 1} \exp\left(-m_n x\right) u(x). \tag{3.12}$$

Figure 3.2 shows the comparison between Rician fading and Nakagami-m fading for different values of m_n and K_n. Nakagami-m fading can be considered as a good approximation for Rician fading. However, the two distributions are still not equal. For example, [24] compares the two distributions by matching their first and second moments. In that case, the relation between the parameters is given by [23, 24]

$$m_n = \frac{(K_n + 1)^2}{2K_n + 1}. \tag{3.13}$$

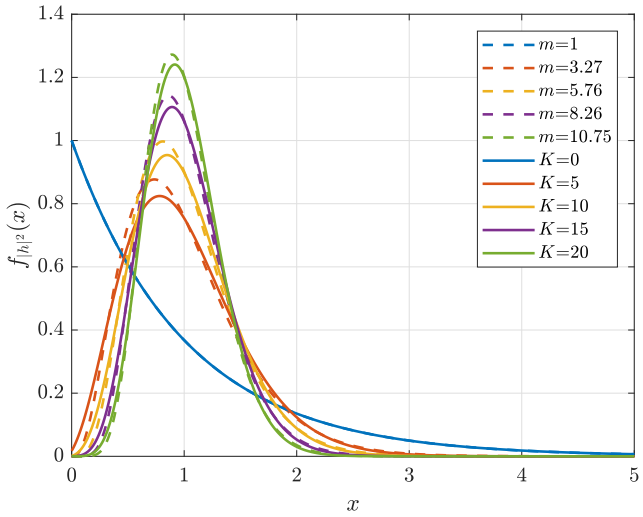

Figure 3.2: Comparison between Nakagami-m fading (dashed lines) and Rician fading (solid lines) for different values of m and K.

By evaluating the outage probability with the two models, differences owing to the behaviour of the distributions in deep fades are noticed.

Nakagami-m fading is often preferred to Rician fading, as in [19, 20, 25], because of the Bessel functions which do not appear in the former.

3.3.4 LoS Probability Model

The flying capability of UAVs enables to achieve higher probability for the links to be in LoS compared to G2G links. Therefore, for A2G links, new LoS probability models are needed to model it correctly.

Ground-to-Ground links

Different LoS probability models have been proposed in previous studies. For example, [22] proposes a comparison of different models based on data measured in Aalborg in Denmark:

- The 3rd Generation Partnership Project (3GPP) d_1/d_2 model [26], also used in [11], with a LoS probability given by

$$p_{GL}(r) = \min\left(\frac{d_1}{r}, 1\right)\left(1 - \exp\left(-\frac{r}{d_2}\right)\right) + \exp\left(-\frac{r}{d_2}\right), \tag{3.14}$$

  where d_1 and d_2 are respectively called the near-field and far-field critical distances;

- a model proposed by the New York University (NYU) [27], similar to the 3GPP d_1/d_2 model, with a LoS probability given by

$$p_{GL}(r) = \left(\min\left(\frac{d_1}{r}, 1\right)\left(1 - \exp\left(-\frac{r}{d_2}\right)\right) + \exp\left(-\frac{r}{d_2}\right)\right)^2; \tag{3.15}$$

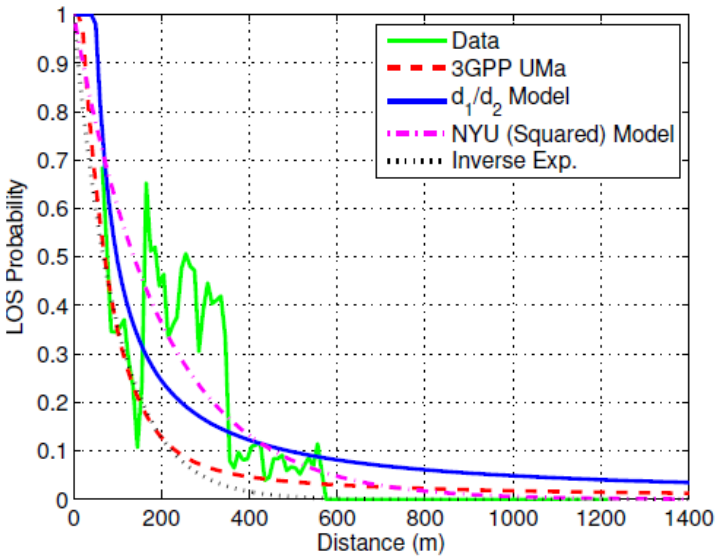

Figure 3.3: LoS probability for the Aalborg data set with four models proposed in [22], and given in Equation (3.14), (3.15) and (3.16). Among these models, the red curve corresponds to the 3GPP d_1/d_2 model in the Urban Macro-cellular (UMa) scenario for a UE at a height of 1.5 meters, with near-field and far-field critical distances set to 18 and 63 meters (Source: [22]).

- an inverse exponential model [28], with a LoS probability given by

$$p_{GL}(r) = \frac{1}{1 + \exp\left(d_1(r - d_2)\right)}. \tag{3.16}$$

Depending on the scenario, d_1 and d_2 are tuned arbitrarily to fit some measurements. In [22], the parameters are computed using the Minimum Mean Square Error (MMSE) criterion. Figure 3.3 illustrates these different models.

Air-to-Ground Links

A very popular closed-form formula to model the LoS probability for LAPs is proposed in [29]:

$$p_{AL}(r) = \prod_{n=0}^{m} \left(1 - \exp\left(-\frac{\left(H_F - \frac{(n+\frac{1}{2})(H_F - H_G)}{m-1}\right)^2}{2\gamma^2}\right)\right), \tag{3.17}$$

where $m = \left\lfloor r\sqrt{\alpha\beta} - 1 \right\rfloor$, H_F is the LAP's altitude, H_G is the ground platform's altitude, and r is the distance between the LAP and the ground platform.

Three parameters are involved in this model:

- the ratio of built-up land area to the total land area α;
- the mean number of buildings per unit area β;
- a scale parameter γ that describes the buildings' heights, according to a Rayleigh distribution.

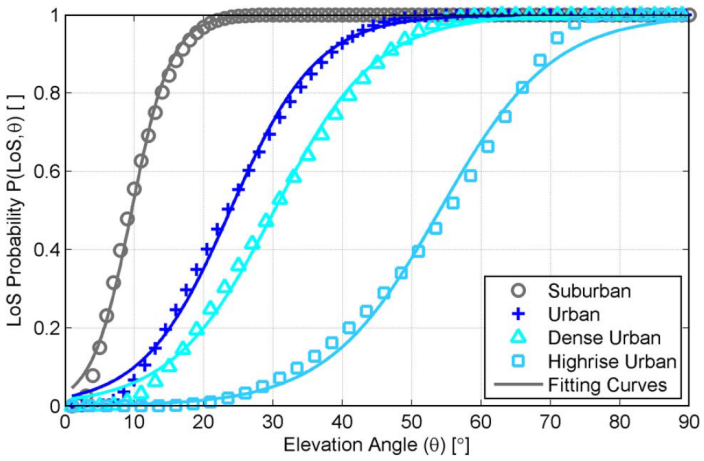

Figure 3.4: A2G LoS probability models for four different environments. Markers show the results obtained with Equation (3.17), while solid lines show the approximation given by Equation (3.18) (Source: [29]).

In practice, it is assumed that $H_F >> H_B >> H_G$, where H_B is the average height of the buildings. With this assumption, it has been shown in [29] that the trends can be closely approximated by a sigmoid function:

$$p_{AL}(r) = \frac{1}{1 + a \exp\left(-b\left(\frac{180}{\pi}\arctan\left(\frac{H_F}{r}\right) - a\right)\right)}, \tag{3.18}$$

where a and b are two parameters related to α, β and γ. Figure 3.4 illustrates the results obtained for four different environments (suburban, urban, dense urban and highrise urban). The corresponding parameters are summarised in Table 3.1.

Equation (3.17) and (3.18) are usually the LoS probability models adopted for A2G links involving UAVs with SG [7, 11, 20, 25, 30].

Environment	α	β	γ	a	b
Suburban	0.1	750	8	4.88	0.429
Urban	0.3	500	15	9.612	0.158
Dense Urban	0.5	300	20	12.081	0.114
Highrise Urban	0.5	300	50	27.23	0.078

Table 3.1: Parametrisation of different environments for the A2G LoS probability model from [29].

3.3.5 Putting Everything Together

The total attenuations for LoS or NLoS wireless links are given by

$$L_L(\|\boldsymbol{x}\|) = \frac{A_L\|\boldsymbol{x}\|^{\alpha_L}}{S_L|h_L|^2} \quad \sim \quad p_{R,L}(r), \tag{3.19}$$

$$L_N(\|\boldsymbol{x}\|) = \frac{A_N\|\boldsymbol{x}\|^{\alpha_N}}{S_N|h_N|^2} \quad \sim \quad p_{R,N}(r). \tag{3.20}$$

For G2G links, the distance $\|\boldsymbol{x}\|$ corresponds usually to the ground distance between the source and the destination node, since the height of the terrestrial nodes is often omitted. However, for A2G links, the altitude of the aerial nodes cannot be neglected. Therefore the distance $\|\boldsymbol{x}\|$ is expressed as $\|\boldsymbol{x}\| = \sqrt{r^2 + H_F^2}$, where r is the ground distance between the source and the destination node, and H_F is the altitude of the aerial node.

The links are in LoS or NLoS with a probability given by the models presented in Section 3.3.4, different for G2G and A2G links. The fading phenomena are taken into account through the path-loss coefficients A_n, the PLEs α_n, the shadowing RVs S_n and the fast fading RVs h_n. These parameters differ if the links are in LoS or NLoS, but they are usually identical for all the nodes of the same kind.

Note that, in order to avoid any convergence issue with the numerical integration of the SG expressions, as in [11], the distance $\|\boldsymbol{x}\|$ is sometimes replaced by $1+\|\boldsymbol{x}\|$ and the path-loss parameters are adapted accordingly. It is also the case in this study for direct links.

3.4 Association Rule

The association rule defines which source node should be selected to communicate with the destination node. In order to achieve the best performance, the destination node should naturally be associated with the source node which can provide the highest SINR in order to achieve the best possible coverage and spectral efficiency. However, this leads to non tractable results for most of the scenarios.

Another approach considers rather the long-term average power instead of the SINR [31], since the performance of the link is closely related to the target link's received power. Indeed, the cell-level association in cellular networks acts on the order of seconds, and therefore fast fading effects are averaged out [30]. A bias factor is also introduced in [32].

Thus, with the **maximum biased average power association** rule, the node $\tilde{\boldsymbol{\phi}}$ is selected among all the nodes in $\boldsymbol{\Phi}$ to communicate with a node located at position $\boldsymbol{x}$ if

$$\begin{aligned}\tilde{\boldsymbol{\phi}} &= \underset{\boldsymbol{\phi}_i \in \boldsymbol{\Phi}}{\operatorname{argmax}} \left\{ b_{\boldsymbol{\Phi}}\, \mathbb{E}_{|h_{n_i}|^2} \left[P_i G_i L_{n_i}^{-1}(\|\boldsymbol{\phi_i} - \boldsymbol{x}\|) \right] \right\} \\ &= \underset{\boldsymbol{\phi}_i \in \boldsymbol{\Phi}}{\operatorname{argmax}} \left\{ b_{\boldsymbol{\Phi}} \frac{P_i G_i}{K_{n_i}} \|\boldsymbol{\phi}_i - \boldsymbol{x}\|^{-\alpha_{n_i}} S_{n_i} \right\}, \end{aligned} \tag{3.21}$$

where $b_{\boldsymbol{\Phi}}$ is the bias factor, P_i is the transmit power of the node $\boldsymbol{\phi}_i$, G_i is the total beamforming gain between the source and the destination node, and L_{n_i} is the total attenuation of the link.

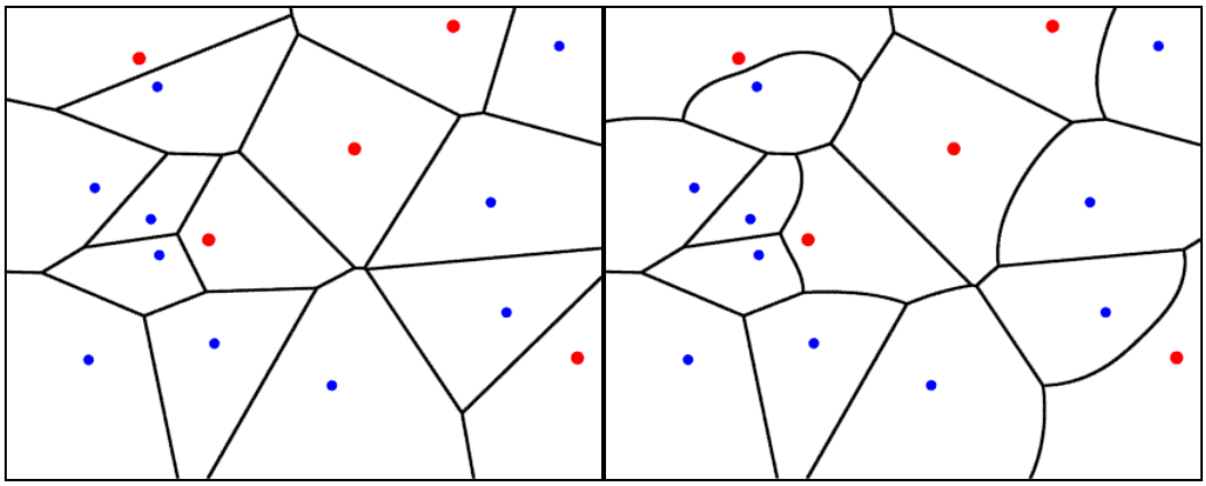

Figure 3.5: Regions of association with the nearest neighbour (left) and the maximum average power (right) assocation rules. The red and blue dots represent respectively nodes with a LoS or NLoS link. All the propagation parameters are equal in both cases, except for the path-loss coefficients ($A_N = 10A_L$) and the PLEs ($\alpha_L = 3, \alpha_N = 4$).

Instead of the maximum biased average power criterion, the **nearest neighbour association** rule is also often considered in SG thanks to its mathematical tractability. With this criterion, the node $\tilde{\boldsymbol{\phi}}$ is selected among all the nodes in $\boldsymbol{\Phi}$ to communicate with a node located at position $\boldsymbol{x}$ if

$$\tilde{\boldsymbol{\phi}} = \underset{\boldsymbol{\phi}_i \in \boldsymbol{\Phi}}{\operatorname{argmax}} \left\{ \|\boldsymbol{\phi}_i - \boldsymbol{x}\| \right\}. \tag{3.22}$$

Note that the two criteria are identical if the following assumptions are fulfilled:

- the transmitted power and the total beamforming gain are identical for all the nodes $\boldsymbol{\phi}_i$ in $\boldsymbol{\Phi}$;
- the propagation parameters are identical in the LoS and NLoS case.

Figure 3.5 highlights the differences between the two presented association rules when the path-loss parameters are not the same for LoS and NLoS links.

3.5 Additional Models for Wireless Relay Networks

For wireless networks involving relays, the performance of the relay link (from the source to the destination through the RN) are analysed. The achieved performance can also vary depending on the relay transmission protocol. Moreover, direct links are either neglected or taken into account. Therefore, the study of wireless relay networks needs additional considerations about the association scheme and the transmission protocol which are adopted.

3.5.1 Relay Association Scheme

The performance of two-hop relay links does not only depend on the second hop (from the RN to the destination node), but it also varies depending on the first hop (from the source node to the RN). Therefore, the association rule presented in Section 3.4 must be extended for wireless relay networks.

The destination node should naturally be associated with the link which can provide the highest SINR in order to achieve the best possible coverage and spectral efficiency. This should be estimated for relay links but also for direct links. For direct links, the best link can be selected following the association rules presented in Section 3.4. This is not the case for relay links, since their performances also depend on the first hop. To overcome this issue, different strategies have been adopted.

In [16, 19, 20, 25], the density of RNs which are able to decode the signal coming from the source is first computed based on the received Signal-to-Noise Ratio (SNR). Then, either the destination node combines the signals coming from these RNs, or it selects the best link among this subset based on the received power or the SNR.

Another solution adopted by [32] is to first choose the RN which provides the highest average power to the destination node, and then to choose the TBS which provides the highest average power to the selected RN. However, with this approach, a RN very close to the destination node could be selected even if the performance of another RN's link is better, depending on the first hop.

Furthermore, depending on the transmission protocol, the best direct link and relay link are combined, or the best of the two is selected. The selection is done in [32] by comparing the average power received at the destination node from the selected RN and TBS. Contrariwise, [16, 19, 20, 25] consider only the relay links, assuming that direct links suffer from strong shadowing.

3.5.2 Relay Transmission Protocol

In wireless relay networks, the relay transmission protocol should be specified, since it impacts the expression of the SINR for the relay link. Therefore, in studies focused on relay networks, two protocols are commonly applied: the **Amplify-and-Forward** (AF) and **Decode-and-Forward** (DF) protocols [33–38].

Amplify-and-Forward Protocol

With the AF protocol, the signal received at the relay node is amplified and directly re-emitted. The communication from the source to the destination is executed in one step. If the channel attenuations of all the links are modelled following a simple flat fading channel model, [35] shows that the SNR of the complete link is given by

$$SNR_{AF} = SNR_{SD} + \frac{SNR_{SR}SNR_{RD}}{SNR_{SR} + SNR_{SD} + 1}, \tag{3.23}$$

where SNR_{SD}, SNR_{SR} and SNR_{RD} are respectively the SNR from the source to the destination, from the source to the RN, and from the RN to the destination.

The SNR expressed in Equation (3.23) is achieved by combining the contribution from the direct link and the relay link. This is also the expression adopted in [33, 37, 38].

However, when the direct link is supposed to be strongly obstructed, or when the relay link is considered separately, the contribution of the direct link is removed from Equation (3.23):

$$SNR_{SRD,AF} = \frac{SNR_{SR}SNR_{RD}}{SNR_{SR} + SNR_{SD} + 1}. \tag{3.24}$$

Moreover, in [16], an approximation of Equation (3.24) is adopted, as suggested by [36]:

$$SNR_{SRD,AF} \approx \frac{SNR_{SR}SNR_{RD}}{SNR_{SR} + SNR_{SD}}. \tag{3.25}$$

Note that Equation (3.24) can be further extended to take into account interfering links [34].

Decode-and-Forward Protocol

With the DF protocol, the signal received at the RN is first decoded, and then re-emitted. In that case, the performance of the two-hop link is limited by the rate at which the RN can decode the signal from the source. With this protocol, the SNR of the complete link to the destination is given by [33]

$$SNR_{DF} = \min\left(SNR_{SR}, SNR_{SD} + SNR_{RD}\right), \tag{3.26}$$

where SNR_{SD}, SNR_{SR} and SNR_{RD} are respectively the SNR from the source to the destination, from the source to the RN, and from the RN to the destination. The SNR expressed in Equation (3.26) is achieved by combining the contributions of both the direct and relay links. However, in most works using the DF protocol, the transmission is done in two steps [19, 20, 32]. In that case, Equation (3.26) can be simplified:

$$SNR_{SRD,DF} = \min\left(SNR_{SR}, SNR_{RD}\right). \tag{3.27}$$

Equation (3.27) can be further extended to take into account interfering links in a simple way:

$$\chi_{SRD,DF} = \min\left(\chi_{SR}, \chi_{RD}\right). \tag{3.28}$$

where χ_{SRD}, χ_{SR} and χ_{RD} are respectively the SINR of the complete relay link, from the source to the RN and from the RN to the destination.

Amplify-and-Forward Protocol vs Decode-and-Forward protocol

In practice, the AF protocol is easier to implement since the received signal must only be amplified and not decoded. However, even if it can lead to better performance than the DF protocol depending on the scenario [33–35], mathematics are intractable when the propagation models are complexified. Therefore, the DF protocol is used in most works evaluating the performance of wireless relay networks using SG, and particularly when interfering links are also taken into account.

3.6 Performance Metrics

Numerous metrics are defined for each scenario in order to estimate the performance of wireless networks. However, for communication purposes, the same popular metrics, based on the SNR, Signal-to-Interference Ratio (SIR), or SINR at the destination node, are evaluated in almost all scenarios. In SG, these quantities are always RVs, function of the topology of the network and the propagation conditions. Therefore, the appropriate metrics are based on the following RVs' statistics (PDF, moments, ...).

3.6.1 Typical Metrics

Coverage and Outage Probability

The **Coverage Probability** (CP) $\mathcal{P}$ is defined as the probability that the SINR at the typical node χ is higher or equal than a predefined SINR threshold β. It is defined by contrast with the **Outage Probability** (OP) $\mathcal{O}$, the probability that the SINR at the typical node is lower than this predefined threshold:

$$\mathcal{P}(\beta) = \mathbb{P}_\chi\left(\chi \geq \beta\right) = 1 - \mathbb{P}_\chi\left(\chi < \beta\right) = 1 - \mathcal{O}(\beta). \tag{3.29}$$

The CP corresponds to the probability that the typical node is able to decode without error the incoming signal transmitted over a bandwidth B, at a rate $R = B\log_2(1+\beta)$.

Note that the OP and the CP are respectively equal to the Cumulative Distribution Function (CDF) and the CCDF of the SINR at the typical node. Therefore, its PDF can be obtained by deriving the CP or the OP:

$$f_\chi(x) = \left.\frac{\mathrm{d}\mathcal{O}}{\mathrm{d}\beta}\right|_{\beta=x} = -\left.\frac{\mathrm{d}\mathcal{P}}{\mathrm{d}\beta}\right|_{\beta=x}. \tag{3.30}$$

Average Rate and Spectral Efficiency

The **rate** (or **capacity**) is defined as the maximum number of bits per second that the typical node is able to decode without error. Under standard modelling assumptions [39], for a given bandwidth B and a SINR at the typical node χ, it is expressed as

$$R = B\log_2\left(1+\chi\right) \quad \left[\frac{\text{bits}}{\text{s}}\right]. \tag{3.31}$$

Similarly, the **Spectral Efficiency** (SE) is defined as the rate over a normalised bandwidth:

$$SE = \frac{\mathcal{R}}{B} = \log_2\left(1+\chi\right) \quad \left[\frac{\text{bits}}{\text{s}\cdot\text{Hz}}\right]. \tag{3.32}$$

With SG, since the SINR value is a RV, these metrics are not evaluated directly. Instead, the **average** (or **ergodic**) **rate** and **spectral efficiency** are actually computed:

$$\mathcal{R} = \mathbb{E}_R[R] \qquad = B\,\mathbb{E}_\chi[\log_2(1+\chi)] \quad \left[\frac{\text{bits}}{\text{s}}\right], \tag{3.33}$$

$$\mathcal{S} = \mathbb{E}_{SE}[SE] = \frac{\mathcal{R}}{B} = \mathbb{E}_\chi[\log_2(1+\chi)] \quad \left[\frac{\text{bits}}{\text{s}\cdot\text{Hz}}\right]. \tag{3.34}$$

Note that the average SE can be computed based on the CP:

$$\begin{aligned}\mathcal{S} &= \int_0^\infty \mathbb{P}_\chi(\log_2(1+\chi) > \gamma)\,\mathrm{d}\gamma = \int_0^\infty \mathbb{P}_\chi(\chi > 2^\gamma - 1)\,\mathrm{d}\gamma \\ &= \frac{1}{\ln 2}\int_0^\infty \frac{\mathbb{P}_\chi(\chi > \beta)}{1+\beta}\mathrm{d}\beta = \frac{1}{\ln 2}\int_0^\infty \frac{\mathcal{P}(\beta)}{1+\beta}\mathrm{d}\beta.\end{aligned} \tag{3.35}$$

Some studies use another definition of the average rate [13, 39–41]: for a given SINR threshold β, the average rate is given by

$$\tilde{\mathcal{R}}(\beta) = B\log_2(1+\beta)\mathcal{P}(\beta) \quad \left[\frac{\text{bits}}{\text{s}}\right]. \tag{3.36}$$

With Equation (3.33), an average over the possible realisations of the SINR is computed. Therefore, it assumes that the channel statistics remain unchanged (stationarity) for every realisation of the network, and ergodism (short channel coherence time) is needed for estimation in real networks. Strictly speaking, in Equation (3.36), no average is computed. However, the rate which would be achieved if a SINR threshold β is needed to decode successfully the signal, is pondered by the probability that the SINR at the typical node is higher than β. The first definition is adopted in this study.

Average Energy Efficiency

The average rate is a relevant metric as long as the power needed for the network to achieve this rate stays realistic. Since it should always be evaluated in regards to the consumed power, the metric of energy efficiency has been introduced.

The **Energy Efficiency** (EE) is defined as the ratio of the achievable rate and the total power consumption of the network P_T:

$$E = \frac{R}{P_T} = \frac{B\log_2(1+\chi)}{P_T} \quad \left[\frac{\text{bits}}{\text{J}}\right]. \tag{3.37}$$

As for the average rate, the **average energy efficiency** is the actual metric which is computed. Depending on the adopted definition of the average rate (respectively Equation (3.33) or (3.36)), it is expressed as

$$\mathcal{E} = \frac{\mathcal{R}}{P_T} = \frac{B\,\mathbb{E}_\chi[\log_2(1+\chi)]}{P_T} \quad \left[\frac{\text{bits}}{\text{J}}\right], \tag{3.38}$$

or

$$\tilde{\mathcal{E}} = \frac{\tilde{\mathcal{R}}}{P_T} = \frac{B \log_2(1+\beta)\mathcal{P}(\beta)}{P_T} \quad \left[\frac{\text{bits}}{\text{J}}\right]. \tag{3.39}$$

Note that studies sometimes define the average EE in regards to the average SE per unit area and the total power consumption per unit area [7, 39, 42]. However, the total noise power is a function of the bandwidth, therefore the expressions presented in Equation (3.38) and (3.39) are relevant only when the noise is not neglected.

Average Exposure

With the release of the new generation of networks as the Fifth Generation (5G) scheduled for the next few years, a new metric of interest is introduced: the **exposure**. It is defined as the total (electromagnetic) power to which a user is exposed.

If a typical node which communicates with its associated source node, receives a power U and an additional power I from all the interfering nodes, the exposure at the typical node is given by

$$X_c = U + I \quad [\text{W}]. \tag{3.40}$$

If the typical node does not communicate with any transmitter, all the emitting nodes are considered as interferers, and the exposure is then given by

$$X = I \quad [\text{W}]. \tag{3.41}$$

As for the other metrics, the **average exposure** $\mathcal{X}$ is the actual metric which is computed. Depending on the scenario, it is given by

$$\mathcal{X}_c = \mathbb{E}_{X_c}[X_c] = \mathbb{E}_U[U] + \mathbb{E}_I[I] \quad [\text{W}] \tag{3.42}$$

or

$$\mathcal{X} = \mathbb{E}_X[X] = \mathbb{E}_I[I] \quad [\text{W}]. \tag{3.43}$$

3.6.2 Other Metrics

Other metrics are very specific to some kind of scenario. For example, in [13], a UAV is deployed to act as a flying base station in order to serve some users in a disk of radius R, while other D2D users are communicating simultaneously with each other in the same area. In that case, the achievable rate for both UAV-served and D2D UEs must be evaluated. Therefore, the study defines the **system sum-rate** $\tilde{\mathcal{R}}_{\mathcal{T}}$ based on Equation (3.36):

$$\tilde{\mathcal{R}}_{\mathcal{T}}(\beta) = \underbrace{\pi R^2 \lambda_U \, B \log_2(1+\beta)\mathcal{P}_U(\beta)}_{\text{total average rate for UAV-served users}} + \underbrace{\pi R^2 \lambda_D \, B \log_2(1+\beta)\mathcal{P}_D(\beta)}_{\text{total average rate for D2D users}} \quad \left[\frac{\text{bits}}{\text{s}}\right], \tag{3.44}$$

where λ_U, $\mathcal{P}_U$ and λ_D, $\mathcal{P}_D$ are respectively the densities and the coverage probabilities of UAV-served and D2D UEs.

Moreover, with mobile UAV BSs, some users could be out of coverage at some time owing to the mobility of the BS. Therefore, it should also be quantified. Still in [13], the **delay between two transmissions** is expressed as a function of the coverage radius of the UAV, the time needed for a transmission and the number of stop points. In [43], stochastic trajectories are evaluated for mobile UAV BSs. In this scenario, they define the **average fade duration** as the average time between entering into a fading situation and going out of it.

3.7 Applications

As described in Chapter 1, UAVs have a lot of attractive features, which make them good candidates to be integrated in tomorrow's wireless networks. In this section, some existing works studying the performance of UAV-based networks in numerous specific scenarios are presented. More particularly, we focus on three applications in which the key features of UAVs (and more particularly LAPs) are necessary, or at least enable some performance enhancement: post-disaster and hotspot scenarios, relay networks, and mobile BSs.

3.7.1 Post-disaster and Hotspot Scenarios

A terrestrial cellular network can be subject to destructions or failures due to natural or man-made phenomena, which result in coverage holes, while communication is precisely critical in that kind of scenarios. Drone empowered Small Cellular Networks (DSCN) seem very attractive to overcome these shortcomings. Their flying capability and mobility enable fast displacements to the areas of interest, regardless to the ground topology. Even if endurance is limited, this new network structure is supposed to be temporary by definition.

Quite similarly, UAVs are also an attractive solution for hotspot scenarios. Indeed, a large and unusual number of UEs are temporary regrouped in some localised areas, such that the capacity need is beyond what the terrestrial cellular network can provide. In that situation, the ease of deployment and the associated costs of UAVs seem an appealing solution. Limited endurance is not really an issue since that kind of events is supposed to be temporary.

In these scenarios, it is quite realistic to assume that the UEs are clustered in some localised area, either because of a temporary event or owing to a natural disaster. In order to meet the Quality of Service (QoS) requirements, one or numerous UAVs may be deployed to help or replace the damaged TBSs which should serve this area. Therefore, the position of the users and the position of the UAVs are naturally modelled using PCPs. This kind of model has been adopted in [7, 30].

In [7], TBSs are destroyed independently with a certain probability to model a disaster. Around each destroyed point, a fixed number of UAVs is deployed to replace it, following a MCP or a TCP, in a radius (or with a standard deviation) depending on the coverage radius of the destroyed TBS. There can be multiple UAVs for each destroyed TBS since the UAVs' capacity is more limited. This scenario is illustrated in Figure 3.6. The distribution of UEs is supposed to be the same as the distribution of UAVs, with the same density. Additionally, every UAV is associated with only one user in the same channel resource block.

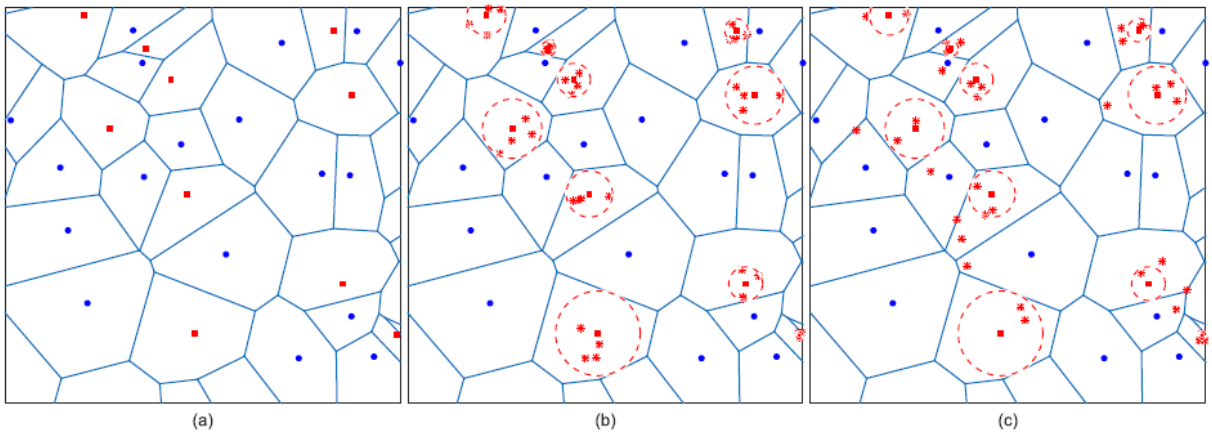

Figure 3.6: Generation of the post-disaster network. In (a), TBS are destroyed with probability 0.3 (red squares). Then, Four UAVs (red stars) are deployed around the destroyed BSs, following a MCP in (b) and a TCP in (c) (Source: [7]).

A propagation model with LoS and NLoS large-scale fading and a Rayleigh distributed small-scale fading is supposed. The LoS probability model for the UAV-UE links is the one classically used for LAPs, given by Equation (3.18). The UEs are assumed to be served with the nearest UAV. The performance metrics which are evaluated are the CP, the average area SE and the average SE.

A different approach is followed in [44]: TBSs are also destroyed independently with a certain probability to model a disaster, but only in a disk with fixed radius. Consequently, the density of the TBSs which have not been destroyed follows an IHPPP with a piece-wise constant density. The UAVs are distributed in the disk following a BPP, and a typical UE located at the center of the disk is considered. The propagation model is identical to the one adopted in [7], with also the same LoS probability model, and the same association rule. An analytical expression of the CP is provided.

Finally, [30] consider an urban environment with multiple demand hotspots. The UEs are therefore distributed following a MCP, and the number of UEs is random. Each UAV is positioned exactly at the center of each hotspot. They suppose a propagation model with LoS and NLoS large-scale fading and a Nakagami-m distributed small-scale fading. The LoS probability model for the UAV-UE links is given by Equation (3.17). The UEs are assumed to be served by the UAV which provides the highest long-term average received power, as given by Equation (3.21). The CP and the average SE are the metrics of interest.

3.7.2 Relay Networks

In scenarios with strong shadowing, harsh environment which makes ground displacement difficult, or even in post-disaster and hotspots scenarios as previously described, UAVs are good candidates for relaying purposes. Indeed, compared to TBSs, there is no ground topology constraint. Furthermore, a high probability for the link between the UAV and the UE to be in LoS can be achieved thanks to their flying capability, while it would not be possible with a terrestrial link. This feature is particularly required in mmWave scenarios where LoS links and a large number of relays are needed owing to the high

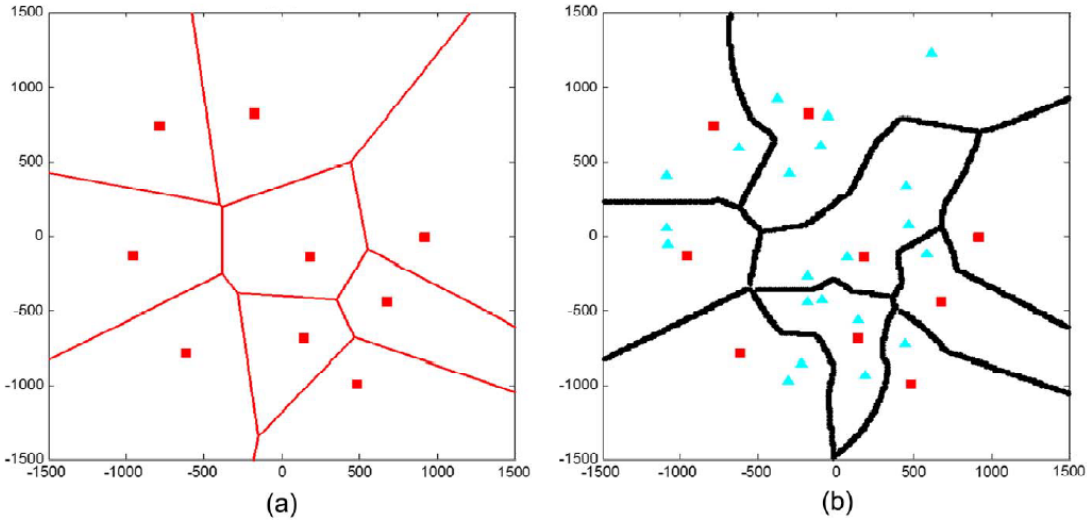

Figure 3.7: Regions of association in absence of shadowing, without relays (a) or with relays (b). Squares and triangles denote respectively BSs and RNs (Source: [32]).

path-loss. Additionally, deployment is easier, and mobility enables dynamic adjustments of the UAVs' positions and speeds to enhance the performance of the network.

When we focus on relay networks, besides the performance of the link between the UE and the RN or the TBS, the performance of the link from the TBS to the RN (or from any other source which provides informations to the relay) should also be studied. Indeed, the SINR of the whole two-hop link can be expressed as a function of the SINR of each hop, depending on the relay transmission protocol which is used. This has been detailed for the AF and DF protocols in Section 3.5.2. Additionally, direct links are also considered depending on the scenario. Therefore, the association rule must also be adapted, as presented in Section 3.5.1. Different frameworks have been developed with terrestrial RNs to this end.

In [32], a mathematical framework for the analysis and the optimisation of two-hop relay-aided cellular networks is provided. Base stations, RNs and mobile terminals are modelled by three HPPPs. A best biased average received power association rule is considered, and direct links are compared with two-hops links using the same criterion. Figure 3.7 illustrates the modification of the coverage regions owing to the presence of RNs in this study. A linear path-loss model is adopted, with log-normally distributed shadowing and Rayleigh small-scale fading. The DF protocol is selected for the relay transmissions. The CP and average rate are the metrics of interest.

In a mmWave scenario, [16, 19] evaluate the performance of a two hop link. In the former, the source and the destination are at a fixed position, and the RN locations are modelled by a HPPP. They suppose a propagation model with linear path-loss and Nakagami-m small-scale fading. Different selection modes (direct link only, best relay, ...) are compared. The DF transmission scheme is selected. In the latter, the sources and the RNs are modelled by two independent HPPPs. They suppose a propagation model with linear path-loss and log-normally distributed shadowing. Small-scale fading is neglected. The AF transmission scheme is selected. In both studies, the CP and the average SE are evaluated.

However, these frameworks developed for terrestrial RNs cannot be directly exploited for UAV RNs since the altitude of these UAVs plays a major role for the performance of the network.

In [20], UAV relay links are studied in a secrecy context with mmWaves: cooperative jamming UAV degrades the quality of eavesdropping channels to enhance the security. Relay nodes and eavesdroppers are modelled as two independent HPPPs. A propagation model with linear path-loss and Nakagami-m small-scale fading is supposed. LoS and NLoS links are considered following the LoS probability model for LAPs given by Equation (3.18). The secrecy OP is evaluated.

Finally, the performance of a cooperative UAV relay network is evaluated in [25], for a Non Orthogonal Multiple Access (NOMA) scenario involving two users at fixed locations. The number of UAV RNs and their locations are also fixed, but the interfering nodes on the ground are modelled using a HPPP. The selected propagation models are identical to those used in [20]. The evaluated performance metrics are the OP and the average sum-rate of the users.

3.7.3 Mobile UAVs

Compared to TBSs, which can potentially be mounted on ground vehicles, UAVs are not constrained by the ground topology, and are easier to deploy. This increased mobility enables dynamic adjustments of their position and speed to enhance the performance of the networks.

When the performance of a wireless network including UAVs is evaluated, the mobility scheme must be specified. It can be separated in deterministic or stochastic trajectories, in two (fixed altitude) or three (varying altitude) dimensions.

With deterministic trajectories, in [13], a UAV flying at a fixed altitude is moving around a circular area in order to provide coverage for multiple UEs. Other D2D UEs also communicate with each other in the same area. Both are modelled using independent HPPPs. The system model is illustrated in Figure 3.8a. LoS and NLoS link following the classical LoS probability model for LAPs, given by Equation (3.18), and a linear path-loss model with Rayleigh-distributed small-scale fading is considered. The UAV circulates through an arbitrary number of stop points, in order to cover the whole area after all the stop points have been visited. The number and the position of the stop points are defined depending on the coverage radius of the UAV and the radius of the area (disk covering problem). The metrics of interest are the average sum-rate and the time required for the UAV to cover the whole area, which is also the time between two requests.

An uplink scenario where IoT devices transmit their data to numerous UAVs flying at a fixed altitude, and distributed periodically on a line with an initial uniformly distributed shift is presented in [45]. The fleet flies in the orthogonal direction with a fixed speed. A linear path-loss model with Nakagami-m small-scale fading is considered. From the UAVs' perspective, the CP and the mean data rate are evaluated, while the mean amount of data transmitted is evaluated from the IoT's perspective.

With stochastic trajectories, in [46], a fixed number of UAVs are distributed following a BPP in a circular area at a fixed altitude. They flight independently with each other,

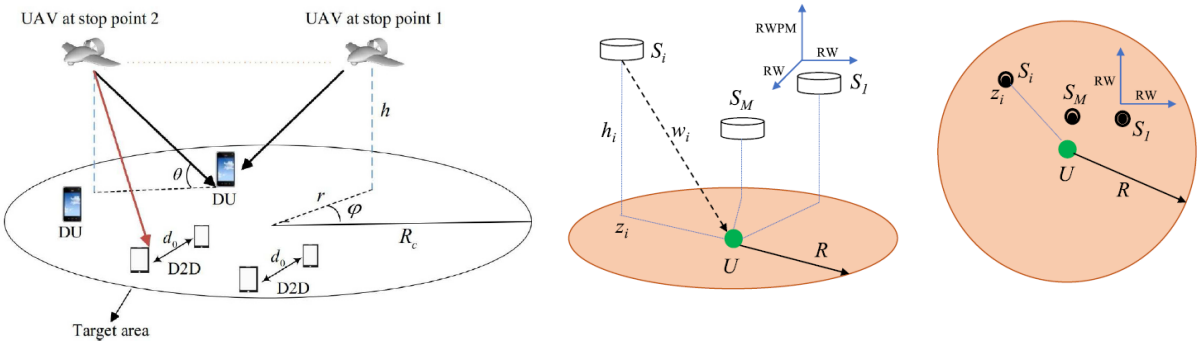

(a) (b)

Figure 3.8: Network model (a) in [13] and (b) in [47] (Source: [13, 47]).

and follow an arbitrary trajectory process. In order to provide an uniform coverage at each time step, two families of trajectory processes (referred as spiral and oval) have been identified. Deterministic counterparts of important trajectories of the two families are also developed. A propagation model with linear path-loss and Nakagami-m small-scale fading is assumed. The associated UAV is selected using a nearest neighbour association rule. For these trajectories, the CP and the average fade duration are evaluated.

Another mobility scheme in three dimensions is considered in [47]. A fixed number of UAVs are deployed uniformly in a cylindrical area. Their altitudes are modified independently following a Random WayPoint Mobility (RWPM) model, while their horizontal locations are modified following a Random Walk (RW) model. This system model is illustrated in Figure 3.8b. A linear path-loss model with Nakagami-m small-scale fading is considered. The associated UAV is either selected uniformly between all the UAVs, or following the nearest neighbour criterion. The metric of interest is the CP.

Finally, in [48], a fleet of UAVs are distributed at a fixed altitude following an HPPP. Two mobility scheme are selected: in both cases, the interfering UAVs fly in independent directions at a fixed speed. The serving UAV is selected following the nearest neighbour criterion: either it flies in a random direction, or towards the typical UE and hovers above it. A propagation model with linear path-loss and Rayleigh small-scale fading is supposed, and the CP and average rate are evaluated.

Chapter 4

UAV-based Relay Networks with Fixed Position

Numerous studies relative to UAV-based relay networks have been presented in Section 3.7. However, direct links are often neglected, and the performance obtained for the whole link from a TBS to the typical UE through a UAV RN, where both the TBSs and the RNs are modelled using two HPPPs has not been evaluated yet. Therefore, in this chapter, a general framework for the study of UAV-based relay networks with fixed position using SG is described.

4.1 System Model

We consider a typical UE located at ground level at position $(0, 0)$ in $\mathbb{R}^2$. Both locations of TBSs and UAV RNs are modelled using two independent HPPPs $\mathbf{\Phi}_T$ and $\mathbf{\Phi}_R$ of density λ_T and λ_R in $\mathbb{R}^2$. TBSs are distributed at ground level, while UAV RNs are flying at a fixed altitude H_R. Additionally, we suppose $\lambda_R >> \lambda_T$, and a highly congested network. In that case, all the RNs or TBSs are interfering with each other while transmitting.

The selected relay transmission protocol is decode-and-forward. We assume that the protocol is executed in two steps. First, the TBSs transmit the information to the RNs. Then, the information is decoded and re-transmitted by the RNs to the UEs.

Both TBSs and UAV RNs are equipped with antenna arrays. This is modelled using the sectored antenna model given by Equation (3.2). The achieved beamforming gains are summarised in Table 4.1.

For the propagation model, LoS and NLoS links are considered. The selected LoS probability models for G2G and A2G links are respectively given by Equations (3.14) and

	Target	Interference
TBS-RN	$G_{SR,M} = G_{TM}G_{RM}$	$G_{SR,m} = G_{Tm}G_{Rm}$
TBS-UE	$G_{SD,M} = G_{TM}$	$G_{SD,m} = G_{Tm}$
RN-UE	$G_{RD,M} = G_{RM}$	$G_{RD,m} = G_{Rm}$

Table 4.1: Beamforming gains for the different links.

		Model	Equation	Parameters	Units
TBSs		HPPP in $\mathbb{R}^2$ at ground	–	λ_T	$[m^{-2}]$
		constant power		P_T	$[W]$
UAV RNs		HPPP in $\mathbb{R}^2$	–	λ_R	$[m^{-2}]$
		fixed altitude		H_R	$[m]$
		constant power		P_R	$[W]$
Beamforming	G2G	Sectored antenna model	(3.2)	G_{TM}, G_{Tm}	[\ ]
	A2G			G_{RM}, G_{Rm}	[\ ]
Path-loss	G2G	Linear path-loss model	(3.3)	A_{GL}, A_{GN}	[\ ]
				α_{GL}, α_{GN}	[\ ]
	A2G			A_{AL}, A_{AN}	[\ ]
				α_{AL}, α_{AN}	[\ ]
Shadowing	G2G	Log-normal shadowing	(3.5)	$\sigma^2_{GL}, \sigma^2_{GN}$	[\ ]
	A2G			$\sigma^2_{AL}, \sigma^2_{AN}$	[\ ]
Small-scale fading	G2G	Rice	(3.10)	K_{GL}, K_{GN}	[\ ]
	A2G			K_{AL}, K_{AN}	[\ ]
	G2G	Nakagami-m	(3.12)	m_{GL}, m_{GN}	[\ ]
	A2G			m_{AL}, m_{AN}	[\ ]
LoS probability	G2G	3GPP d_1/d_2 model	(3.14)	d_1, d_2	$[m]$
	A2G	Sigmoid model	(3.18)	a, b	[\ ]
Association scheme		Nearest neighbour association	(3.22)	–	–
		Selection: direct or relay link	–		
Transmission protocol		DF protocol in two steps	(3.28)	–	–
Additional assumptions		Highly congested network			

Table 4.2: Summary of the system model and parameters involved.

(3.18). We consider a linear path-loss model given by Equation (3.3), with log-normal shadowing and Rician or Nakagami-m fading. The PDFs of the shadowing, of the Rice and of the Nakagami-m channel power gain are respectively given by Equations (3.5), (3.10) and (3.12).

The nearest neighbour association rule given by Equation (3.22) is selected. The typical UE is served by its closest node, either a TBS or a UAV RN. If a RN is selected, this RN itself is served by its closest TBS. Figure 4.1 illustrates the geometry of the scenario. Table 4.2 summarises all the considered models and their related parameters.

Three links must be studied:

- the link from the typical UE to its closest TBS, namely the **direct link**;
- the link from the typical UE to its closest UAV RN, namely the **first hop** of the relay link;

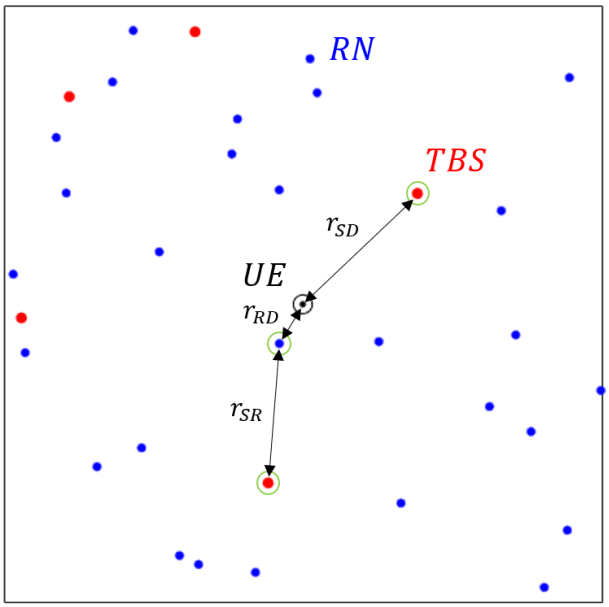

Figure 4.1: Illustration of the scenario: the typical UE is positioned at position $(0, 0)$ in $\mathbb{R}^2$. The RNs and the TBSs are respectively represented by blue and red dots. The selected TBS, the selected RN and its closest TBS are circled in green.

- the link from the selected RN to its closest TBS, namely the **second hop** of the relay link.

The quantities related to these three links are respectively denoted using the acronyms SD, SR and RD, and quantities related to the relay link are denoted with the acronym SRD.

4.1.1 Signal to Interference plus Noise Ratio

In order to develop mathematical expressions of the performance metrics, the SINR of each link must be precised.

Direct Link

The SINR of the direct link at the typical UE for a LoS or NLoS propagation is given by

$$\chi_{SD,n} = \frac{U_{SD,n}}{I_{SD} + \sigma^2}, \tag{4.1}$$

with $U_{SD,n}$ and I_{SD}, respectively the power from the selected TBS at the typical UE in LoS or NLoS and the aggregate interference of the TBSs at the typical UE. If we define

$$C_{SD,n} = \frac{P_T G_{SD,M}}{A_{Gn}} = \frac{P_T G_{TM}}{A_{Gn}} \quad \text{and} \quad c_{SD,n} = \frac{P_T G_{SD,m}}{A_{Gn}} = \frac{P_T G_{Tm}}{A_{Gn}}, \tag{4.2}$$

these powers are expressed as

$$U_{SD,n} = P_T G_{SD,M} L_{Gn}^{-1}(r_{SD}) = C_{SD,n}(1 + r_{SD})^{-\alpha_{Gn}} |h_{SD,n}|^2 S_{SD,n} \tag{4.3}$$

$$I_{SD} = \sum_{\phi_j \in \mathbf{\Phi}_{SDI}} P_T G_{SD,m} L_{Gn_j}^{-1}(\|\boldsymbol{\phi}_j\|)$$
$$= \sum_{n=\{L,N\}} \sum_{\phi_j \in \mathbf{\Phi}_{SDI,n}} c_{SD,n}(1+\|\boldsymbol{\phi}_j\|)^{-\alpha_{Gn}} |h_{SD,n,j}|^2 S_{SD,n,j}, \tag{4.4}$$

where r_{SD} is the distance between the typical UE and its closest TBS and σ^2 is the noise power. The PP in $\mathbb{R}^2$ corresponding to the locations of the interfering TBSs is denoted by $\mathbf{\Phi}_{SDI} = \mathbf{\Phi}_T \setminus \{\tilde{\boldsymbol{\phi}}_{SD}\}$, with $\tilde{\boldsymbol{\phi}}_{SD}$ being the TBS which is the closest to the typical UE. The PPs of the TBSs interferers in LoS and NLoS are respectively denoted by $\mathbf{\Phi}_{SDI,L}$ and $\mathbf{\Phi}_{SDI,N}$.

Relay Link

The SINR at the typical UE and at the selected RN for LoS or NLoS links are respectively given by

$$\chi_{SR,n} = \frac{U_{SR,n}}{I_{SR} + \sigma^2} \qquad \text{and} \qquad \chi_{RD,n} = \frac{U_{RD,n}}{I_{RD} + \sigma^2}, \tag{4.5}$$

with $U_{SR,n}$, $U_{RD,n}$, I_{SR} and I_{RD}, respectively the power from the TBS serving at the selected RN in LoS or NLoS, the power from the selected RN at the typical UE in LoS or NLoS, the aggregate interference of the TBSs at the selected RN, and the aggregate interference of the UAV RNs at the typical UE. If we define

$$\begin{aligned} C_{SR,n} &= \frac{P_T G_{SR,M}}{A_{An}} = \frac{P_T G_{TM} G_{RM}}{A_{An}}, \qquad c_{SR,n} = \frac{P_T G_{SR,m}}{A_{An}} = \frac{P_T G_{Tm} G_{Rm}}{A_{An}}, \\ C_{RD,n} &= \frac{P_R G_{RD,M}}{A_{An}} = \frac{P_R G_{RM}}{A_{An}} \quad \text{and} \quad c_{RD,n} = \frac{P_R G_{RD,m}}{A_{An}} = \frac{P_R G_{Rm}}{A_{An}}, \end{aligned} \tag{4.6}$$

these powers are expressed as

$$U_{SR,n} = P_T G_{SR,M} L_{An}^{-1}\left(\sqrt{r_{SR}^2 + H_R^2}\right) = C_{SR,n}(r_{SR}^2 + H_R^2)^{-\frac{\alpha_{An}}{2}} |h_{SR,n}|^2 S_{SR,n} \tag{4.7}$$

$$U_{RD,n} = P_R G_{RD,M} L_{An}^{-1}\left(\sqrt{r_{RD}^2 + H_R^2}\right) = C_{RD,n}(r_{RD}^2 + H_R^2)^{-\frac{\alpha_{An}}{2}} |h_{RD,n}|^2 S_{RD,n} \tag{4.8}$$

$$I_{SR} = \sum_{\phi_j \in \mathbf{\Phi}_{SRI}} P_T G_{SR,m} L_{An_j}^{-1}\left(\sqrt{\|\boldsymbol{\phi}_j\|^2 + H_R^2}\right)$$
$$= \sum_{n=\{L,N\}} \sum_{\phi_j \in \mathbf{\Phi}_{SRI,n}} c_{SR,n}(\|\boldsymbol{\phi}_j\|^2 + H_R^2)^{-\frac{\alpha_{An}}{2}} |h_{SR,n,j}|^2 S_{SR,n,j}, \tag{4.9}$$

$$I_{RD} = \sum_{\phi_j \in \mathbf{\Phi}_{RDI}} P_R G_{RD,m} L_{An_j}^{-1}\left(\sqrt{\|\boldsymbol{\phi}_j\|^2 + H_R^2}\right)$$
$$= \sum_{n=\{L,N\}} \sum_{\phi_j \in \mathbf{\Phi}_{RDI,n}} c_{RD,n}(\|\boldsymbol{\phi}_j\|^2 + H_R^2)^{-\frac{\alpha_{An}}{2}} |h_{RD,n,j}|^2 S_{RD,n,j}, \tag{4.10}$$

where r_{SR} is the distance from the selected RN to its closest TBS and r_{RD} is the distance from the typical UE to the selected RN. The PP in $\mathbb{R}^2$ corresponding to the locations of the interfering TBSs is denoted by $\mathbf{\Phi}_{SRI} = \mathbf{\Phi}_T \setminus \{\tilde{\boldsymbol{\phi}}_{SR}\}$, with $\tilde{\boldsymbol{\phi}}_{SR}$ being the TBS which is the closest to the selected RN, and the PP in $\mathbb{R}^2$ corresponding to the locations of the interfering RNs is denoted by $\mathbf{\Phi}_{RDI} = \mathbf{\Phi}_R \setminus \{\tilde{\boldsymbol{\phi}}_{RD}\}$, with $\tilde{\boldsymbol{\phi}}_{RD}$ being the selected RN. The

PPs of the terrestrial and RNs interferers in LoS and NLoS are respectively denoted by $\mathbf{\Phi}_{SRI,L}$, $\mathbf{\Phi}_{SRI,N}$, $\mathbf{\Phi}_{RDI,L}$, and $\mathbf{\Phi}_{RDI,N}$,.

With the DF protocol, as given by Equation (3.28), the SINR of the relay link is:

$$\chi_{SRD} = \min\left(\chi_{SR}, \chi_{RD}\right). \tag{4.11}$$

4.1.2 Interferers' Point Processes

Owing to the highly congested network assumption, all the TBSs and RNs are supposed to be active, each at their respective time slot, since the transmission is executed in two steps. Additionally, according to the Slivnyak-Mecke's theorem, the exclusion of the two selected TBSs and the selected RN from these PPs does not affect their statistical properties.

Since the links between every couple of nodes are independent (there is no spatial correlation involved in the model), the PPs of the interferer nodes in LoS or NLoS are obtained by applying an independent thinning on the complete interferers PPs, respectively with probability $p_{GL}(r)$ and $p_{GN}(r) = 1 - p_{GL}(r)$ between two nodes at a distance r for G2G links, or $p_{AL}(r)$ and $p_{AN}(r) = 1 - p_{GL}(r)$ between two nodes at a ground distance r for A2G links. Therefore, the LoS or NLoS interferers PPs are distributed as two independent IHPPPs. Knowing r_{SD}, r_{SR} and r_{RD}, their densities are given by

$$\lambda_{SDI,n|r_{SD}}(r) = p_{Gn}(r)\lambda_{SDI|r_{SD}}(r) = p_{Gn}(r)\,\lambda_T\,u(r - r_{SD}), \tag{4.12}$$
$$\lambda_{SRI,n|r_{SR}}(r) = p_{An}(r)\lambda_{SRI|r_{SR}}(r) = p_{An}(r)\,\lambda_T\,u(r - r_{SR}), \tag{4.13}$$
$$\lambda_{RDI,n|r_{RD}}(r) = p_{An}(r)\lambda_{RDI|r_{RD}}(r) = p_{An}(r)\,\lambda_R\,u(r - r_{RD}). \tag{4.14}$$

4.1.3 Useful Lemmas

In this section, different lemmas are presented, useful for the development of an analytical expression for the CP of the complete link, or for the analysis of the numerical results presented in Chapter 6.

First, an expression of the PDFs of r_{SD}, r_{SR} and r_{RD} is given by Lemma 4.1.

Lemma 4.1. With the nearest neighbour association rule, the PDF of the distance between the typical UE and its closest TBS, the PDF of the distance between the selected RN and its closest TBS and the distance between the selected RN and the typical UE are respectively given by

$$f_{r_{SD}}(r_{SD}) = 2\pi\lambda_T\,r_{SD}\,\exp\left(-\pi\lambda_T r_{SD}^2\right), \tag{4.15}$$
$$f_{r_{SR}}(r_{SR}) = 2\pi\lambda_T\,r_{SR}\,\exp\left(-\pi\lambda_T r_{SR}^2\right), \tag{4.16}$$
$$f_{r_{RD}}(r_{RD}) = 2\pi\lambda_R\,r_{RD}\,\exp\left(-\pi\lambda_R r_{RD}^2\right). \tag{4.17}$$

Based on Lemma 4.1, the PDF of the elevation angle is given by Lemma 4.2.

Lemma 4.2. With the nearest neighbour association rule, the PDF of the elevation angle between the selected RN and its closest TBS, and the elevation angle between the typical UE and the selected RN are respectively given by

$$f_{\theta_{SR}}(\theta_{SR}) = 2\pi\lambda_T H_R^2 \frac{\cos\theta_{SR}}{\sin^3\theta_{SR}} \exp\left(-\frac{\pi\lambda_T H_R^2}{\tan^2\theta_{SR}}\right), \tag{4.18}$$

$$f_{\theta_{RD}}(\theta_{RD}) = 2\pi\lambda_R H_R^2 \frac{\cos\theta_{RD}}{\sin^3\theta_{RD}} \exp\left(-\frac{\pi\lambda_R H_R^2}{\tan^2\theta_{RD}}\right). \tag{4.19}$$

Finally, using Lemma 4.1, the probability of association with the direct link or the relay link using the nearest neighbour association rule is given by Lemma 4.3.

Lemma 4.3. With the nearest neighbour association rule, the probability that the typical UE selects the direct link or the relay link are respectively given by

$$p_{A,SD} = 1 - \frac{\lambda_R}{\lambda_R + \lambda_T} \exp\left(-\pi\lambda_T H_R^2\right), \tag{4.20}$$

$$p_{A,SRD} = \frac{\lambda_R}{\lambda_R + \lambda_T} \exp\left(-\pi\lambda_T H_R^2\right). \tag{4.21}$$

4.2 Coverage Probability

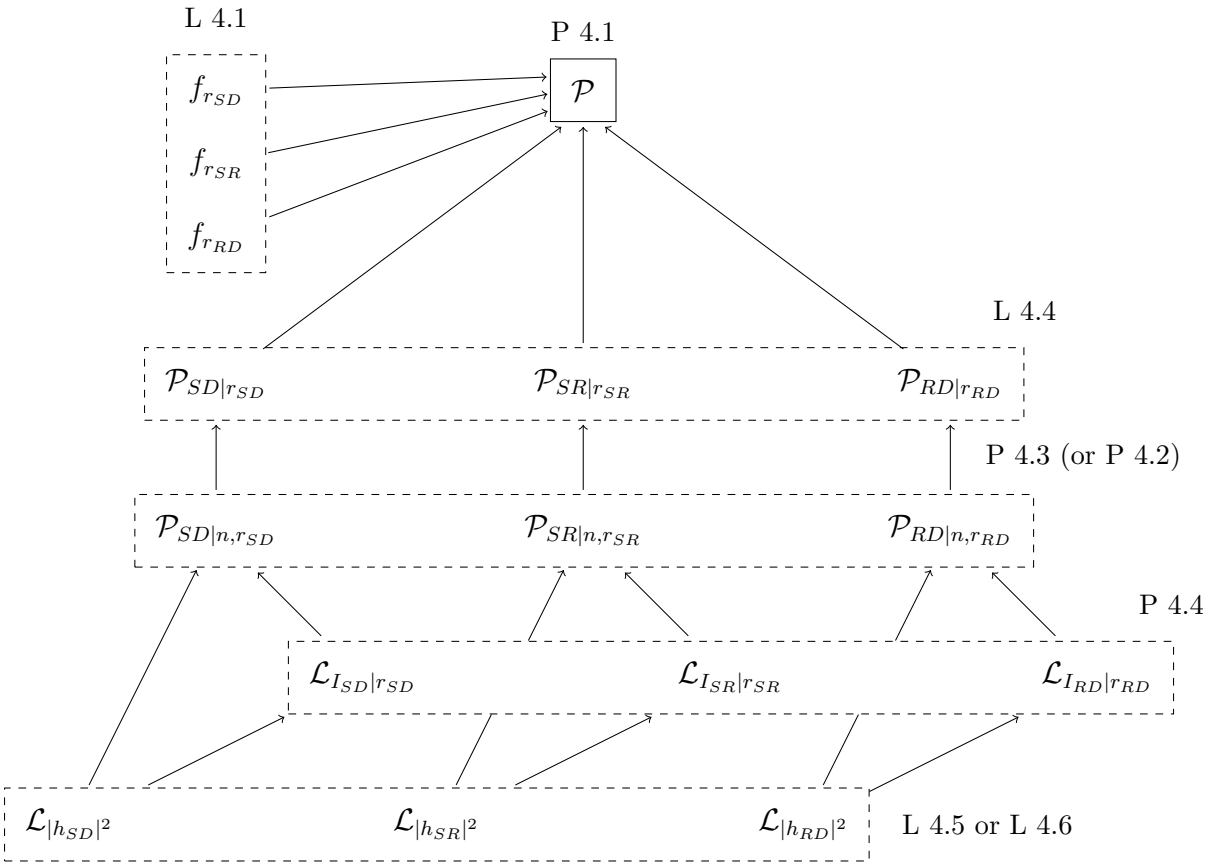

Figure 4.2: Summary of the different quantities to be evaluated in order to obtain an analytical expression of the CP for the complete link. The acronyms L and P are abbreviations for Lemma and Proposition.

Based on the scenario depicted in Section 4.1, an analytical expression of the CP of the complete link $\mathcal{P}$ can be developed using SG. For this purpose, Figure 4.2 summarises all the different quantities which will be evaluated in this section.

First, Proposition 4.1 gives an analytical expression of $\mathcal{P}$ based on Lemma 4.1.

Then, Proposition 4.1 requires the CPs of the direct link, the first hop and the second hop, respectively conditioned on r_{SD}, r_{SR} and r_{RD}. Since these links are either in LoS or NLoS, these quantities can be further developed as in Lemma 4.4.

Next, in numerous studies [6, 9, 11, 15], the CP of a link conditioned on the distance between the two nodes is developed based on the CDF of the small-scale fading channel power gain, which introduces a lot of complexity in the closed-form expressions when Nakagami-m or Rician fading are used. It is illustrated by Proposition 4.2 with Nakagami-m fading: the evaluation of these expressions require the computation of multiple numerical derivatives of the LTs of the aggregate interference.

Proposition 4.1. With the nearest neighbour association rule and selection between direct and relay link, the CP of the complete link for a given SINR threshold β is given by

$$\mathcal{P}(\beta) = \mathcal{I}_{SD}^{(a)}(\beta) + \mathcal{I}_{SD}^{(b)}(\beta) + \mathcal{I}_{SRD}(\beta), \tag{4.22}$$

with

$$\begin{aligned}
\mathcal{I}_{SD}^{(a)}(\beta) &= 2\pi\lambda_T \int_0^{H_R} \mathcal{P}_{SD|r_{SD}}(\beta)\, r_{SD} \exp\left(-\pi\lambda_T r_{SD}^2\right) \mathrm{d}r_{SD}, \\
\mathcal{I}_{SD}^{(b)}(\beta) &= 2\pi\lambda_T \exp\left(\pi\lambda_R H_R^2\right) \int_{H_R}^{\infty} \mathcal{P}_{SD|r_{SD}}(\beta)\, r_{SD} \exp\left(-\pi(\lambda_R+\lambda_T) r_{SD}^2\right) \mathrm{d}r_{SD}, \\
\mathcal{I}_{SRD}(\beta) &= 2\pi\lambda_R \exp\left(-\pi\lambda_T H_R^2\right) \mathcal{P}_{SR}(\beta) \int_0^{\infty} \mathcal{P}_{RD|r_{RD}}(\beta)\, r_{RD} \exp\left(-\pi(\lambda_R+\lambda_T) r_{RD}^2\right) \mathrm{d}r_{RD},
\end{aligned}$$

and

$$\mathcal{P}_{SR}(\beta) = 2\pi\lambda_T \int_0^{\infty} \mathcal{P}_{SR|r_{SR}}(\beta)\, r_{SR} \exp\left(-\pi\lambda_T r_{SR}^2\right) \mathrm{d}r_{SR}. \tag{4.23}$$

In these expressions,

- $\mathcal{P}_{SD|r_{SD}}$ is the CP of the direct link, conditioned on r_{SD};
- $\mathcal{P}_{SR|r_{SR}}$ is the CP of the first hop, conditioned on r_{SR};
- $\mathcal{P}_{RD|r_{RD}}$ is the CP of the second hop, conditioned on r_{RD}.

If direct links are neglected, the CP of the relay link for a given SINR threshold β is expressed as

$$\mathcal{P}_{SRD}(\beta) = 2\pi\lambda_R\, \mathcal{P}_{SR}(\beta) \int_0^{\infty} \mathcal{P}_{RD|r_{RD}}(\beta)\, r_{RD} \exp\left(-\pi\lambda_R r_{RD}^2\right) \mathrm{d}r_{RD}. \tag{4.24}$$

Lemma 4.4. The CPs of the direct link, the first hop and the second hop, respectively conditioned on r_{SD}, r_{SR} and r_{RD} are respectively given by

$$\mathcal{P}_{SD|r_{SD}}(\beta) = p_{GL}(r_{SD})\mathcal{P}_{SD|L,r_{SD}}(\beta) + p_{GN}(r_{SD})\mathcal{P}_{SD|N,r_{SD}}(\beta), \tag{4.25}$$

$$\mathcal{P}_{SR|r_{SR}}(\beta) = p_{AL}(r_{SR})\,\mathcal{P}_{SR|L,r_{SR}}(\beta) + p_{AN}(r_{SR})\,\mathcal{P}_{SR|N,r_{SR}}(\beta), \tag{4.26}$$

$$\mathcal{P}_{RD|r_{RD}}(\beta) = p_{AL}(r_{RD})\mathcal{P}_{RD|L,r_{RD}}(\beta) + p_{AN}(r_{RD})\mathcal{P}_{RD|N,r_{RD}}(\beta), \tag{4.27}$$

where p_{Gn} and p_{An} are the LoS and NLoS probability respectively for G2G and A2G links. In these expressions,

- $\mathcal{P}_{SD|n,r_{SD}}$ is the CP of the direct link conditioned on r_{SD} if the link is in LoS or NLoS;
- $\mathcal{P}_{SR|n,r_{SR}}$ is the CP of the first hop conditioned on r_{SR} if the link is in LoS or NLoS;
- $\mathcal{P}_{RD|n,r_{RD}}$ is the CP of the second hop conditioned on r_{RD} if the link is in LoS or NLoS.

Proposition 4.2. With Nakagami-m fading, the CPs of the direct link, the first hop and the second hop if these links are in LoS or NLoS, and respectively conditioned on r_{SD}, r_{SR} and r_{RD} are given by

$$\mathcal{P}_{SD|n,r_{SD}}(\beta) = \mathbb{E}_{S_{SD,n}}\left[\exp\left(-\frac{\sigma^2}{D_{SD,n}}\right)\sum_{i=0}^{m_{Gn}-1}\sum_{k=0}^{i}\frac{(-1)^k}{i!D_{SD,n}^i}\binom{i}{k}(\sigma^2)^{i-k}\frac{\partial^k\mathcal{L}_{I_{SD}|r_{SD}}}{\partial s^k}\Big|_{s=\frac{1}{D_{SD,n}}}\right], \tag{4.28}$$

$$\mathcal{P}_{SR|n,r_{SR}}(\beta) = \mathbb{E}_{S_{SR,n}}\left[\exp\left(-\frac{\sigma^2}{D_{SR,n}}\right)\sum_{i=0}^{m_{An}-1}\sum_{k=0}^{i}\frac{(-1)^k}{i!D_{SR,n}^i}\binom{i}{k}(\sigma^2)^{i-k}\frac{\partial^k\mathcal{L}_{I_{SR}|r_{SR}}}{\partial s^k}\Big|_{s=\frac{1}{D_{SR,n}}}\right], \tag{4.29}$$

$$\mathcal{P}_{RD|n,r_{RD}}(\beta) = \mathbb{E}_{S_{RD,n}}\left[\exp\left(-\frac{\sigma^2}{D_{RD,n}}\right)\sum_{i=0}^{m_{An}-1}\sum_{k=0}^{i}\frac{(-1)^k}{i!D_{RD,n}^i}\binom{i}{k}(\sigma^2)^{i-k}\frac{\partial^k\mathcal{L}_{I_{RD}|r_{RD}}}{\partial s^k}\Big|_{s=\frac{1}{D_{RD,n}}}\right], \tag{4.30}$$

with

$$\begin{aligned}
D_{SD,n} &= \frac{C_{SD,n}(1+r_{SD})^{-\alpha_{Gn}}S_{SD,n}}{m_{Gn}\beta},\\
D_{SR,n} &= \frac{C_{SR,n}(r_{SR}^2+H_R^2)^{-\frac{\alpha_{An}}{2}}S_{SR,n}}{m_{An}\beta},\\
D_{RD,n} &= \frac{C_{RD,n}(r_{RD}^2+H_R^2)^{-\frac{\alpha_{An}}{2}}S_{RD,n}}{m_{An}\beta}.
\end{aligned}$$

In these expressions,

- $\mathcal{L}_{I_{SD}|r_{SD}}$ is the LT of I_{SD} conditioned on r_{SD};
- $\mathcal{L}_{I_{SR}|r_{SR}}$ is the LT of I_{SR} conditioned on r_{SR};
- $\mathcal{L}_{I_{RD}|r_{RD}}$ is the LT of I_{RD} conditioned on r_{RD}.

However, this complexity can be avoided using the Gil-Pelaez theorem presented in Section 2.3. Using this theorem, the CP of each link in LoS or NLoS, conditioned on the distance between the two nodes of interest can also be computed, based on characteristic functions. Their expressions are given in Proposition 4.3. By means of this method, the multiple numerical derivations are replaced by one numerical integration.

Proposition 4.3. The CPs of the direct link, the first hop and the second hop if these links are in LoS or NLoS, and respectively conditioned on r_{SD}, r_{SR} and r_{RD} are given by

$$\mathcal{P}_{SD|n,r_{SD}}(\beta) = \frac{1}{2} + \frac{1}{\pi}\mathbb{E}_{S_{SD,n}}\left[\int_0^\infty \frac{1}{\tau}\mathrm{Im}\left[\phi_{Z_{SD}|r_{SD}}(\tau)\exp\left(-j\tau\beta\sigma^2\right)\right]\mathrm{d}\tau\right], \tag{4.31}$$

$$\mathcal{P}_{SR|n,r_{SR}}(\beta) = \frac{1}{2} + \frac{1}{\pi}\mathbb{E}_{S_{SR,n}}\left[\int_0^\infty \frac{1}{\tau}\mathrm{Im}\left[\phi_{Z_{SR}|r_{SR}}(\tau)\exp\left(-j\tau\beta\sigma^2\right)\right]\mathrm{d}\tau\right], \tag{4.32}$$

$$\mathcal{P}_{RD|n,r_{RD}}(\beta) = \frac{1}{2} + \frac{1}{\pi}\mathbb{E}_{S_{RD,n}}\left[\int_0^\infty \frac{1}{\tau}\mathrm{Im}\left[\phi_{Z_{RD}|r_{RD}}(\tau)\exp\left(-j\tau\beta\sigma^2\right)\right]\mathrm{d}\tau\right], \tag{4.33}$$

with

$$\begin{aligned}
\phi_{Z_{SD}|r_{SD}}(\tau) &= \mathcal{L}_{|h_{SD,n}|^2}\left(-j\tau C_{SD,n}(1+r_{SD})^{-\alpha_{G_n}}S_{SD,n}\right)\mathcal{L}_{I_{SD}|r_{SD}}(j\tau\beta),\\
\phi_{Z_{SR}|r_{SR}}(\tau) &= \mathcal{L}_{|h_{SR,n}|^2}\left(-j\tau C_{SR,n}(r_{SR}^2+H_R^2)^{-\frac{\alpha_{An}}{2}}S_{SR,n}\right)\mathcal{L}_{I_{SR}|r_{SR}}(j\tau\beta),\\
\phi_{Z_{RD}|r_{RD}}(\tau) &= \mathcal{L}_{|h_{RD,n}|^2}\left(-j\tau C_{RD,n}(r_{RD}^2+H_R^2)^{-\frac{\alpha_{An}}{2}}S_{RD,n}\right)\mathcal{L}_{I_{RD}|r_{RD}}(j\tau\beta).
\end{aligned}$$

In these expressions,

- $\mathcal{L}_{|h_{SD,n}|^2}$ is the LT of $|h_{SD,n}|^2$;
- $\mathcal{L}_{|h_{SR,n}|^2}$ is the LT of $|h_{SR,n}|^2$;
- $\mathcal{L}_{|h_{RD,n}|^2}$ is the LT of $|h_{RD,n}|^2$;
- $\mathcal{L}_{I_{SD}|r_{SD}}$ is the LT of I_{SD} conditioned on r_{SD};
- $\mathcal{L}_{I_{SR}|r_{SR}}$ is the LT of I_{SR} conditioned on r_{SR};
- $\mathcal{L}_{I_{RD}|r_{RD}}$ is the LT of I_{RD} conditioned on r_{RD}.

Finally, the last steps are the evaluation of the LTs of the small-scale fading channel power gains and the LTs of the aggregate interferences for each link.

With Nakagami-m fading, since the small-scale fading channel power gain follows a Gamma distribution, its LT is an already known result, given by Lemma 4.5.

Lemma 4.5. With Nakagami-m fading, the LT of the small-scale fading channel power gain is given by

$$\mathcal{L}_{|h|^2}(s) = \left(\frac{m}{m+s}\right)^m, \tag{4.34}$$

where $m = m_{Gn}$ for G2G links in LoS or NLoS, and $m = m_{An}$ for A2G links in LoS or NLoS.

However, with Rician fading, developments to obtain the LT based on the PDF of the small-scale fading channel power gain are less straightforward. Lemma 4.6 gives the expression of this LT.

Lemma 4.6. With Rician fading, The LT of the small-scale fading channel power gain is given by

$$\mathcal{L}_{|h|^2}(s) = \frac{K+1}{K+1+s} \exp\left(-\frac{Ks}{K+1+s}\right), \tag{4.35}$$

where $K = K_{Gn}$ for G2G links in LoS or NLoS, and $K = K_{An}$ for A2G links in LoS or NLoS.

At last, the LT of the aggregate interference for each link is given by Proposition 4.4.

Proposition 4.4. The LTs of the aggregate interference of the direct link, the first hop or the second hop, respectively conditioned on r_{SD}, r_{SR} and r_{RD} are given by

$$\mathcal{L}_{I_{SD}|r_{SD}}(s) = \exp\Big(-2\pi\lambda_T \mathbb{E}_{\tilde{S}_{SD,L},\tilde{S}_{SD,N}} \Big[\int_{r_{SD}}^{\infty} \iota_{SD}(r,s)\ r\mathrm{d}r \Big] \Big), \tag{4.36}$$

$$\mathcal{L}_{I_{SR}|r_{SR}}(s) = \exp\Big(-2\pi\lambda_T \mathbb{E}_{\tilde{S}_{SR,L},\tilde{S}_{SR,N}} \Big[\int_{r_{SR}}^{\infty} \iota_{SR}(r,s)\ r\mathrm{d}r \Big] \Big), \tag{4.37}$$

$$\mathcal{L}_{I_{RD}|r_{RD}}(s) = \exp\Big(-2\pi\lambda_R \mathbb{E}_{\tilde{S}_{RD,L},\tilde{S}_{RD,N}} \Big[\int_{r_{RD}}^{\infty} \iota_{RD}(r,s)\ r\mathrm{d}r \Big] \Big), \tag{4.38}$$

with

$$\iota_{SD}(r,s) = 1 - \sum_{n=\{L,N\}} p_{Gn}(r) \mathcal{L}_{|\tilde{h}_{SD,n}|^2}\left(s\, c_{SD,n} (1+r)^{-\alpha_{Gn}} \tilde{S}_{SD,n}\right),$$

$$\iota_{SR}(r,s) = 1 - \sum_{n=\{L,N\}} p_{An}(r) \mathcal{L}_{|\tilde{h}_{SR,n}|^2}\left(s\, c_{SR,n} (r^2+H_R^2)^{-\frac{\alpha_{An}}{2}} \tilde{S}_{SR,n}\right),$$

$$\iota_{RD}(r,s) = 1 - \sum_{n=\{L,N\}} p_{An}(r) \mathcal{L}_{|\tilde{h}_{RD,n}|^2}\left(s\, c_{RD,n} (r^2+H_R^2)^{-\frac{\alpha_{An}}{2}} \tilde{S}_{RD,n}\right).$$

In these expressions, The RVs $|\tilde{h}_{SD,n}|^2$, $|\tilde{h}_{SR,n}|^2$, $|\tilde{h}_{RD,n}|^2$, $\tilde{S}_{SD,n}$, $\tilde{S}_{SR,n}$ and $\tilde{S}_{RD,n}$ are equivalent to the small-scale fading channel power gains and the shadowings of the corresponding links.

4.3 Enhancements of the Model

An analytical expression of the CP has been developed in Section 4.2 for a specific scenario summarised in Table 4.2. However, the shadowing induces a lot of complexity (four additional integrations for each link) in the presented framework. Additionally, direct links are not taken into account, and a nearest neighbour association rule is considered while the maximum biased average power association rule would be more realistic. In this section, some clues are given in order to enhance the developed framework and overcome these drawbacks. Note that the propositions and lemmas presented in this section have not been yet validated numerically!

4.3.1 Shadowing

An alternative way to incorporate shadowing has been proposed by some authors [49–51] a new PP is defined, the **propagation process** in $\mathbb{R}^+$:

$$\mathbf{\Phi}'_R = \left\{ \phi'_i = \frac{L_{n_i}(\|\phi_i\|)}{S_i} \;\middle|\; \phi_i \in \mathbf{\Phi}_R \right\}. \tag{4.39}$$

The density of this new PP can be computed using the displacement theorem given by Equation (2.17). However, in the presented framework, unlike these studies, it does not enable to reduce the mathematical complexity of the analytical expressions owing to the LoS probability model given by Equation (3.18) and the RNs' altitude.

Unfortunately, for this framework, there is no other way to handle it with the channel models presented in Section 3.3, except if an analytical expression of the LT of the product between the small-scale fading channel power gain and shadowing RVs exists. However, the $\kappa-\mu$ and $\eta-\mu$ channel models presented in [6, 52, 53] are other alternatives for the channel modelling which replace the small-scale fading and shadowing RVs in order to obtain more accurate results. Since the LT for these two models exists, a possible improvement of the analytical expressions is straightforward. This might be analysed in a future study.

4.3.2 Association Rule

The closest node is not necessarily the node which provides the highest power if the link is in NLoS. This applies for the direct link, the first hop, the second hop but also for the selection between the direct link and the relay link. Therefore, the maximum biased average power association rule overcomes this drawback.

However, the mathematical complexity is highly increased. The TBSs' PP and the UAV RNs' PP must be splitted in four different PPs for which all the links of the same PP are in LoS or NLoS. For the selection, the closest nodes of these PPs must be compared to select the one which provides the highest power. In case of a TBS, direct link is chosen, while relay link is selected in case of a UAV RN.

If the distances between the typical UE and its closest TBS in LoS and NLoS are denoted by $r_{SD,n}$, the distances between the selected RN and its closest TBS in LoS or NLoS are denoted $r_{SR,n}$, and the distances between the typical UE and its closest RN in LoS or NLoS are denoted by $r_{RD,n}$, assuming that the realisations of the shadowings of

each link are known, the biased average powers of the direct link and the second hop are defined as

$$\bar{U}_{SD,n} = b_{\mathbf{\Phi}_T} C_{SD,n} (1 + r_{SD,n})^{-\alpha_{Gn}} S_{SD,n}, \tag{4.40}$$

$$\bar{U}_{RD,n} = b_{\mathbf{\Phi}_R} C_{RD,n} \left(r_{RD,n}^2 + H_R^2 \right)^{-\frac{\alpha_{An}}{2}} S_{RD,n}. \tag{4.41}$$

Therefore, with the maximum biased average power association rule, knowing the tuple $\boldsymbol{x} = (r_{SD,L}, r_{SD,N}, r_{RD,L}, r_{RD,N}, S_{SD,L}, S_{SD,N}, S_{RD,L}, S_{RD,N})$, the regions of association of the typical UE are defined as

$$\Omega_{SD,L} = \left\{ \boldsymbol{x} \,\middle|\, \bar{U}_{SD,L} > \bar{U}_{SD,N}, \bar{U}_{SD,L} > \bar{U}_{RD,L}, \bar{U}_{SD,L} > \bar{U}_{RD,N} \right\}, \tag{4.42}$$

$$\Omega_{SD,N} = \left\{ \boldsymbol{x} \,\middle|\, \bar{U}_{SD,N} > \bar{U}_{SD,L}, \bar{U}_{SD,N} > \bar{U}_{RD,L}, \bar{U}_{SD,N} > \bar{U}_{RD,N} \right\}, \tag{4.43}$$

$$\Omega_{RD,L} = \left\{ \boldsymbol{x} \,\middle|\, \bar{U}_{RD,L} > \bar{U}_{SD,L}, \bar{U}_{RD,L} > \bar{U}_{SD,N}, \bar{U}_{RD,L} > \bar{U}_{RD,N} \right\}, \tag{4.44}$$

$$\Omega_{RD,N} = \left\{ \boldsymbol{x} \,\middle|\, \bar{U}_{RD,N} > \bar{U}_{SD,L}, \bar{U}_{RD,N} > \bar{U}_{SD,N}, \bar{U}_{RD,N} > \bar{U}_{RD,L} \right\}. \tag{4.45}$$

Lemma 4.7 gives the PDF of these distances with this new association rule.

Lemma 4.7. With the maximum biased average power association rule, the PDF of the distance between the typical UE and its closest TBS if the link is in LoS or NLoS, the PDF of the distance between the selected RN and its closest TBS if the link is in LoS or NLoS and the PDF of the distance between the selected RN and the typical UE if the link is in LoS or NLoS are respectively given by

$$f_{r_{SD,n}}(r) = 2\pi\lambda_T \, p_{Gn}(r) \, r \exp\left(-2\pi\lambda_T \int_0^r p_{Gn}(r) r \mathrm{d}r \right), \tag{4.46}$$

$$f_{r_{SR,n}}(r) = 2\pi\lambda_T \, p_{An}(r) \, r \exp\left(-2\pi\lambda_T \int_0^r p_{An}(r) r \mathrm{d}r \right), \tag{4.47}$$

$$f_{r_{RD,n}}(r) = 2\pi\lambda_R \, p_{An}(r) \, r \exp\left(-2\pi\lambda_R \int_0^r p_{An}(r) r \mathrm{d}r \right). \tag{4.48}$$

Assuming that direct links are strongly obstructed, only relay links are considered, and the problem is restricted to the region $\Omega_{RD} = \Omega_{RD,L} \cup \Omega_{RD,N}$. With this assumption, using Lemma 4.7, Proposition 4.5 gives the CP of the second hop, and the mathematical expressions are similar for the first hop. Then, as in Proposition 4.1, the CP of the relay link is given by

$$\mathcal{P}_{SRD}(\beta) = \mathcal{P}_{SR}(\beta) \mathcal{P}_{RD}(\beta). \tag{4.49}$$

Note that the CP of the second hop for a LoS or NLoS link, conditioned on $r_{RD,n}$ can be computed with Proposition 4.3.

In the particular case where the small-scale fading parameters are chosen to be identical for the LoS and NLoS links, this expression can be further simplified following the approach

Proposition 4.5. Assuming that direct links are strongly obstructed, with the maximum biased average power association rule, the CP of the relay link for a given SINR threshold β is given by

$$\mathcal{P}_{SRD}(\beta) = \begin{cases} \mathcal{P}_{RD}^{(a)}(\beta) & \text{if} \quad d_{RD,L} \geq 0 \text{ and } d_{RD,N} = 0 \\ \mathcal{P}_{RD}^{(b)}(\beta) & \text{if} \quad d_{RD,L} = 0 \text{ and } d_{RD,N} > 0 \end{cases}, \tag{4.50}$$

where

$$d_{RD,L} = \left(\max \left\{ \left(\frac{C_{RD,L} S_{RD,L}}{C_{RD,N} S_{RD,N}} H_R^{\alpha_{AN}} \right)^{\frac{2}{\alpha_{AL}}} - H_R^2, 0 \right\} \right)^{\frac{1}{2}},$$
$$d_{RD,N} = \left(\max \left\{ \left(\frac{C_{RD,N} S_{RD,N}}{C_{RD,L} S_{RD,L}} H_R^{\alpha_{AL}} \right)^{\frac{2}{\alpha_{AN}}} - H_R^2, 0 \right\} \right)^{\frac{1}{2}},$$

and with

$$\mathcal{P}_{RD}^{(a)}(\beta) = \mathbb{E}_{S_{RD,L}} \left[\mathcal{I}_{RD,L|S_{RD,L}}^{(a)} + \mathcal{I}_{RD,L|S_{RD,L}}^{(b)} \right] + \mathbb{E}_{S_{SR,N}} \left[\mathcal{I}_{RD,N|S_{RD,N}} \right],$$
$$\mathcal{P}_{RD}^{(b)}(\beta) = \mathbb{E}_{S_{RD,L}} \left[\mathcal{I}_{RD,L|S_{RD,L}} \right] + \mathbb{E}_{S_{SR,N}} \left[\mathcal{I}_{RD,N|S_{RD,N}}^{(a)} + \mathcal{I}_{RD,N|S_{RD,N}}^{(b)} \right].$$

In these expressions,

$$\mathcal{I}_{RD,L|S_{RD,L}}^{(a)} = \int_0^{d_{RD,L}} \mathcal{P}_{RD,L|S_{RD,L},r_{RD,L}}(\beta) \; f_{r_{RD,L}}(r_{RD,L}) \, \mathrm{d}r_{RD,L},$$
$$\mathcal{I}_{RD,L|S_{RD,L}}^{(b)} = \int_{d_{RD,L}}^{\infty} \mathcal{P}_{RD,L|S_{RD,L},r_{RD,L}}(\beta) \; \tilde{f}_{r_{RD,L}}(r_{RD,L}) \, \mathrm{d}r_{RD,L},$$
$$\mathcal{I}_{RD,N|S_{RD,N}} = \int_0^{\infty} \mathcal{P}_{RD,N|S_{RD,N},r_{RD,N}}(\beta) \tilde{f}_{r_{RD,N}}(r_{RD,N}) \mathrm{d}r_{RD,N},$$
$$\mathcal{I}_{RD,L|S_{RD,L}} = \int_0^{\infty} \mathcal{P}_{RD,L|S_{RD,L},r_{RD,L}}(\beta) \; \tilde{f}_{r_{RD,L}}(r_{RD,L}) \, \mathrm{d}r_{RD,L},$$
$$\mathcal{I}_{RD,N|S_{RD,N}}^{(a)} = \int_0^{d_{RD,N}} \mathcal{P}_{RD,N|S_{RD,N},r_{RD,N}}(\beta) f_{r_{RD,N}}(r_{RD,N}) \mathrm{d}r_{RD,N},$$
$$\mathcal{I}_{RD,N|S_{RD,N}}^{(b)} = \int_{d_{RD,N}}^{\infty} \mathcal{P}_{RD,N|S_{RD,N},r_{RD,N}}(\beta) \tilde{f}_{r_{RD,N}}(r_{RD,N}) \mathrm{d}r_{RD,N},$$

$$\tilde{f}_{r_{RD,L}}(r_{RD,L}) = f_{r_{RD,L}}(r_{RD,L}) \; \exp\left(-2\pi\lambda_R \int_0^{\sqrt{g_{RD,N}(r_{RD,L})}} p_{AN}(r) r \mathrm{d}r \right),$$
$$\tilde{f}_{r_{RD,N}}(r_{RD,N}) = f_{r_{RD,N}}(r_{RD,N}) \exp\left(-2\pi\lambda_R \int_0^{\sqrt{g_{RD,L}(r_{RD,N})}} p_{AL}(r) r \mathrm{d}r \right),$$

and

$$g_{RD,N}(r_{RD,L}) = \left(\frac{C_{RD,N} S_{RD,N}}{C_{RD,L} S_{RD,L}} \right)^{\frac{2}{\alpha_{AN}}} \left(r_{RD,L}^2 + H_R^2 \right)^{\frac{\alpha_{AL}}{\alpha_{AN}}} - H_R^2,$$
$$g_{RD,L}(r_{RD,N}) = \left(\frac{C_{RD,L} S_{RD,L}}{C_{RD,N} S_{RD,N}} \right)^{\frac{2}{\alpha_{AL}}} \left(r_{RD,N}^2 + H_R^2 \right)^{\frac{\alpha_{AN}}{\alpha_{AL}}} - H_R^2.$$

Proposition 4.6. With the maximum biased power association rule, if the small-scale fading parameters are identical for LoS and NLoS links, the CP of the second hop is given by

$$\mathcal{P}_{RD}(\beta) = \mathbb{E}_{S_{RD,L},S_{RD,N}}\left[\int_0^{\infty} \mathcal{P}_{RD,L|r'_{RD}}(\beta) f_{r'_{RD}}(r'_{RD}) \mathrm{d}r'_{RD}\right], \tag{4.51}$$

where $f_{r'_{RD}}$ is the PDF of the closest RN in an equivalent PPP where all the RNs are in LoS. This PDF is given by

$$f_{r'_{RD}}(r'_{RD}) = 2\pi\lambda_R\, r'_{RD} \exp\left(-2\pi\lambda_R \int_0^{r'_{RD}} p_{AL}(r) r \mathrm{d}r\right) \tilde{f}_{r'_{RD}}(r'_{RD}), \tag{4.52}$$

with

$$\tilde{f}_{r'_{RD}}(r) = \begin{cases} \exp\left(-2\pi\lambda_R \int_0^{r} p_{AN}(r') r' \mathrm{d}r'\right)\left(p_{AL}(r) + p_{AN}(r)\dfrac{\mathrm{d}}{\mathrm{d}r}\tilde{g}^{-1}(r)\right) & \text{if } r > d_{min} \\ p_{AL}(r) & \text{otherwise} \end{cases}.$$

The function $\tilde{g}^{-1}$ and d_{min} are defined as

$$\tilde{g}^{-1}(r) = \left(\left(\frac{C_{RD,N}S_{RD,N}}{C_{RD,L}S_{RD,L}}\right)^{\frac{2}{\alpha_{AN}}}\left(r^2 + H_R^2\right)^{\frac{\alpha_{AL}}{\alpha_{AN}}} - H_R^2\right)^{\frac{1}{2}},$$

and

$$d_{min} = \left(\max\left\{\left(\frac{C_{RD,L}S_{RD,L}}{C_{RD,N}S_{RD,N}} H_R^{\alpha_{AN}}\right)^{\frac{2}{\alpha_{AL}}} - H_R^2, 0\right\}\right)^{\frac{1}{2}}.$$

The derivative of $\tilde{g}^{-1}(r)$ when $r > d_{min}$ is given by

$$\frac{\mathrm{d}}{\mathrm{d}r}\tilde{g}^{-1}(r) = \frac{\left(\frac{C_{RD,L}S_{RD,L}}{C_{RD,N}S_{RD,N}}\right)^{\frac{2}{\alpha_{AN}}} \frac{\alpha_{AL}}{\alpha_{AN}} \left(r^2 + H_R^2\right)^{\frac{\alpha_{AL}}{\alpha_{AN}}-1} r}{\left(\left(\frac{C_{RD,L}S_{RD,L}}{C_{RD,N}S_{RD,N}}\right)^{\frac{2}{\alpha_{AN}}} \left(r^2 + H_R^2\right)^{\frac{\alpha_{AL}}{\alpha_{AN}}} - H_R^2\right)^{\frac{1}{2}}}.$$

.

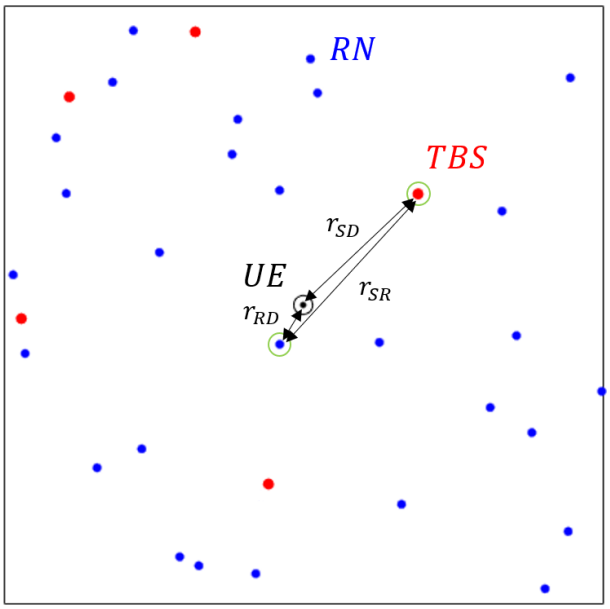

Figure 4.3: Illustration of the new scenario, where the same TBS serves both the typical UE and the selected RN. The typical UE is positioned at position $(0, 0)$ in $\mathbb{R}^2$. The RNs and the TBSs are respectively represented by blue and red dots. The selected TBS and the selected RN are circled in green.

of [54] the LoS and NLoS RNs' PPs are respectively denoted by $\mathbf{\Phi}_{R,L}$ and $\mathbf{\Phi}_{R,N}$. Assuming that the realisations of the shadowing are known, let us define a transformation g as

$$g : \mathbb{R}^2 \to \mathbb{R}^2 : \boldsymbol{\phi}_i \to \boldsymbol{\phi}'_i = \frac{\boldsymbol{\phi}_i}{\|\boldsymbol{\phi}_i\|} \left(\left(\frac{C_{RD,L} S_{RD,L}}{C_{RD,N} S_{RD,N}} \right)^{\frac{2}{\alpha_{AL}}} \left(\|\boldsymbol{\phi}_i\|^2 + H_R^2 \right)^{\frac{\alpha_{AN}}{\alpha_{AL}}} - H_R^2 \right)^{\frac{1}{2}}. \tag{4.53}$$

This mapping is defined such that a RN in NLoS located at a distance $\|\boldsymbol{\phi}_i\|$ from the typical UE transmits the same average power than a RN in LoS located at a distance $\|\boldsymbol{\phi}'_i\|$ from the typical UE:

$$C_{RD,N}(\|\boldsymbol{\phi}_i\|^2 + H_R^2)^{-\frac{\alpha_{AN}}{2}} S_{RD,N} = C_{RD,L}(\|\boldsymbol{\phi}'_i\|^2 + H_R^2)^{-\frac{\alpha_{AL}}{2}} S_{RD,L}. \tag{4.54}$$

Based on this mapping, we can define a new PP $\mathbf{\Phi}'_R = \mathbf{\Phi}_{R,L} \cup g(\mathbf{\Phi}_{R,N})$ by superposition. With this new PP composed only of nodes in LoS, the nearest neighbour association rule can be applied. Proposition 4.6 gives an expression of the CP of the second hop following this method.

The CP of the second hop for a LoS link, and conditioned on r'_{RD} can be computed with Proposition 4, but the LT of the aggregate interference should be adapted, since an equivalent PPP with only LoS RNs is considered.

4.3.3 Terrestrial Base Station Selection

In this section, we consider that the TBS which serves the typical UE if the direct link is selected is also the TBS which serves the selected RN if the relay link is chosen, as illustrated by Figure 4.3.

With this configuration and the nearest neighbour association rule, the PDFs of r_{RD} and r_{SD} are still given by Lemma 4.1. However, the distance between the selected TBS and the selected RN is now a function of r_{RD} and r_{SD}. Lemma 4.8 gives the PDF of r_{SR}, conditioned on r_{RD} and r_{SD}.

Lemma 4.8. With the nearest neighbour association rule, if the same TBS serves the selected RN and the typical UE, the PDF of the distance between the selected TBS and the selected RN conditioned on r_{RD} and r_{SD} is given by

$$f_{r_{SR}|r_{RD},r_{SD}}(r) = \begin{cases} \frac{1}{\pi} \frac{2r}{\sqrt{4r_{SD}^2 r_{RD}^2 - \left(r^2 - r_{SD}^2 - r_{RD}^2\right)^2}} & \text{if } |r_{RD} - r_{SD}| \leq r \leq r_{RD} + r_{SD} \\ 0 & \text{otherwise} \end{cases}. \tag{4.55}$$

Based on Lemma 4.8, Proposition 4.7 gives the CP of the complete link.

Proposition 4.7. With the nearest neighbour association rule, if the same TBS serves the selected RN of the relay link and the typical UE, the CP of the complete link at a SINR threshold β is given by

$$\mathcal{P}(\beta) = \mathcal{I}_{SD}^{(a)}(\beta) + \mathcal{I}_{SD}^{(b)}(\beta) + \mathcal{I}_{SRD}(\beta), \tag{4.56}$$

with

$$\mathcal{I}_{SD}^{(a)}(\beta) = 2\pi\lambda_T \int_0^{H_R} \mathcal{P}_{SD|r_{SD}}(\beta)\, r_{SD} \exp\left(-\pi\lambda_T r_{SD}^2\right) \mathrm{d}r_{SD},$$

$$\mathcal{I}_{SD}^{(b)}(\beta) = 2\pi\lambda_T \exp\left(\pi\lambda_R H_R^2\right) \int_{H_R}^{\infty} \mathcal{P}_{SD|r_{SD}}(\beta)\, r_{SD} \exp\left(-\pi(\lambda_R + \lambda_T) r_{SD}^2\right) \mathrm{d}r_{SD},$$

$$\mathcal{I}_{SRD}(\beta) =$$

$$\int_0^{\infty} \int_{\sqrt{r_{RD}^2 + H_R^2}}^{\infty} \int_{|r_{SD} - r_{RD}|}^{r_{SD} + r_{RD}} \mathcal{P}_{SR|r_{SR}}(\beta) \mathcal{P}_{SD|r_{SD}}(\beta) \tilde{f}_{r_{SD},r_{SR},r_{RD}}(r_{SD}, r_{SR}, r_{RD}) \mathrm{d}r_{SR} \mathrm{d}r_{SD} \mathrm{d}r_{SD},$$

and

$$\tilde{f}_{r_{SD},r_{SR},r_{RD}}(r_{SD}, r_{SR}, r_{RD}) = \frac{8\pi\lambda_R\lambda_T\, r_{SR} r_{RD} r_{SD} \exp\left(-\pi(\lambda_R r_{RD}^2 + \lambda_T r_{SD}^2)\right)}{\sqrt{4r_{SD}^2 r_{RD}^2 - \left(r^2 - r_{SD}^2 - r_{RD}^2\right)^2}}.$$

In these expressions,

- $\mathcal{P}_{SD|r_{SD}}$ is the CP of the direct link, conditioned on r_{SD};
- $\mathcal{P}_{SR|r_{SR}}$ is the CP of the first hop, conditioned on r_{SR};
- $\mathcal{P}_{RD|r_{RD}}$ is the CP of the second hop, conditioned on r_{RD}.

4.4 Average Exposure

Based on the scenario depicted in Section 4.1, an analytical expression of the average exposure can be developed. We consider a typical UE which communicates either through a direct link or a relay link. Proposition 4.8 gives the average exposure at the typical UE from the TBSs and from the RNs.

Proposition 4.8. With the nearest neighbour association rule, considering a typical UE which communicates either through a direct link or a relay link, the average exposure at the typical UE from the TBSs and from the RNs are respectively given by

$$\mathcal{X}_{c,SD} = 2\pi\lambda_T \int_0^\infty \mathcal{X}_{c,SD|r_{SD}}\ r_{SD} \exp\left(-\pi\lambda_T r_{SD}^2\right) \mathrm{d}r_{SD}, \tag{4.57}$$

$$\mathcal{X}_{c,RD} = 2\pi\lambda_R \int_0^\infty \mathcal{X}_{c,RD|r_{RD}}\ r_{RD} \exp\left(-\pi\lambda_R r_{RD}^2\right) \mathrm{d}r_{SD}, \tag{4.58}$$

with

$$\begin{aligned}
\mathcal{X}_{c,SD|r_{SD}} = & \sum_{n=\{L,N\}} \exp\left(\frac{\ln^2 10}{200}\sigma_{S_{Gn}}^2\right) C_{SD,n}\, p_{Gn}(r_{SD})\, (1+r_{SD})^{-\alpha_{Gn}} \\
& + \sum_{n=\{L,N\}} c_{SD,n} \exp\left(\frac{\ln^2 10}{200}\sigma_{S_{Gn}}^2\right) 2\pi\lambda_T \int_{r_{SD}}^\infty (1+r)^{-\alpha_{Gn}} p_{Gn}(r)\, r\mathrm{d}r, \\
\mathcal{X}_{c,RD|r_{RD}} = & \sum_{n=\{L,N\}} \exp\left(\frac{\ln^2 10}{200}\sigma_{S_{An}}^2\right) C_{RD,n}\, p_{An}(r_{RD})\ \left(r_{RD}^2 + H_R^2\right)^{-\frac{\alpha_{An}}{2}} \\
& + \sum_{n=\{L,N\}} c_{RD,n} \exp\left(\frac{\ln^2 10}{200}\sigma_{S_{An}}^2\right) 2\pi\lambda_R \int_{r_{RD}}^\infty \left(r^2 + H_R^2\right)^{-\frac{\alpha_{An}}{2}} p_{An}(r)\, r\mathrm{d}r.
\end{aligned}$$

When the typical UE does not communicate, Proposition 4.9 gives the average exposure from the TBSs and from the RNs.

Proposition 4.9. With the nearest neighbour association rule, considering a typical UE which does not communicate, the average exposure at the typical UE from the TBSs and from the RNs are respectively given by

$$\mathcal{X}_{SD} = 2\pi\lambda_T \int_0^\infty \mathcal{X}_{SD|r_{SD}}\ r_{SD} \exp\left(-\pi\lambda_T r_{SD}^2\right) \mathrm{d}r_{SD}, \tag{4.59}$$

$$\mathcal{X}_{RD} = 2\pi\lambda_R \int_0^\infty \mathcal{X}_{RD|r_{RD}}\ r_{RD} \exp\left(-\pi\lambda_R r_{RD}^2\right) \mathrm{d}r_{SD}, \tag{4.60}$$

with

$$\begin{aligned}
\mathcal{X}_{SD|r_{SD}} = & \sum_{n=\{L,N\}} c_{SD,n} \exp\left(\frac{\ln^2 10}{200}\sigma_{S_{Gn}}^2\right) 2\pi\lambda_T \int_0^\infty (1+r)^{-\alpha_{Gn}} p_{Gn}(r)\, r\mathrm{d}r, \\
\mathcal{X}_{RD|r_{RD}} = & \sum_{n=\{L,N\}} c_{RD,n} \exp\left(\frac{\ln^2 10}{200}\sigma_{S_{An}}^2\right) 2\pi\lambda_R \int_0^\infty \left(r^2 + H_R^2\right)^{-\frac{\alpha_{An}}{2}} p_{An}(r)\, r\mathrm{d}r.
\end{aligned}$$

4.5 Average Spectral Efficiency

As specified in Section 3.6, knowing the CP of the complete link, the ergodic SE is obtained as follows:

$$\mathcal{S} = \frac{1}{2\ln 2}\int_0^\infty \frac{\mathcal{P}(\beta)}{1+\beta}\mathrm{d}\beta, \tag{4.61}$$

and with the other definition of the average rate given by Equation (3.36),

$$\tilde{\mathcal{S}}(\beta) = \frac{1}{2}\log_2(1+\beta)\mathcal{P}(\beta). \tag{4.62}$$

The factor $1/2$ which appears in these expressions is a consequence of the DF protocol executed in two steps.

However, since the expression of the CP given by Proposition 4.1 is already mathematically complex, Proposition 4.10 shows an alternative way suggested by [55, 56] to compute the ergodic SE of the direct link, first hop and second hop without using the CP.

Proposition 4.10. With the nearest neighbour association rule, the ergodic SE of the direct link, the first hop and the second hop are given by

$$\mathcal{S}_{SD} = \mathbb{E}_{S_{SD,L},S_{SD,N}}\left[\frac{\pi\lambda_T}{\ln 2}\int_0^\infty \mathcal{I}_{\mathcal{S},SD}(s,r_{SD})\; r_{SD}\,\exp\left(-\pi\lambda_T r_{SD}^2\right)\mathrm{d}r_{SD}\right], \tag{4.63}$$

$$\mathcal{S}_{SR} = \mathbb{E}_{S_{SR,L},S_{SR,N}}\left[\frac{\pi\lambda_T}{\ln 2}\int_0^\infty \mathcal{I}_{\mathcal{S},SR}(s,r_{SR})\; r_{SR}\,\exp\left(-\pi\lambda_T r_{SR}^2\right)\mathrm{d}r_{SR}\right], \tag{4.64}$$

$$\mathcal{S}_{RD} = \mathbb{E}_{S_{RD,L},S_{RD,N}}\left[\frac{\pi\lambda_R}{\ln 2}\int_0^\infty \mathcal{I}_{\mathcal{S},RD}(s,r_{RD})\, r_{RD}\,\exp\left(-\pi\lambda_R r_{RD}^2\right)\mathrm{d}r_{RD}\right], \tag{4.65}$$

with

$$\begin{aligned}
\mathcal{I}_{\mathcal{S},SD}(s,r_{SD}) &= \int_0^\infty \mathcal{L}_{I_{SD}|r_{SD}}(s)\;\iota_{\mathcal{X},SD}(r_{SD},s)\,\frac{\exp\left(-s\sigma^2\right)}{s}\mathrm{d}s,\\
\mathcal{I}_{\mathcal{S},SR}(s,r_{SR}) &= \int_0^\infty \mathcal{L}_{I_{SR}|r_{SR}}(s)\;\iota_{\mathcal{X},SR}(r_{SR},s)\,\frac{\exp\left(-s\sigma^2\right)}{s}\mathrm{d}s,\\
\mathcal{I}_{\mathcal{S},RD}(s,r_{RD}) &= \int_0^\infty \mathcal{L}_{I_{RD}|r_{RD}}(s)\,\iota_{\mathcal{X},RD}(r_{RD},s)\frac{\exp\left(-s\sigma^2\right)}{s}\mathrm{d}s,
\end{aligned}$$

and

$$\begin{aligned}
\iota_{\mathcal{S},SD}(r,s) &= 1-\sum_{n=\{L,N\}} p_{Gn}(r)\mathcal{L}_{|h_{SD,n}|^2}\left(s\,C_{SD,n}(1+r)^{-\alpha_{Gn}}S_{SD,n}\right),\\
\iota_{\mathcal{S},SR}(r,s) &= 1-\sum_{n=\{L,N\}} p_{An}(r)\mathcal{L}_{|h_{SR,n}|^2}\left(s\,C_{SR,n}(r^2+H_R^2)^{-\frac{\alpha_{An}}{2}}S_{SR,n}\right),\\
\iota_{\mathcal{S},RD}(r,s) &= 1-\sum_{n=\{L,N\}} p_{An}(r)\mathcal{L}_{|h_{RD,n}|^2}\left(s\,C_{RD,n}(r^2+H_R^2)^{-\frac{\alpha_{An}}{2}}S_{RD,n}\right).
\end{aligned}$$

Unfortunately, the ergodic SE of the relay link is not directly related to the ergodic SEs of each hop taken individually. Therefore, Lemma 4.9 proposes an upper bound for the ergodic SE of the relay link.

Lemma 4.9. With the DF protocol, knowing the ergodic SE of the first hop and of the second hop, an upper bound for the ergodic SE of the relay link is given by

$$\mathcal{S}_{SRD} \leq \min\left(\mathcal{S}_{SR}, \mathcal{S}_{RD}\right). \tag{4.66}$$

Chapter 5

UAV-based Relay Networks with Mobile UAVs

Numerous studies about mobile UAV networks have been presented in Section 3.7. In this chapter, the framework presented in Section 4 is extended by allowing the UAV RNs to move following the mobility schemes presented in [48].

5.1 Introduction of the Mobility Schemes

Two different UAVs' mobility schemes, both at a fixed altitude, are defined in [48]:

1. All the UAV RNs move independently at a constant speed in random directions;
2. All the UAV RNs move independently at a constant speed in random directions, except the selected UAV RN, which moves towards the typical UE and hovers above it.

For the first mobility scheme, Proposition 5.1 suggests that the performance of the network remains unchanged with the introduction of this mobility scheme.

Proposition 5.1. For the first mobility scheme, the resulting PP at time $t \geq 0$ is still an HPPP with density λ_R. Therefore, the performance of the network remains unchanged with the introduction of this mobility scheme.

However, this is not the case for the second one. At time $t \geq 0$, even if the SINR of the direct link at the typical UE is not affected by the RNs' mobility, the SINR of the first and second hop for LoS or NLoS links becomes

$$\chi_{SR,n}(t) = \frac{U_{SR,n}(t)}{I_{SR}(t) + \sigma^2} \qquad \text{and} \qquad \chi_{RD,n}(t) = \frac{U_{RD,n}(t)}{I_{RD}(t) + \sigma^2}, \tag{5.1}$$

with $U_{SR,n}(t)$, $U_{RD,n}(t)$, $I_{SR}(t)$ and $I_{RD,n}(t)$, respectively the power from the TBS serving at the selected RN in LoS or NLoS, the power from the selected RN at the typical UE in

LoS or NLoS, the aggregate interference of the TBSs at the selected RN, and the aggregate interference of the UAV RNs at the typical UE. These powers can be expressed as

$$\begin{aligned} U_{SR,n}(t) &= P_T G_{SR,M} L_{An}^{-1}\left(\sqrt{(r_{SR}(t))^2 + H_R^2}\right) \\ &= C_{SR,n}((r_{SR}(t))^2 + H_R^2)^{-\frac{\alpha_{An}}{2}} |h_{SR,n}|^2 S_{SR,n}, \end{aligned} \tag{5.2}$$

$$\begin{aligned} U_{RD,n}(t) &= P_R G_{RD,M} L_{An}^{-1}\left(\sqrt{(r_{RD}(t))^2 + H_R^2}\right) \\ &= C_{RD,n}((r_{RD}(t))^2 + H_R^2)^{-\frac{\alpha_{An}}{2}} |h_{RD,n}|^2 S_{RD,n}, \end{aligned} \tag{5.3}$$

$$\begin{aligned} I_{SR}(t) &= \sum_{\boldsymbol{\phi}_j \in \boldsymbol{\Phi}_{SRI}(t)} P_T G_{SR,m} L_{An_j}^{-1}\left(\sqrt{\|\boldsymbol{\phi}_j\|^2 + H_R^2}\right) \\ &= \sum_{n=\{L,N\}} \sum_{\boldsymbol{\phi}_j \in \boldsymbol{\Phi}_{SRI,n}(t)} c_{SR,n}(\|\boldsymbol{\phi}_j\|^2 + H_R^2)^{-\frac{\alpha_{An}}{2}} |h_{SR,n,j}|^2 S_{SR,n,j}, \end{aligned} \tag{5.4}$$

$$\begin{aligned} I_{RD}(t) &= \sum_{\boldsymbol{\phi}_j \in \boldsymbol{\Phi}_{RDI}(t)} P_R G_{RD,m} L_{An_j}^{-1}\left(\sqrt{\|\boldsymbol{\phi}_j\|^2 + H_R^2}\right) \\ &= \sum_{n=\{L,N\}} \sum_{\boldsymbol{\phi}_j \in \boldsymbol{\Phi}_{RDI,n}(t)} c_{RD,n}(\|\boldsymbol{\phi}_j\|^2 + H_R^2)^{-\frac{\alpha_{An}}{2}} |h_{RD,n,j}|^2 S_{RD,n,j}, \end{aligned} \tag{5.5}$$

where $r_{SR}(t)$ is the distance from the selected RN to its closest TBS and $r_{RD}(t)$ is the distance from the typical UE to the selected RN. The PP in $\mathbb{R}^2$ corresponding to the locations of the interfering TBSs is denoted by $\boldsymbol{\Phi}_{SRI}(t) = \boldsymbol{\Phi}_T \setminus \{\tilde{\boldsymbol{\phi}}_{SR}(t)\}$, with $\tilde{\boldsymbol{\phi}}_{SR}(t)$ being the TBS which is the closest of the selected RN, and the PP in $\mathbb{R}^2$ corresponding to the locations of the interfering RNs is denoted by $\boldsymbol{\Phi}_{RDI}(t) = \boldsymbol{\Phi}_R \setminus \{\tilde{\boldsymbol{\phi}}_{RD}(t)\}$, with $\tilde{\boldsymbol{\phi}}_{RD}(t)$ being the selected RN. The PPs of the TBSs and RNs interferers in LoS and NLoS at time $t \geq 0$ are respectively denoted by $\boldsymbol{\Phi}_{SRI,L}(t)$, $\boldsymbol{\Phi}_{SRI,N}(t)$, $\boldsymbol{\Phi}_{RDI,L}(t)$, and $\boldsymbol{\Phi}_{RDI,N}(t)$.

Lemma 5.1 shows that the second mobility scheme does not impact the distribution of the SINR and hence the performance of the first hop.

Lemma 5.1. With the second mobility scheme, the SINR of the first hop at time $t \geq 0$ is a RV equivalent to the SINR of the first hop at time $t = 0$:

$$F_{\chi_{SR}(t)}(x) = F_{\chi_{SR}(0)}(x) = F_{\chi_{SR}}(x) \qquad \forall x,\ \forall t \geq 0. \tag{5.6}$$

For the first hop, the selected RN at time $t = 0$ will remain the selected RN for every time $t \geq 0$ since it is initially the closest RN to the typical UE and it moves in its direction at the same speed v than the other RNs. Therefore, the distance between the typical UE and the selected RN is given by

$$r_{RD}(t) = \begin{cases} r_{RD} - vt \text{ if } r_{RD} > vt \\ 0 \qquad\quad \text{otherwise} \end{cases}, \tag{5.7}$$

where the PDF of r_{RD} is given by Lemma 4.1.

Additionally, Lemma 5.2 generalises with the second mobility scheme the probabilities that the typical UE selects either the direct link or the relay link given by Lemma 4.3.

Lemma 5.2. With the nearest neighbour association rule, the probabilities that the typical UE selects a direct or relay link at time $t \geq 0$ are respectively given by

$$p_{A,SD} = 1 - \exp\left(-\pi\lambda_T H_R^2\right)\left(1 - \exp\left(-\pi\lambda_R v^2 t^2\right)\right) - 2\pi\lambda_R \exp\left(-\pi\lambda_T (H_R^2 + v^2 t^2)\right)\mathcal{I}_{A,SD}, \tag{5.8}$$

$$p_{A,SRD} = \exp\left(-\pi\lambda_T H_R^2\right)\left(1 - \exp\left(-\pi\lambda_R v^2 t^2\right)\right) + 2\pi\lambda_R \exp\left(-\pi\lambda_T (H_R^2 + v^2 t^2)\right)\mathcal{I}_{A,SD}, \tag{5.9}$$

with

$$\mathcal{I}_{A,SD} = \int_{vt}^{\infty} r_{RD} \exp\left(-\pi(\lambda_R + \lambda_T) r_{RD}^2 + 2\pi\lambda_T vt\, r_{RD}\right) \mathrm{d}r_{RD}.$$

The first hop interferers' PP is also modified by the second mobility scheme. At time $t \geq 0$, its density conditioned on the initial distance between the typical UE and the selected RN is given by [48]

$$\lambda_{RDI|r_{RD}}(r,t) = \begin{cases} \lambda_R & \text{if } r_{RD} + vt \leq r \\ \dfrac{\lambda_R}{\pi} \arccos\left(\dfrac{r_{RD}^2 - r^2 - v^2 t^2}{2rvt}\right) & \text{if } |r_{RD} - vt| \leq r < r_{RD} + vt\,. \\ \lambda_R\, \mathbb{1}\left(r_{RD} < vt\right) & \text{if } 0 \leq r < |r_{RD} - vt| \end{cases} \tag{5.10}$$

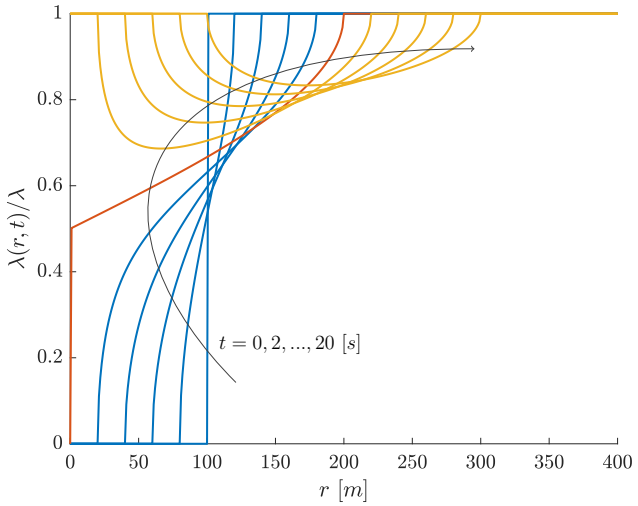

Figure 5.1: Normalised density at time $t = \{0, 2, ..., 20\}$ $[s]$ for an initial distance $r_{RD} = 100$ $[m]$ and a speed $v = 10$ $[m/s]$. Blue curves represent the normalised density for $r_{RD} > vt$, the orange curve for $r_{RD} = vt$ and yellow curves for $r_{RD} < vt$.

Figure 5.1 illustrates this density. For $r_{RD} > vt$, there cannot be any interfering RN closer to the typical UE than the selected RN, therefore this density is zero in the

exclusion zone defined by $r \leq r_{RD} - vt$. For $r_{RD} < vt$, as explained in [48], the density of the interfering RNs can be obtained by substracting the density imposed by the initial exclusion zone to λ_R. Since the RNs inside a circle of radius r_{RD} will not remain at a distance lower than $vt - r_{RD}$ at time $t \geq {}^{r_{RD}}/_{v}$, the density imposed by the initial exclusion zone is zero in this area. Finally, at time $t \to \infty$, this density is spread in the entire area such that the density of the interfering RNs is uniform everywhere.

5.2 Coverage Probability

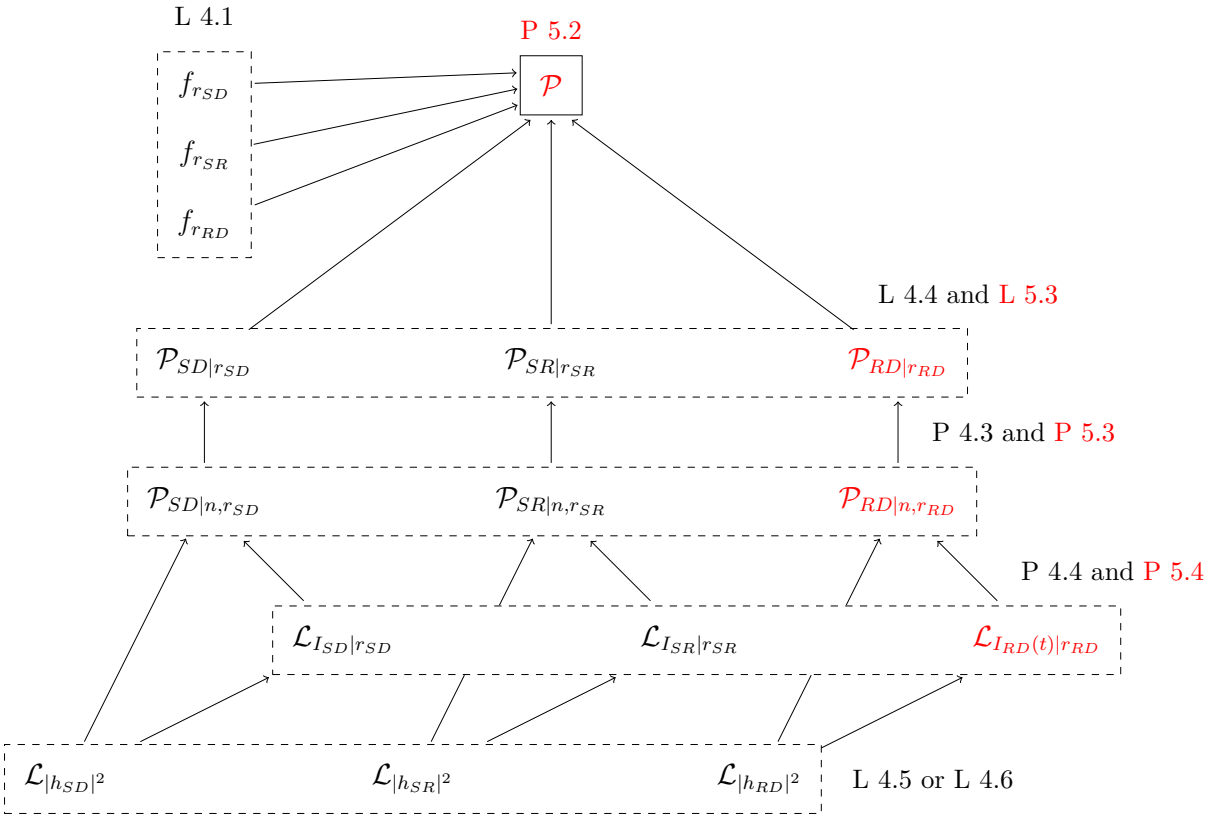

Figure 5.2: Summary of the different quantities to be evaluated in order to obtain an analytical expression of the CP for the complete link at time $t \geq 0$. Quantities in red are the quantities affected by the mobility scheme. The acronyms L and P are abbreviations for Lemma and Proposition.

With the introduction of the second mobility scheme, Figure 5.2 shows the different quantities which must be evaluated in order to obtain an expression of the CP of the complete link using SG. The mathematical expressions obtained in Chapter 4 are still valid for the direct link and the first hop, but the expressions related to the second hop must be adapted.

First, the CP of the complete link given by Proposition 4.1 is generalised with the second mobility scheme in Proposition 5.2.

Proposition 5.2. With the second mobility scheme, considering the nearest neighbour association rule and selection between direct link and relay link, the CP of the complete link at time $t \geq 0$ for a given SINR threshold β is given by

$$\mathcal{P}(\beta,t) = \mathcal{I}_{SD}^{(a)}(\beta,t) + \mathcal{I}_{SD}^{(b)}(\beta,t) + \mathcal{I}_{SRD}^{(a)}(\beta,t) + \mathcal{I}_{SRD}^{(a)}(\beta,t), \tag{5.11}$$

with

$$\begin{aligned}
\mathcal{I}_{SD}^{(a)}(\beta) &= \int_0^{H_R} \mathcal{P}_{SD|r_{SD}}(\beta) f_{r_{SD}}(r_{SD}) \mathrm{d}r_{SD}, \\
\mathcal{I}_{SD}^{(b)}(\beta) &= \int_{H_R}^{\infty} \mathcal{P}_{SD|r_{SD}}(\beta) \tilde{f}_{r_{SD}}(r_{SD}) \mathrm{d}r_{SD}, \\
\mathcal{I}_{SRD}^{(a)}(\beta) &= \mathcal{P}_{SR}(\beta) \int_0^{vt} \mathcal{P}_{RD|r_{RD}}^{(a)}(\beta,t) \tilde{f}_{r_{RD}}^{(a)}(r_{RD}) \mathrm{d}r_{RD}, \\
\mathcal{I}_{SRD}^{(b)}(\beta) &= \mathcal{P}_{SR}(\beta) \int_{vt}^{\infty} \mathcal{P}_{RD|r_{RD}}^{(b)}(\beta,t) \tilde{f}_{r_{RD}}^{(b)}(r_{RD}) \mathrm{d}r_{RD},
\end{aligned}$$

and

$$\mathcal{P}_{SR}(\beta) = \int_0^{\infty} \mathcal{P}_{SR|r_{SR}}(\beta) f_{r_{SR}}(r_{SR}) \mathrm{d}r_{SR}, \tag{5.12}$$

$$\begin{aligned}
\tilde{f}_{r_{SD}}(r_{SD}) &= f_{r_{SD}}(r_{SD}) \exp\left(-\pi\lambda_R \left(v^2t^2 - H_R^2\right)\right) \exp\left(-\pi\lambda_R \left(r_{SD}^2 + 2vt\sqrt{r_{SD}^2 - H_R^2}\right)\right), \\
\tilde{f}_{r_{RD}}^{(a)}(r_{RD}) &= f_{r_{RD}}(r_{RD}) \exp\left(-\pi\lambda_T H_R^2\right), \\
\tilde{f}_{r_{RD}}^{(b)}(r_{RD}) &= f_{r_{RD}}(r_{RD}) \exp\left(-\pi\lambda_T \left(H_R^2 + v^2t^2\right)\right) \exp\left(-\pi\lambda_T (r_{RD}^2 - 2r_{RD}vt)\right).
\end{aligned}$$

In these expressions,

- $\mathcal{P}_{SD|r_{SD}}$ is the CP of the direct link, conditioned on r_{SD};
- $\mathcal{P}_{SR|r_{SR}}$ is the CP of the first hop, conditioned on r_{SR};
- $\mathcal{P}_{RD|r_{RD}}^{(a)}$ is the CP of the second hop at time $t \geq 0$, conditioned on r_{RD} and knowing that $r_{RD} \leq vt$;
- $\mathcal{P}_{RD|r_{RD}}^{(b)}$ is the CP of the second hop at time $t \geq 0$, conditioned on r_{RD} and knowing that $r_{RD} > vt$.

If direct links are neglected, the CP of the relay link at time $t \geq 0$ for a given SINR threshold β becomes

$$\begin{aligned}
\mathcal{P}_{SRD}(\beta,t) = {} & 2\pi\lambda_R \mathcal{P}_{SR}(\beta) \int_0^{vt} \mathcal{P}_{RD|r_{RD}}^{(a)}(\beta,t)\, r_{RD} \exp\left(-\pi\lambda_R r_{RD}^2\right) \mathrm{d}r_{RD} \\
& + 2\pi\lambda_R \mathcal{P}_{SR}(\beta) \int_{vt}^{\infty} \mathcal{P}_{RD|r_{RD}}^{(b)}(\beta,t)\, r_{RD} \exp\left(-\pi\lambda_R r_{RD}^2\right) \mathrm{d}r_{RD}.
\end{aligned} \tag{5.13}$$

Then, Lemma 5.3 gives the CP of the second hop with the second mobility scheme at

time $t \geq 0$, conditioned on r_{RD} and knowing that $r_{RD} \leq vt$ or $r_{RD} > vt$.

Lemma 5.3. With the second mobility scheme, the CPs of the second hop at time $t \geq 0$, conditioned on r_{RD} and knowing that $r_{RD} \leq vt$ or $r_{RD} > vt$ are given by

$$\mathcal{P}^{(a)}_{RD|r_{RD}}(\beta, t) = \mathcal{P}^{(a)}_{RD|L,r_{RD}}(\beta, t), \tag{5.14}$$

$$\mathcal{P}^{(b)}_{RD|r_{RD}}(\beta, t) = p_{AL}(r_{RD} - vt)\mathcal{P}^{(a)}_{RD|L,r_{RD}}(\beta, t) + p_{AN}(r_{RD} - vt)\mathcal{P}^{(b)}_{RD|N,r_{RD}}(\beta, t). \tag{5.15}$$

In these expressions,

- $\mathcal{P}^{(a)}_{RD|n,r_{RD}}$ is the CP of the second hop at time $t \geq 0$ if the link is in LoS or NLoS, conditioned on r_{RD} and knowing that $r_{RD} \leq vt$;
- $\mathcal{P}^{(b)}_{RD|n,r_{RD}}$ is the CP of the second hop at time $t \geq 0$ if the link is in LoS or NLoS, conditioned on r_{RD} and knowing that $r_{RD} > vt$.

Using the Gil-Pelaez theorem and Lemma 5.3, Proposition 5.3 gives the CP of the second hop with the second mobility scheme if the link is in LoS or NLoS, conditioned on r_{RD} and knowing that $r_{RD} \leq vt$ or $r_{RD} > vt$.

Proposition 5.3. With the second mobility scheme, the CPs of the second hop if the link is in LoS or NLoS, conditioned on r_{RD}, at time $t \geq 0$ and knowing that $r_{RD} \leq vt$ or $r_{RD} > vt$ are respectively given by

$$\mathcal{P}^{(a)}_{RD|n,r_{RD}}(\beta, t) = \frac{1}{2} + \frac{1}{\pi}\mathbb{E}_{S_{RD,n}}\left[\int_0^\infty \frac{1}{\tau}\mathrm{Im}\left[\phi^{(a)}_{Z_{RD}|r_{RD}}(\tau)\exp\left(-j\tau\beta\sigma^2\right)\right]\mathrm{d}\tau\right], \tag{5.16}$$

$$\mathcal{P}^{(b)}_{RD|n,r_{RD}}(\beta, t) = \frac{1}{2} + \frac{1}{\pi}\mathbb{E}_{S_{RD,n}}\left[\int_0^\infty \frac{1}{\tau}\mathrm{Im}\left[\phi^{(b)}_{Z_{RD}|r_{RD}}(\tau, t)\exp\left(-j\tau\beta\sigma^2\right)\right]\mathrm{d}\tau\right], \tag{5.17}$$

with

$$\begin{aligned}
\phi^{(a)}_{Z_{RD}|r_{RD}}(\tau) &= \mathcal{L}_{|h_{RD,n}|^2}\left(-j\tau C_{RD,n}H_R^{-\alpha_{An}}S_{RD,n}\right)\mathcal{L}^{(a)}_{I_{RD}|r_{RD}}(j\tau\beta),\\
\phi^{(b)}_{Z_{RD}|r_{RD}}(\tau, t) &= \mathcal{L}_{|h_{RD,n}|^2}\left(-j\tau C_{RD,n}((r_{RD} - vt)^2 + H_R^2)^{-\frac{\alpha_{An}}{2}}S_{RD,n}\right)\mathcal{L}^{(b)}_{I_{RD}(t)|r_{RD}}(j\tau\beta).
\end{aligned}$$

In these expressions,

- $\mathcal{L}_{|h_{RD,n}|^2}$ is the LT of $|h_{RD,n}|^2$ if the link of the second hop is in LoS or NLoS;
- $\mathcal{L}^{(a)}_{I_{RD}(t)|r_{RD}}$ is the LT of $I_{RD}(t)$ conditioned on r_{RD} and knowing that $r_{RD} \leq vt$;
- $\mathcal{L}^{(b)}_{I_{RD}(t)|r_{RD}}$ is the LT of $I_{RD}(t)$ conditioned on r_{RD} and knowing that $r_{RD} > vt$.

Finally, based on the density given by Equation 5.10, the LT of the aggregate interference for the second hop with the second mobility scheme is given by Proposition 5.4.

Proposition 5.4. The LTs of the aggregate interference of the second hop, conditioned on r_{RD}, at time $t \geq 0$ and knowing that $r_{RD} \leq vt$ or $r_{RD} > vt$ are given by

$$\mathcal{L}^{(a)}_{I_{RD}(t)|r_{RD}}(s) = \exp\Big(- 2\pi\lambda_R \mathbb{E}_{\tilde{S}_{RD,L},\tilde{S}_{RD,N}}\Big[\mathcal{I}^{(a,1)}_{I,RD}(s,t) - \mathcal{I}^{(a,2)}_{I,RD}(s,t)\Big]\Big), \tag{5.18}$$

$$\mathcal{L}^{(b)}_{I_{RD}(t)|r_{RD}}(s) = \exp\Big(- 2\pi\lambda_R \mathbb{E}_{\tilde{S}_{RD,L},\tilde{S}_{RD,N}}\Big[\mathcal{I}^{(b,1)}_{I,RD}(s,t) + \mathcal{I}^{(b,2)}_{I,RD}(s,t)\Big]\Big), \tag{5.19}$$

with

$$\begin{aligned}
\mathcal{I}^{(a,1)}_{I,RD}(s,t) &= \int_0^{\infty} \iota_{RD}(r,s,\tilde{S}_{RD,L},\tilde{S}_{RD,N})\, r\mathrm{d}r,\\
\mathcal{I}^{(a,2)}_{I,RD}(s,t) &= \frac{1}{\pi}\int_{vt-r_{RD}}^{vt+r_{RD}} \arccos\left(\frac{r^2+v^2t^2-r_{RD}^2}{2rvt}\right) \iota_{RD}(r,s,\tilde{S}_{RD,L},\tilde{S}_{RD,N})\, r\mathrm{d}r,\\
\mathcal{I}^{(b,1)}_{I,RD}(s,t) &= \int_{r_{RD}+vt}^{\infty} \iota_{RD}(r,s,\tilde{S}_{RD,L},\tilde{S}_{RD,N})\, r\mathrm{d}r,\\
\mathcal{I}^{(b,2)}_{I,RD}(s,t) &= \frac{1}{\pi}\int_{r_{RD}-vt}^{r_{RD}+vt} \arccos\left(\frac{r_{RD}^2-r^2-v^2t^2}{2rvt}\right) \iota_{RD}(r,s,\tilde{S}_{RD,L},\tilde{S}_{RD,N})\, r\mathrm{d}r,
\end{aligned}$$

and

$$\iota_{RD}(r,s,\tilde{S}_{RD,L},\tilde{S}_{RD,N}) = 1 - \sum_{n=\{L,N\}} p_{An}(r)\mathcal{L}_{|\tilde{h}_{RD,n}|^2}\left(s\, c_{RD,n}(r^2+H_R^2)^{-\frac{\alpha_{An}}{2}}\tilde{S}_{RD,n}\right).$$

In these expressions, the RVs $|\tilde{h}_{RD,n}|^2$ and $\tilde{S}_{RD,n}$ are equivalent to the small-scale fading channel power gains and the shadowings RVs of the second hop.

5.3 Enhancements of the Model

In this section, the correlated model for the TBS selection proposed in Section 4.3 is generalised with the second mobility scheme. Additionally, the introduction of distance-dependent small-scale fading parameters is considered. Note that the propositions and lemmas presented in this section have not been yet validated numerically!

5.3.1 Terrestrial Base Station Selection

We consider that the TBS which serves the typical UE if the direct link is selected is also the TBS which serves the selected RN if the relay link is chosen. At time $t \geq 0$, with the nearest neighbour association rule, the PDFs of r_{RD} and r_{SD} are still given by Lemma 4.1. However, the distance between the selected TBS and the selected RN is now a function of $r_{RD}(t)$, given by Equation (5.7), and r_{SD}. Lemma 5.4 gives the PDF of the distance between the selected TBS and the selected RN, conditioned on r_{RD} and r_{SD}.

Lemma 5.4. With the nearest neighbour association rule, if the same TBS serves the selected RN and the typical UE, the PDFs of r_{SR} conditioned on r_{RD} and r_{SD}, at time $t \geq 0$ and knowing that $r_{RD} \leq vt$ or $r_{RD} > vt$ are respectively given by

$$f^{(a)}_{r_{SR}|r_{RD},r_{SD}}(r) = \delta(r - r_{SD}), \tag{5.20}$$

and

$$f^{(b)}_{r_{SR}|r_{RD},r_{SD}}(r) = \begin{cases} \frac{1}{\pi} \frac{2r}{\sqrt{4r_{SD}^2(r_{RD}-vt)^2 - (r^2 - r_{SD}^2 - (r_{RD}-vt)^2)^2}} & \text{if } \begin{array}{r} |r_{RD} - vt - r_{SD}| \leq r \\ r \leq r_{RD} - vt + r_{SD} \end{array} . \\ 0 & \text{otherwise} \end{cases} \tag{5.21}$$

Finally, based on Lemma 5.4, Proposition 5.5 gives the CP of the complete link.

5.3.2 Distance-Dependent Rician Fading

In the scenario depicted in Chapter 4, we assumed that the parameters of the propagation model are identical for every G2G or A2G link. However, this does not apply in practice, especially when some mobility is introduced. In this section, we introduce some dependency with the distance in the small-scale fading model.

Considering a Rician fading with K-factor K_L and K_N for a LoS or NLoS link, these parameters are replaced by $K_L(r)$ and $K_N(r)$, with r the ground distance between the two nodes.

Lemma 5.5 is a generalisation of Lemma 4.6 with distance-dependent Rician K-factor.

Lemma 5.5. With Rician fading, the LT of the small-scale fading channel power gain with distance-dependent K-factor is given by

$$\mathcal{L}_{|h(r)|^2}(s) = \frac{K(r)+1}{K(r)+1+s} \exp\left(-\frac{K(r)\,s}{K(r)+1+s}\right), \tag{5.23}$$

where $K(r) = K_{Gn}(r)$ for G2G links in LoS or NLoS, and $K(r) = K_{An}(r)$ for A2G links in LoS or NLoS, and r is the ground distance between the two nodes.

The introduction of a distance-dependent LT for the small-scale fading channel power gain is straightforward in the previous developments: in Proposition 5.3, the distance between the two nodes is known, and in Proposition 5.4, the small-scale fading RVs of each link are functions only of the ground distances of these links, therefore the PGFL of a PPP is still applicable.

Proposition 5.5. With the second mobility scheme, considering the nearest neighbour association rule and selection between direct link and relay link, the CP of the complete link at time $t \geq 0$ for a given SINR threshold β is given by

$$\mathcal{P}(\beta,t) = \mathcal{I}_{SD}^{(a)}(\beta,t) + \mathcal{I}_{SD}^{(b)}(\beta,t) + \mathcal{I}_{SRD}^{(a)}(\beta,t) + \mathcal{I}_{SRD}^{(a)}(\beta,t), \tag{5.22}$$

with

$$\mathcal{I}_{SD}^{(a)}(\beta) = \int_0^{H_R} \mathcal{P}_{SD|r_{SD}}(\beta) f_{r_{SD}}(r_{SD}) \mathrm{d}r_{SD},$$
$$\mathcal{I}_{SD}^{(b)}(\beta) = \int_{H_R}^{\infty} \mathcal{P}_{SD|r_{SD}}(\beta) \tilde{f}_{r_{SD}}(r_{SD}) \mathrm{d}r_{SD},$$

$$\mathcal{I}_{SRD}^{(a)}(\beta) = \mathcal{P}_{SR}(\beta) \int_0^{vt} \mathcal{P}_{RD|r_{RD}}^{(a)}(\beta,t) \int_{H_R}^{\infty} \mathcal{P}_{SR|r_{SR}}(\beta)\Big|_{r_{SR}=r_{SD}} \mathcal{P}_{RD|r_{RD}}^{(a)}(\beta,t) \cdot f_{r_{SD},r_{RD}}(r_{SD},r_{RD}) \mathrm{d}r_{SD} \mathrm{d}r_{RD},$$

$$\mathcal{I}_{SRD}^{(b)}(\beta) = \int_{vt}^{\infty} \int_{\sqrt{(r_{RD}-vt)^2+H_R^2}}^{\infty} \int_{|r_{SD}-r_{RD}+vt|}^{r_{SD}+r_{RD}-vt} \mathcal{P}_{SR|r_{SR}}(\beta) \mathcal{P}_{RD|r_{RD}}^{(b)}(\beta,t) \cdot \tilde{f}_{r_{SD},r_{SR},r_{RD}}^{(b)}(r_{SD},r_{SR},r_{RD}) \mathrm{d}r_{SR} \mathrm{d}r_{SD} \mathrm{d}r_{RD},$$

and

$$\tilde{f}_{r_{SD}}(r_{SD}) = f_{r_{SD}}(r_{SD}) \exp\left(-\pi\lambda_R \left(v^2t^2 - H_R^2\right)\right) \exp\left(-\pi\lambda_R \left(r_{SD}^2 + 2vt\sqrt{r_{SD}^2 - H_R^2}\right)\right),$$
$$f_{r_{SD},r_{RD}}(r_{SD},r_{RD}) = 4\pi^2\lambda_R\lambda_T \, r_{SD} r_{RD} \exp\left(-\pi(\lambda_R r_{RD}^2 + \lambda_T r_{SD}^2)\right),$$
$$\tilde{f}_{r_{SD},r_{SR},r_{RD}}^{(b)}(r_{SD},r_{SR},r_{RD}) = \frac{8\pi\lambda_R\lambda_T \, r_{SR} r_{RD} r_{SD} \exp\left(-\pi(\lambda_R r_{RD}^2 + \lambda_T r_{SD}^2)\right)}{\sqrt{4r_{SD}^2(r_{RD}-vt)^2 - \left(r^2 - r_{SD}^2 - (r_{RD}-vt)^2\right)^2}}.$$

In these expressions,

- $\mathcal{P}_{SR|r_{SR}}$ is the CP of the first hop conditioned on r_{SR};
- $\mathcal{P}_{RD|r_{RD}}^{(a)}$ is the CP of the second hop at time $t \geq 0$, conditioned on r_{RD} and knowing that $r_{RD} \leq vt$;
- $\mathcal{P}_{RD|r_{RD}}^{(b)}$ is the CP of the second hop at time $t \geq 0$, conditioned on r_{RD} and knowing that $r_{RD} > vt$;
- $\mathcal{P}_{SD|r_{SD}}$ is the CP of the direct link, conditioned on r_{SD}.

5.4 Average Exposure

As in Chapter 4, we still consider a typical UE which communicates either through a direct link or a relay link. Proposition 4.8 gives the average exposure at the typical UE from the RNs with the second mobility scheme, at time $t \geq 0$.

Proposition 5.6. With the second mobility scheme, considering the nearest neighbour association rule and a typical UE which communicates either through a direct or a relay link, the average exposure at the typical UE from the RNs at time $t \geq 0$ is given by

$$\begin{aligned}\mathcal{X}_{c,RD}(t) = {} & 2\pi\lambda_R \int_0^{vt} \mathcal{X}^{(a)}_{c,RD|r_{RD}}(t)\, r_{RD} \exp\left(-\pi\lambda_R r_{RD}^2\right) \mathrm{d}r_{RD} \\ & + 2\pi\lambda_R \int_{vt}^{\infty} \mathcal{X}^{(b)}_{c,RD|r_{RD}}(t)\, r_{RD} \exp\left(-\pi\lambda_R r_{RD}^2\right) \mathrm{d}r_{RD}, \end{aligned} \tag{5.24}$$

with

$$\begin{aligned}\mathcal{X}^{(a)}_{c,RD|r_{RD}} = {} & \exp\left(\frac{\ln^2 10}{200}\sigma^2_{S_{AL}}\right) C_{RD,L}\, H_R^{-\alpha_{AL}} \\ & + \sum_{n=\{L,N\}} c_{RD,n} \exp\left(\frac{\ln^2 10}{200}\sigma^2_{S_{An}}\right) 2\pi\lambda_R \left(\mathcal{I}^{(a,1)}_{\mathcal{X},RD} - \mathcal{I}^{(a,2)}_{\mathcal{X},RD}\right), \\ \mathcal{X}^{(b)}_{c,RD|r_{RD}} = {} & \sum_{n=\{L,N\}} \exp\left(\frac{\ln^2 10}{200}\sigma^2_{S_{An}}\right) C_{RD,n}\, p_{An}(r_{RD} - vt) \left((r_{RD} - vt)^2 + H_R^2\right)^{-\frac{\alpha_{An}}{2}} \\ & + \sum_{n=\{L,N\}} c_{RD,n} \exp\left(\frac{\ln^2 10}{200}\sigma^2_{S_{An}}\right) 2\pi\lambda_R \left(\mathcal{I}^{(b,1)}_{\mathcal{X},RD} + \mathcal{I}^{(b,2)}_{\mathcal{X},RD}\right), \end{aligned}$$

and

$$\begin{aligned}\mathcal{I}^{(a,1)}_{\mathcal{X},RD} = {} & \int_0^{\infty} \left(r^2 + H_R^2\right)^{-\frac{\alpha_{An}}{2}} p_{An}(r)\, r\mathrm{d}r, \\ \mathcal{I}^{(a,2)}_{\mathcal{X},RD} = {} & \frac{1}{\pi} \int_{vt-r_{RD}}^{vt+r_{RD}} \arccos\left(\frac{r^2 + v^2t^2 - r_{RD}^2}{2rvt}\right) \left(r^2 + H_R^2\right)^{-\frac{\alpha_{An}}{2}} p_{An}(r)\, r\mathrm{d}r, \\ \mathcal{I}^{(b,1)}_{\mathcal{X},RD} = {} & \int_{r_{RD}+vt}^{\infty} \left(r^2 + H_R^2\right)^{-\frac{\alpha_{An}}{2}} p_{An}(r)\, r\mathrm{d}r, \\ \mathcal{I}^{(b,2)}_{\mathcal{X},RD} = {} & \frac{1}{\pi} \int_{r_{RD}-vt}^{r_{RD}+vt} \arccos\left(\frac{r_{RD}^2 - r^2 - v^2t^2}{2rvt}\right) \left(r^2 + H_R^2\right)^{-\frac{\alpha_{An}}{2}} p_{An}(r)\, r\mathrm{d}r. \end{aligned}$$

5.5 Average Spectral Efficiency

Knowing the CP of the complete link at time $t \geq 0$, the expressions of the ergodic SE given in Chapter 4 are generalised as follows:

$$\mathcal{S}(t) = \frac{1}{2\ln 2} \int_0^{\infty} \frac{\mathcal{P}(\beta, t)}{1+\beta} \mathrm{d}\beta, \tag{5.25}$$

and

$$\tilde{\mathcal{S}}(\beta,t)=\frac{1}{2}\log_2(1+\beta)\mathcal{P}(\beta,t). \tag{5.26}$$

However, since the expression of the CP given by Proposition 5.2 is mathematically complex, as in Chapter 4, Proposition 5.7 shows an alternative way to compute the ergodic SE of the second hop at time $t \geq 0$ without using the CP.

Proposition 5.7. With the second mobility scheme, considering the nearest neighbour association rule, the ergodic SE of the second hop at time $t \geq 0$ is given by

$$\begin{aligned}\mathcal{S}_{RD}(t)=&\,\mathbb{E}_{S_{RD,L},S_{RD,N}}\left[\frac{\pi\lambda_R}{\ln 2}\int_0^{vt}\mathcal{I}^{(a)}_{\mathcal{S},RD}(s,t)\,r_{RD}\exp\left(-\pi\lambda_R r_{RD}^2\right)\mathrm{d}r_{RD}\right]\\&+\mathbb{E}_{S_{RD,L},S_{RD,N}}\left[\frac{\pi\lambda_R}{\ln 2}\int_{vt}^{\infty}\mathcal{I}^{(b)}_{\mathcal{S},RD}(s,t)\,r_{RD}\exp\left(-\pi\lambda_R r_{RD}^2\right)\mathrm{d}r_{RD}\right],\end{aligned} \tag{5.27}$$

with

$$\begin{aligned}\mathcal{I}^{(a)}_{\mathcal{S},RD}(s,t)&=\int_0^{\infty}\mathcal{L}^{(a)}_{I_{RD}(t)|r_{RD}}(s)\,\iota^{(a)}_{\mathcal{X},RD}(s)\,\frac{\exp\left(-s\sigma^2\right)}{s}\mathrm{d}s,\\ \mathcal{I}^{(b)}_{\mathcal{S},RD}(s,t)&=\int_0^{\infty}\mathcal{L}^{(b)}_{I_{RD}(t)|r_{RD}}(s)\,\iota^{(b)}_{\mathcal{X},RD}(r_{RD}-vt,s)\,\frac{\exp\left(-s\sigma^2\right)}{s}\mathrm{d}s,\end{aligned}$$

and

$$\begin{aligned}\iota^{(a)}_{\mathcal{S},RD}(s)&=1-\mathcal{L}_{|h_{RD,L}|^2}\left(s\,C_{RD,L}H_R^{-\alpha_{An}}S_{RD,L}\right),\\ \iota^{(b)}_{\mathcal{S},RD}(r,s)&=1-\sum_{n=\{L,N\}}p_{An}(r)\mathcal{L}_{|h_{RD,n}|^2}\left(s\,C_{RD,n}(r^2+H_R^2)^{-\frac{\alpha_{An}}{2}}S_{RD,n}\right).\end{aligned}$$

The ergodic SE of the relay link is still not directly related to the ergodic SEs of each hop taken individually. Therefore, Lemma 4.9 proposes a generalisation of the upper bound presented in Lemma 4.9 at time $t \geq 0$ with the second mobility scheme.

Lemma 5.6. With the second mobility scheme, considering the DF protocol, knowing the ergodic SE of the first hop and of the second hop at time $t \geq 0$, an upper bound of the ergodic SE of the relay link is given by

$$\mathcal{S}_{SRD}(t)\leq\min\left(\mathcal{S}_{SR}(t),\mathcal{S}_{RD}(t)\right). \tag{5.28}$$

Chapter 6

Numerical Evaluation of the Performance

In this chapter, the performance of a network with parameters given by Table 6.1 is evaluated using the framework developed in Chapter 4 and 5.

We consider an interference-limited network without shadowing in an urban environment. First, the UAVs hover at fixed positions. Then, displacements are allowed following the second mobility scheme. The impact of the RNs' density and altitude is studied in particular, when direct links are neglected or taken into consideration.

Finally, SG expressions are compared to MC simulations in terms of computation time.

G2G Links	
A_{GL}	0.01
A_{GN}	0.01
α_{GL}	3
α_{GN}	4
σ^2_{GL}	0
σ^2_{GN}	0
K_{GL}	10
K_{GN}	0
d_1	18 $[m]$
d_2	63 $[m]$

A2G Links	
A_{AL}	0.01
A_{AN}	0.01
α_{AL}	3
α_{AN}	4
σ^2_{AL}	0
σ^2_{AN}	0
K_{AL}	10
K_{AN}	0
a	9.612
b	0.158

UAV RNs	
P_R	1 $[W]$
λ_R	$10^{-7} - 10^{-5}$ $[m^{-2}]$
H_R	$100 - 4000$ $[m]$
v	$0 - 40$ $[m/s]$
G_{RM}	1
G_{Rm}	1

TBSs	
P_T	1 $[W]$
λ_T	$5 \cdot 10^{-8}$ $[m^{-2}]$
G_{TM}	2
G_{Tm}	0.5

Other parameters	
σ^2	10^{-10} [W]

MC simulations	
Iterations	$10000 - 50000$
Radius	100 $[km]$

Table 6.1: Network parameters.

6.1 UAVs at Fixed Positions

6.1.1 Coverage Probability

Relay Link Only

One of the main features of UAVs are their flying capability, leading to an increased probability for the link to be in LoS compared to G2G links. Following the A2G LoS probability model given by Equation (3.18), the LoS probability of the link between the terrestrial nodes the selected RN is a function of the elevation angles between these nodes. These elevation angles themselves are functions of the RNs' altitude and the distance between couple of nodes.

Elevation Angles

Figure 6.1 shows the PDFs of the elevation angles of the first and second hop, respectively denoted by θ_{SR} and θ_{RD}. These PDFs can be compared to the A2G LoS probability model for an urban environment in Figure 3.4, in which a LoS probability of 0.5 is reached when

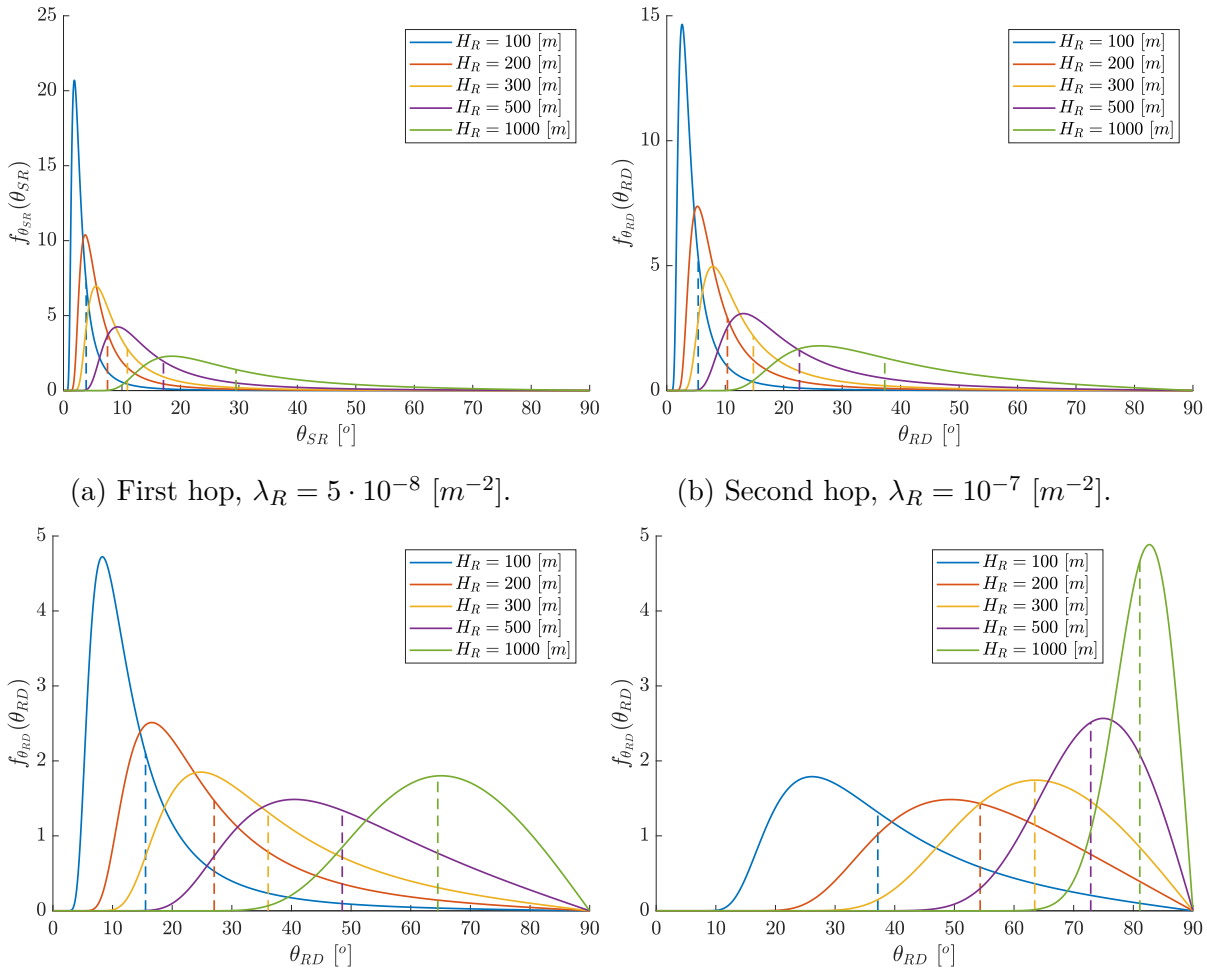

(a) First hop, $\lambda_R = 5 \cdot 10^{-8}$ $[m^{-2}]$.

(b) Second hop, $\lambda_R = 10^{-7}$ $[m^{-2}]$.

(c) Second hop, $\lambda_R = 10^{-6}$ $[m^{-2}]$.

(d) Second hop, $\lambda_R = 10^{-5}$ $[m^{-2}]$.

Figure 6.1: PDFs of the elevation angles of the first hop and second hop (solid lines) and their mean values (dashed lines).

the elevation angle is close to 25°. Since the TBSs' density is low ($5 \cdot 10^{-8}$ $[m^{-2}]$), the first hop's link is mainly in NLoS, as well as the second hop's link when the RNs' density is low (10^{-7} $[m^{-2}]$). For that range of densities, the PDFs of θ_{SR} and θ_{RD} are narrow and concentrated around small elevation angles.

A higher RNs' altitude helps to increase the probability for these links to be in LoS, since the PDF of θ_{SR} and θ_{RD} spreads over the possible elevation angles, with a mean value which exceeds 25° at 1000 meters.

Otherwise, for the second hop, an increase of the RNs' density also enables to reach a high LoS probability, even at low altitudes. At high RNs' density (10^{-5} $[m^{-2}]$), the PDF of θ_{RD} is spread over the elevation angles with a mean value close to 40° at an altitude of 100 meters, and becomes narrow and concentrated around 80° when the altitude is increased to 1000 meters.

CP of the First and Second Hop

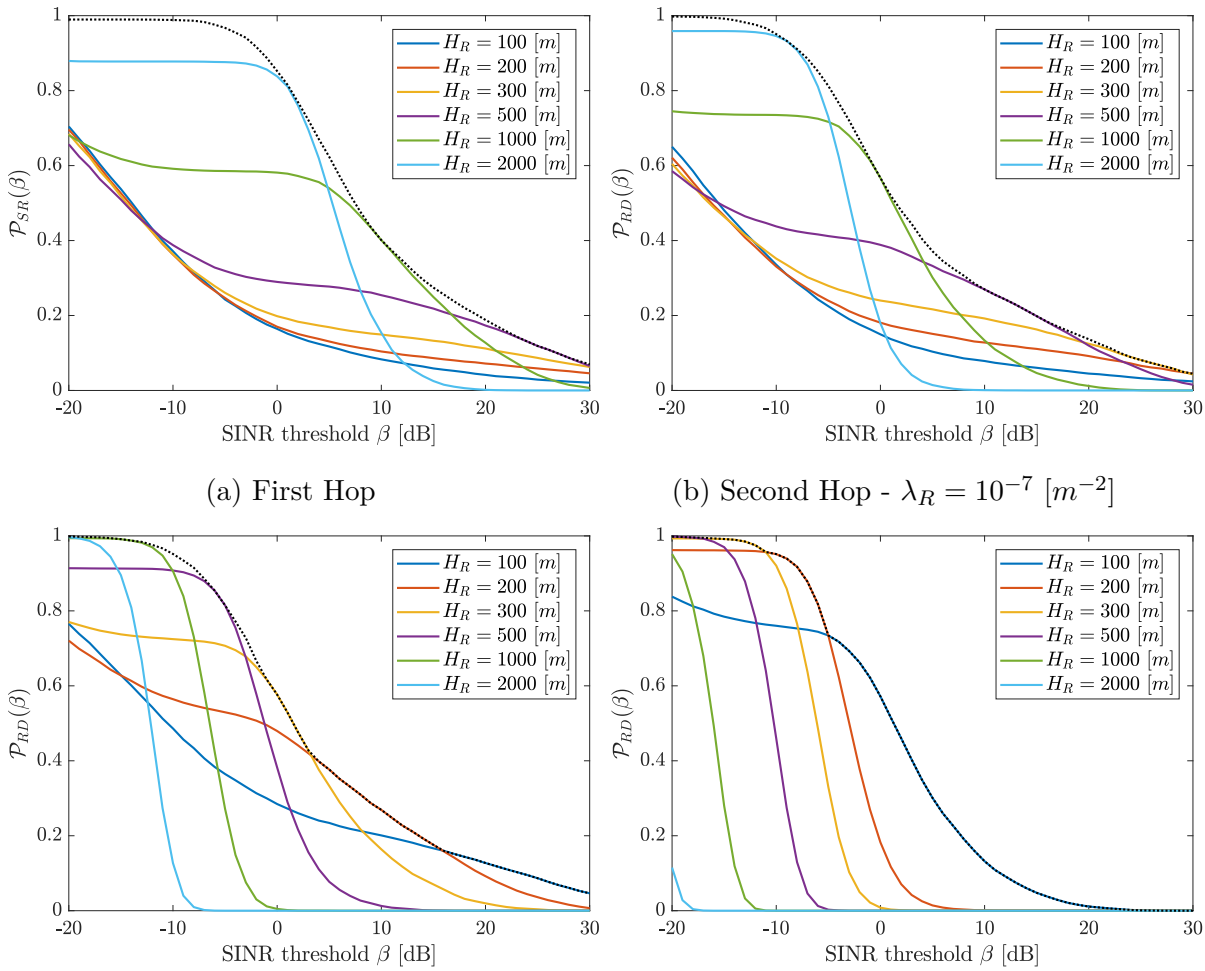

(a) First Hop

(b) Second Hop - $\lambda_R = 10^{-7}$ $[m^{-2}]$

(c) Second Hop - $\lambda_R = 10^{-6}$ $[m^{-2}]$

(d) Second Hop - $\lambda_R = 10^{-5}$ $[m^{-2}]$

Figure 6.2: CP of the first hop and second hop for different RNs' densities and altitudes (solid lines). The dotted curves represent the best CPs which can be achieved for each SINR threshold when the RNs' altitude is selected accordingly between the following values: $H_R = \{100, 200, ..., 4000\}$ $[m]$.

Figure 6.2 illustrates the CP of the first and second hop for different RNs' densities and altitudes, and the best CP which could be achieved for each SINR threshold for a finite set of RNs' altitudes. The increased probability for the A2G links to be in LoS directly impacts the shape of the CP curves. Depending on the type of link (in LoS or in NLoS), two different peaks appear in the PDF of the power from the selected TBS (resp. the selected RN) at the selected RN (resp. at the typical UE), and therefore also on the PDF of the SINR of the first hop (resp. the second hop).

Consequently, when the link is mainly in LoS or NLoS, the CP smoothly decreases straight from high values to low values. For the second hop, it applies for low RNs' densities and altitudes (link mainly in NLoS), or for high RNs' densities and altitudes (link mainly in LoS). Since the first hop does not depend on the RNs' density but on the TBSs' density, the RNs' altitude is the only parameter which matters in that case. However, when the LoS probability is closer to 0.5, owing to the presence of two distinct peaks in the PDF, a stair appears in the CP curves. Additionally, since the small-scale fading channel gain follows a Rice distribution with a larger K-factor when the link is in LoS, its PDF is more concentrated around 1 compared to the PDF for NLoS links. Therefore, the slope of the

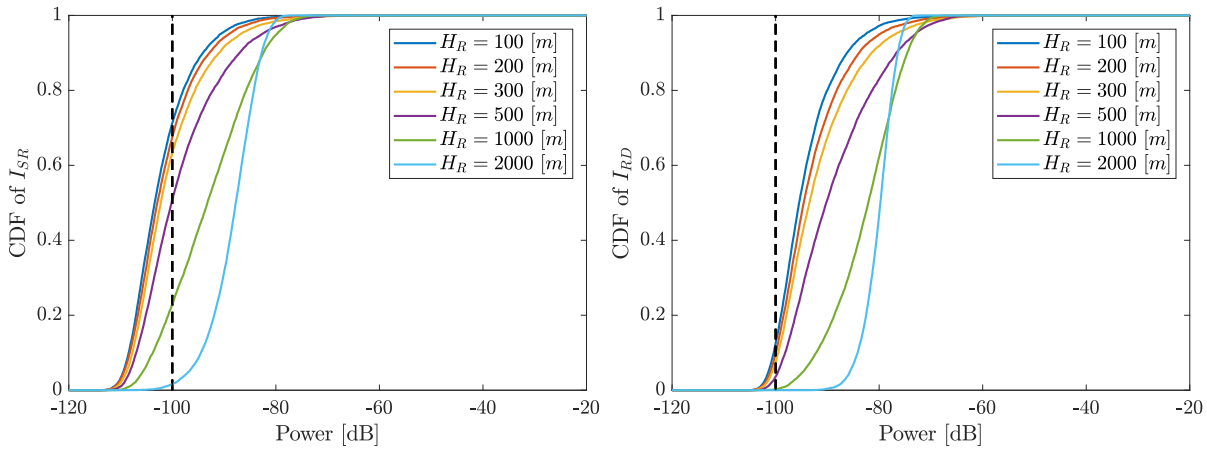

(a) First Hop

(b) Second Hop - $\lambda_R = 10^{-7}$ $[m^{-2}]$

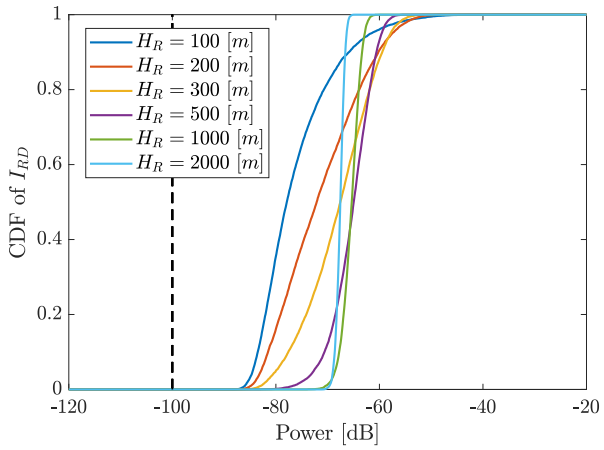

(c) Second Hop - $\lambda_R = 10^{-6}$ $[m^{-2}]$

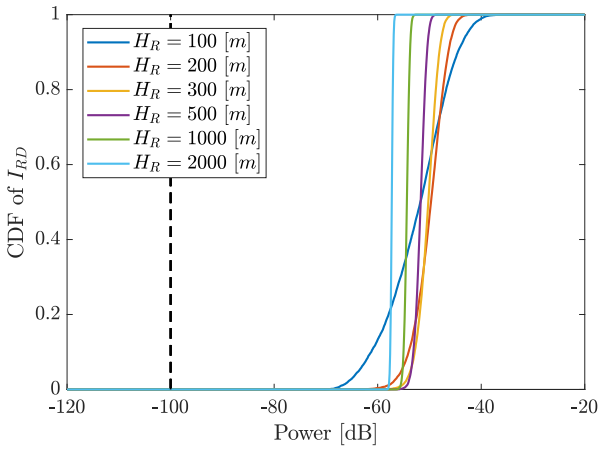

(d) Second Hop - $\lambda_R = 10^{-5}$ $[m^{-2}]$

Figure 6.3: CDF of I_{SR} and I_{RD} (solid lines) for different RNs' densities and altitudes, compared to the noise power (dashed lines).

second hop's CP is steeper in that case.

For this network configuration, the SINR of the second hop is mainly interference-limited. This is confirmed by Figure 6.3, which shows the CDF of the aggregate interference of the first hop and the second hop for different RNs' densities and altitudes, compared to the noise power. Indeed, even if a larger RNs' density or a higher RNs' altitude helps to increase the LoS probability of the first hop and second hop links, the power of the aggregate interference also increases. Moreover, the number of interfering nodes for the second hop is proportional to the former parameter.

CP of the Relay Link

Figure 6.4 illustrates the CP of the relay link for different RNs' densities and altitudes, and the best CP which could be achieved for each SINR threshold, for a finite set of RNs' altitudes. The CP of the relay link is limited by the performance of the worst link between

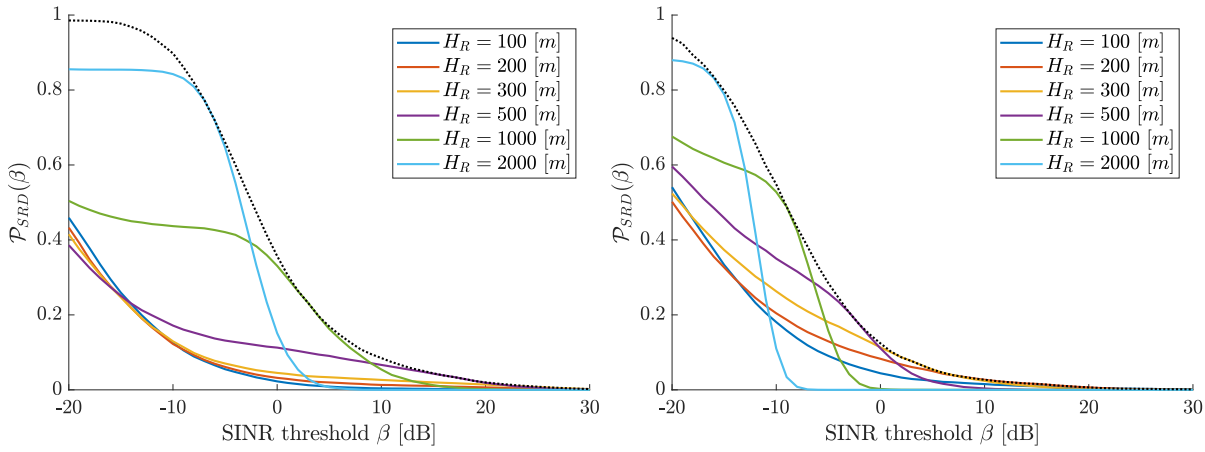

(a) Relay Link - $\lambda_R = 10^{-7}$ $[m^{-2}]$

(b) Relay Link - $\lambda_R = 10^{-6}$ $[m^{-2}]$

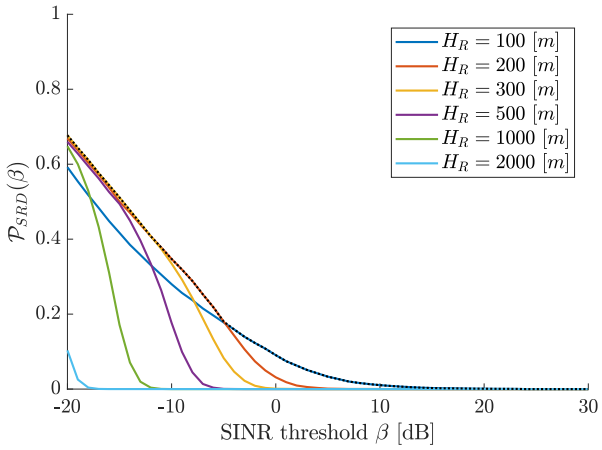

(c) Relay Link - $\lambda_R = 10^{-5}$ $[m^{-2}]$

Figure 6.4: CP of the relay link for different RNs' densities and altitudes (solid lines). The dotted curves represent the best CPs which can be achieved for each SINR threshold when the RNs' altitude is selected accordingly to the following values: $H_R = \{100, 200, ..., 4000\}$ $[m]$.

the first hop and the second hop:

$$\mathcal{P}_{SRD}(\beta) = \mathcal{P}_{SR}(\beta)\mathcal{P}_{RD}(\beta) \leq \min\left(\mathcal{P}_{SR}(\beta), \mathcal{P}_{RD}(\beta)\right). \tag{6.1}$$

It has been shown that a higher RNs' altitude enables to achieve a higher probability for the first and second hops' links to be in LoS, but this also impacts positively or negatively the powers of the aggregate interferences for each link. Moreover, when the RNs' altitude increases, the distances between the typical UE and its closest RNs tend all to be equal to the RNs' altitude, degrading the SINR of the first and second hop.

Besides, a larger RNs' density also enables to achieve a higher LoS probability for the first and second hop, at the price of an increased power of the aggregate interference.

Therefore, since both parameters have positive and negative impacts on each link, they should be optimised together in order to achieve the best relay link's CP at a given SINR threshold. For instance, at 0 [dB], the best CP is achieved at a low RNs' density (10^{-7} $[m^{-2}]$), for a RNs' altitude close to 1000 meters.

Relay Link and Direct Link

When direct links are not neglected, the performance of the relay link must be compared to the performance of the direct link to evaluate if some improvements are possible.

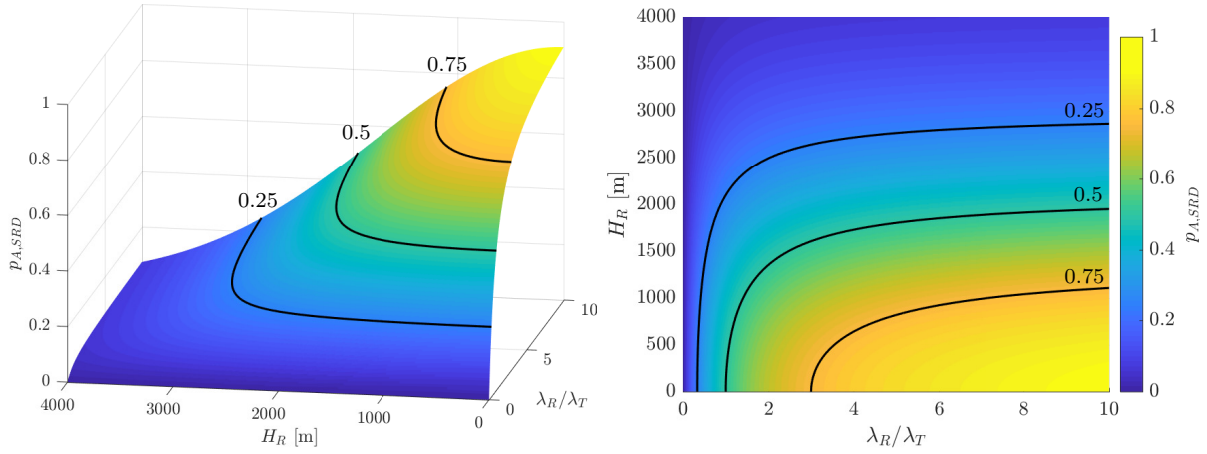

Figure 6.5: Probability of association with the relay link for different RNs' altitudes and densities.

Figure 6.5 shows the probability of association with the relay link for different RNs' altitudes and densities, with the nearest neighbour association rule. The relay link is often selected when the RNs' density increases, but when this density is large compared to the TBSs' density, the RNs' altitude has the largest impact. This can be shown mathematically through the asymptotic behaviour of the probability of association with the relay link: when the RNs' altitude is low, we have

$$\lim_{H_R \to 0} p_{A,SRD} = \frac{\lambda_R}{\lambda_R + \lambda_T}, \tag{6.2}$$

and when the RNs' density is large compared to the TBSs' density, we have

$$\lim_{\lambda_R/\lambda_T \to \infty} p_{A,SRD} = \exp\left(-\pi \lambda_T H_R^2\right). \tag{6.3}$$

Therefore, with this criterion of association, even if the RNs' density and altitude have been optimised for a given SINR threshold in order to obtain the best relay link's CP, the typical UE could select the direct link with a high probability, leading to a lower CP for the complete link. The comparison with the maximum average power association rule might be analysed in future studies.

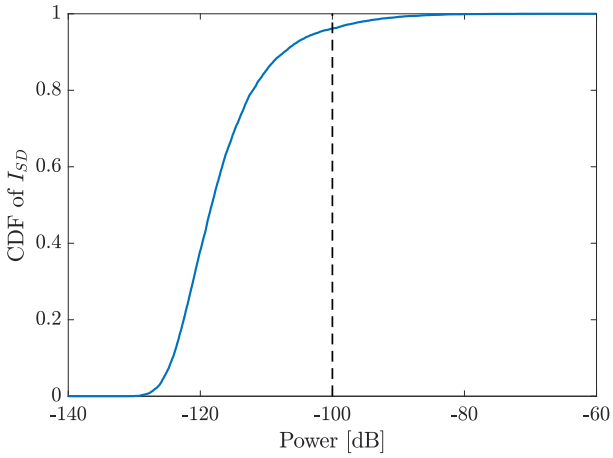

Figure 6.6: CDF of I_{SD} (solid lines), compared to the noise power (dashed lines).

Unlike the second hop's SINR, the SINR of the direct link is noise-limited: since the TBSs' density is low, all the TBSs are mostly in NLoS. This is illustrated by Figure 6.6, which shows the CDF of the aggregate interference of the direct link compared to the noise power.

Figure 6.7 shows the CP of the direct link and the complete link for different RNs' densities and altitudes, and the best CP which could be achieved for each SINR threshold for a finite set of RNs' altitudes. Regarding the G2G LoS probability model presented in Figure 3.3, for a TBSs' density of $5 \cdot 10^{-8}$ $[m^{-2}]$, since the distance between the typical UE and its closest TBS is Rayleigh distributed with mean $\mathbb{E}_{r_{SD}}[r_{SD}] = \sqrt{1/4\lambda_T} = 2236$ $[m]$, the link between these two nodes is nearly always in NLoS.

For this network configuration, when direct links are not completely neglected, with low RNs' densities and high altitudes, the relay link helps to improve the CP of the typical UE, even if the probability of selection of the relay link is low. Therefore, in that case, a low RNs' density to limit the interference from the RNs, and a high altitude to increase the LoS probability of the first and second hop enable to improve the CP of the typical UE. However, if these two parameters are not adjusted correctly, the selection of the relay link can worsen the CP of the typical UE compared to a scenario without UAV RNs.

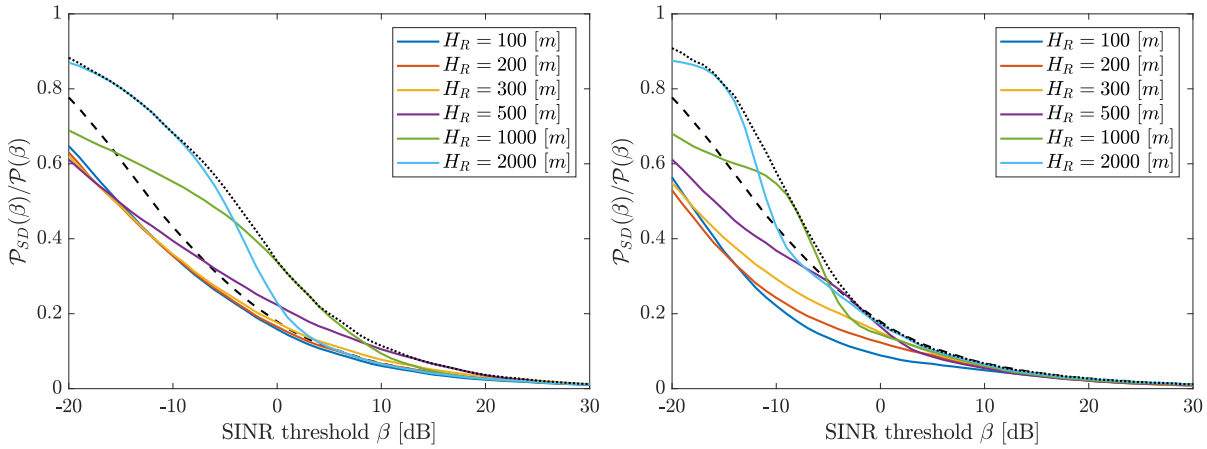

(a) Complete link - $\lambda_R = 10^{-7}$ $[m^{-2}]$

(b) Complete link - $\lambda_R = 10^{-6}$ $[m^{-2}]$

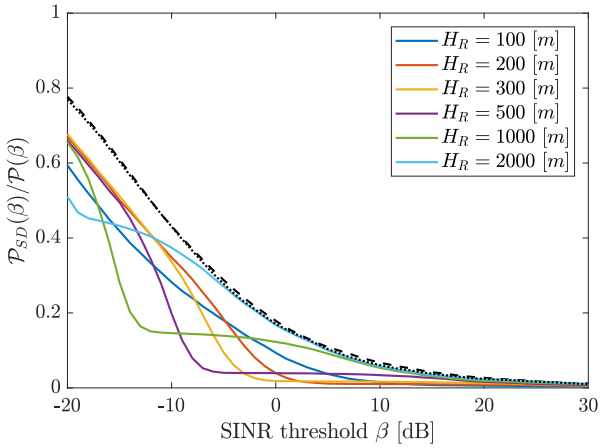

(c) Complete link - $\lambda_R = 10^{-5}$ $[m^{-2}]$

Figure 6.7: CP of the direct link (dashed lines) and the complete link (solid lines) for different RNs' densities and altitudes, with $\lambda_T = 5{\cdot}10^{-8}$ $[m^{-2}]$. The dotted curves represent the best CPs which can be achieved for each SINR threshold when the RNs' altitude is selected accordingly between the following values: $H_R = \{100, 200, ..., 4000\}$ $[m]$.

6.1.2 Average Spectral Efficiency

Relay Link Only

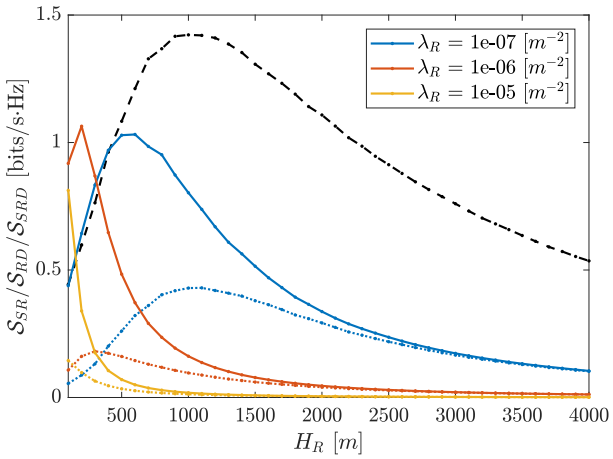

Figure 6.8: Average SE of the first hop (dashed line), second hop (solid lines), and relay link (dotted lines) for different RNs' densities and altitudes.

Figure 6.8 shows the average SE of the first hop, second hop and relay link for different RNs' densities and altitudes. The upper bound for the average SE of the relay link presented in Lemma 4.9 seems to be close to the exact average SE only when the RNs' altitude increases. In that configuration, it is nearly equal to the average SE of the second hop, which is the bottleneck of the relay link.

For the RNs' densities which are considered, except at very low altitudes (less than 400 meters), the lowest RNs' density (10^{-7} $[m^{-2}]$) enables to reach the best average SE of the relay link at RNs' altitudes close to one kilometer. The best values are reached at the same range of RNs' altitudes than for the average SE of the first hop, except for higher RNs' densities. Unfortunately, for that set of values, the upper bound does not help to approximate accurately the average SE of the relay link.

Relay Link and Direct Link

Figure 6.9 shows the average SE of the direct link and complete link for different RNs' densities and altitudes. For the considered network configuration, the average SE of the complete link can be improved compared to the average SE reached with the direct link when the RNs' density is low (10^{-7} $[m^{-2}]$), and the best performance is achieved for RNs' altitudes close to one kilometer. In other conditions, the introduction of the relay link can possibly worsen the achieved average SE.

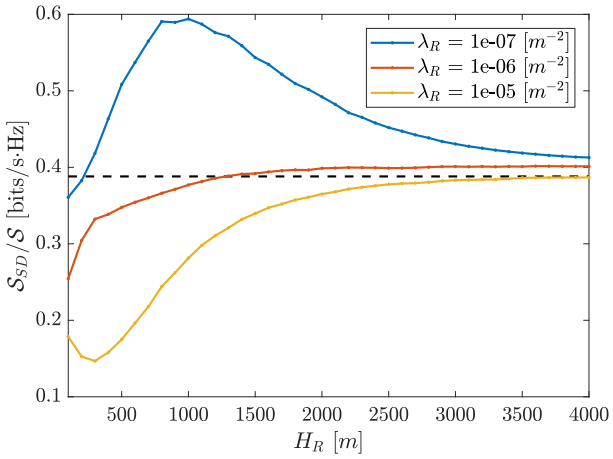

Figure 6.9: Average SE of the direct link (dashed line) and complete link (solid lines) for different RNs' densities and altitudes.

6.1.3 Average Exposure

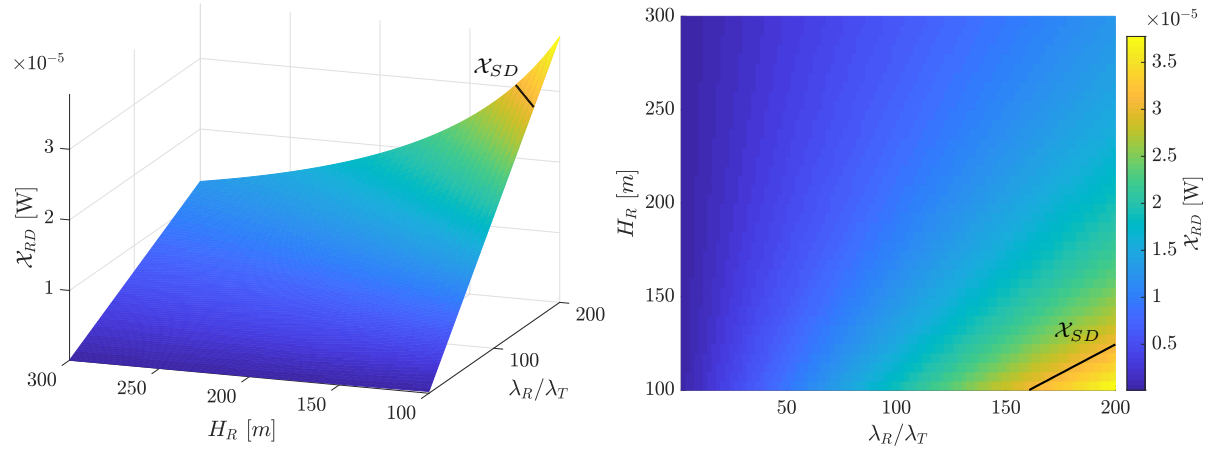

Figure 6.10: Average exposure at the typical UE for different RNs' densities and altitudes.

Figure 6.10 shows the average exposure at the typical UE from the UAV RNs and the TBSs for different RNs' densities and altitudes. It increases linearly with the RNs' density, while it decreases exponentially with the RNs' altitude.

The average exposure from the TBSs is mainly coming from the TBS which is the closest to the typical UE, while the contributions of the selected RN and all the other interfering RNs are equivalent for the average exposure from the UAV RNs. For the network parameters presented in Table 6.1, the average exposure from the UAV RNs is nearly always lower than the average exposure from the TBSs, except at high RNs' densities (about 10^{-5} [m^{-2}]) and low altitudes (about 100 meters).

6.2 Mobile UAVs

6.2.1 Coverage Probability

Relay Link Only

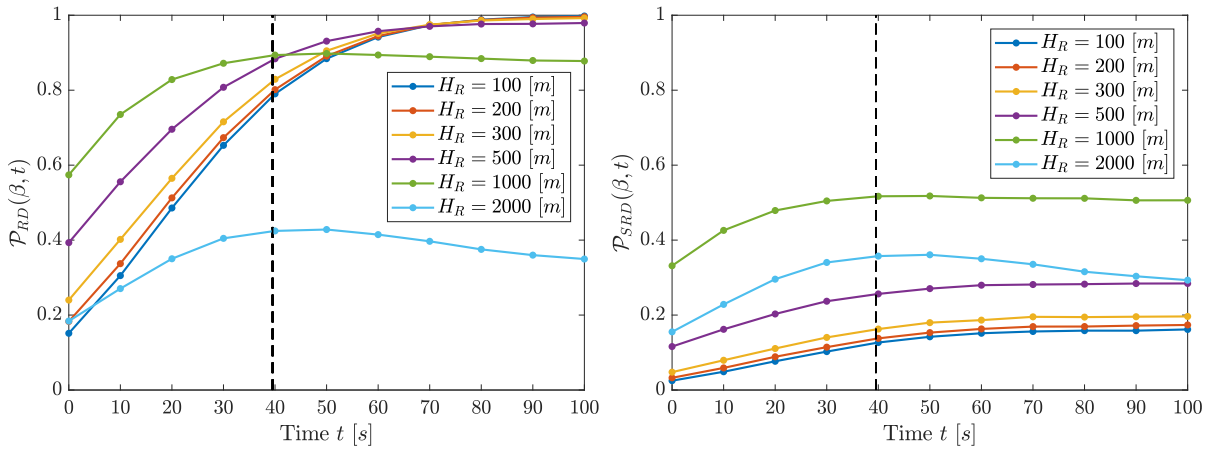

(a) Second Hop

(b) Relay Link

Figure 6.11: Evolution of the CP of the second hop and relay link (solid lines) with time for a SINR threshold of 0 [dB] and for different RNs' altitudes, with $\lambda_R = 10^{-7}$ $[m^{-2}]$. The dashed lines represent the expected travel time $\bar{T} = \mathbb{E}_{r_{RD}}[r_{RD}]/v$.

Figure 6.11 and 6.12 illustrate the evolution with time of the CP of the second hop and relay link for different RNs' altitudes. Thanks to its mobility, the selected RN is moving towards the typical UE. Therefore, the ground distance between the selected RN and the typical UE decreases to zero, and the probability for the link to be in LoS increases to one. This enables a large increase for the CP of the second hop. However, a smaller improvement is visible for the CP of the relay link since the mobility scheme does not have any impact on the CP of the first hop.

At high altitudes, the best CP is not achieved at stationarity ($t \to \infty$) but it is reached at a time close to the expected travel time, defined as $\bar{T} = \mathbb{E}_{r_{RD}}[r_{RD}]/v$. Indeed, after that the selected RN reaches the position of the typical UE and starts to hover above it, the interfering RNs' density close to the typical UE increases drastically, as shown by Figure 5.1, leading to a decrease of the SINR. It is visible in particular for high RNs' altitudes since the LoS probability and the power coming from the interferers RNs are higher. Therefore, at stationarity, the coverage improvement is less noticeable. It is also the case at higher densities (10^{-6} and 10^{-5} $[m^{-2}]$), even at low altitudes owing to the same reasons.

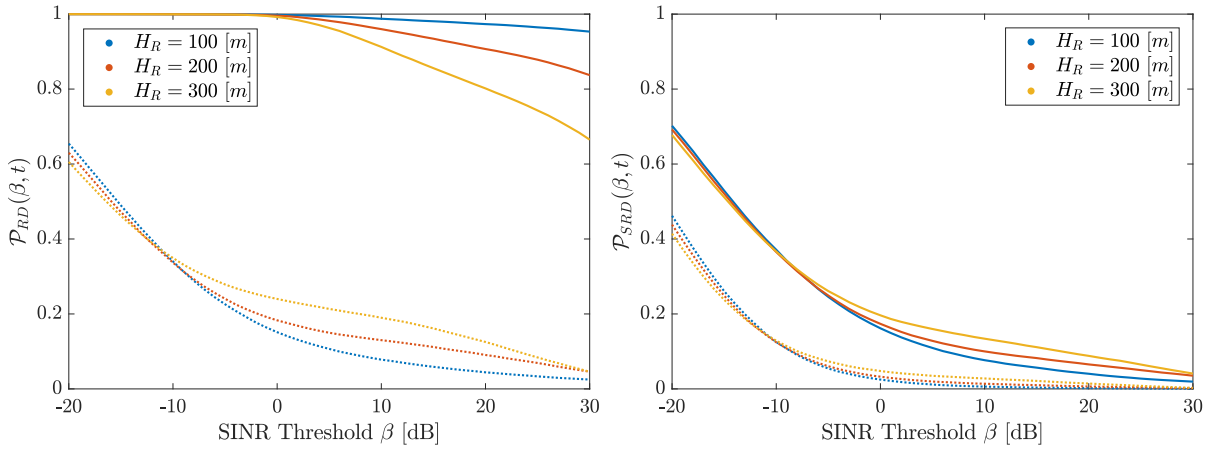

(a) Second Hop - $H_R = 100 - 300$ [m]

(b) Relay Link - $H_R = 100 - 300$ [m]

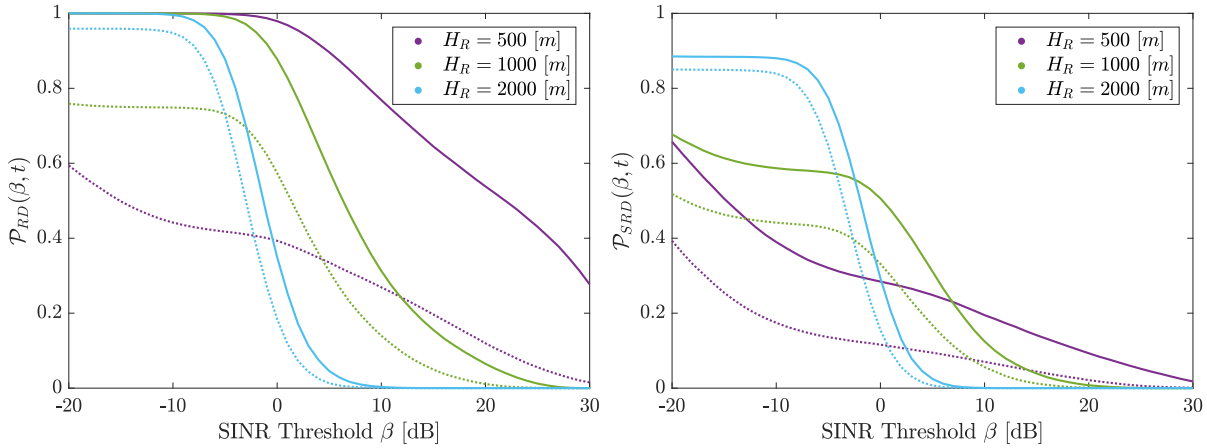

(c) Second Hop - $H_R = 500 - 2000$ [m]

(d) Relay Link - $H_R = 500 - 2000$ [m]

Figure 6.12: CP of the second hop and relay link at time $t = 0$ [s] (dotted lines) and time $t = 100$ [s] (solid lines), for different RNs' altitudes, with $\lambda_R = 10^{-7}$ [m^{-2}].

Relay Link and Direct Link

Figure 6.13 shows the probability of association with the relay link for different RNs' altitudes, densities, and time instants. In comparison with Figure 6.5, with the nearest neighbour association rule, since the selected RN moves toward the typical UE, the probability for the typical UE to select the relay link increases with time, especially at low RNs' density. Indeed, the probability for the selected RN to be initially close to the typical UE decreases with the RNs' density.

At stationarity, the probability of association with the relay link becomes independent with the RNs' density. Actually, whatever the initial distance between the typical UE and the selected RN, the selected RN is hovering above the typical UE, and the RNs' altitude becomes the only factor to influence the association for a fixed TBSs' density. Mathematically, it is expressed as

$$\lim_{t \to \infty} p_{A,SRD} = \exp\left(-\pi \lambda_T H_R^2\right). \tag{6.4}$$

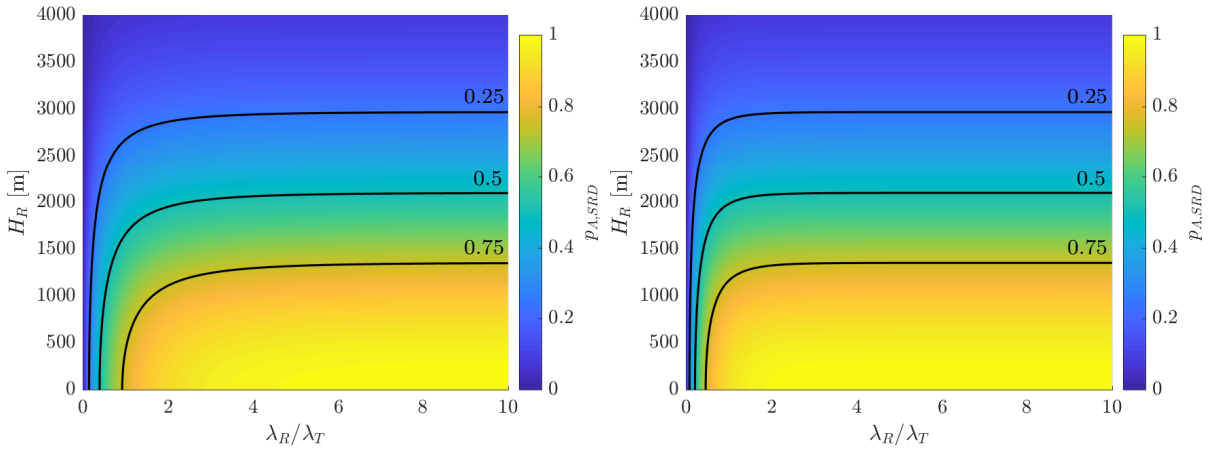

(a) $t = 30$ $[s]$ (b) $t = 60$ $[s]$

Figure 6.13: Probability of association with the relay link for different RNs' altitudes and densities at time $t = 30$ $[s]$ and $t = 60$ $[s]$, with $v = 40$ $[m/s]$.

Therefore, for a RNs' density of 10^{-7} $[m^{-2}]$, the typical UE will select mostly the relay link.

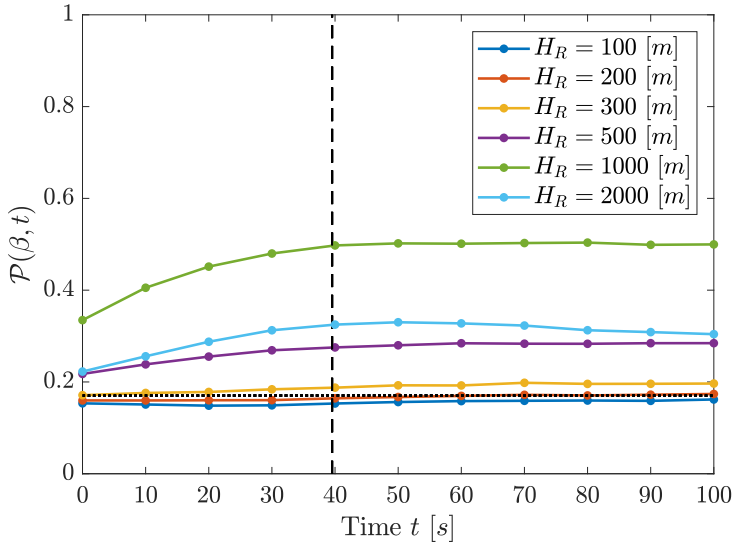

Figure 6.14: Evolution of the CP of the complete link with time (solid lines) compared to the CP of the direct link (dotted line) for a SINR threshold of 0 [dB] and for different RNs' altitudes, with $\lambda_R = 10^{-7}$ $[m^{-2}]$. The dashed line represents the expected travel time $\bar{T} = {}^{\mathbb{E}_{r_{RD}}[r_{RD}]}/_{v}$.

Figure 6.14 and 6.15 illustrate the evolution of the CP of the complete link compared to the CP of the direct link with time for different RNs' altitudes. For the considered density, the CP of the complete link is improved thanks to the introduction of the second mobility scheme. This effect is mostly visible for high SINR thresholds at low altitudes, and for low SINR thresholds at high altitudes. For instance, at 0 [dB], an enhancement is visible for RNs' altitudes higher than 200 meters.

At low altitudes, the CP of the first hop is a bottleneck which limits considerably the

achievable coverage. In contrary, at high altitudes, the interfering power is increased and it limits the possible enhancement of the coverage for high SINR thresholds.

At higher densities, even at low altitudes, the achievable improvements are limited as the interfering power is larger. Furthermore, since the probability of association with the relay link is increased, the CP of the complete link can be lowered!

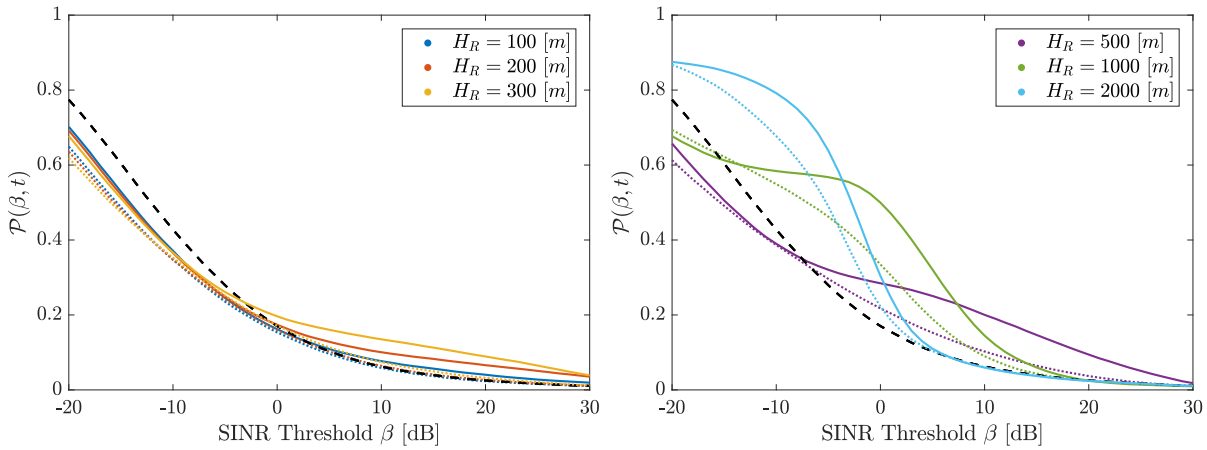

(a) Relay Link - $\lambda_R = 10^{-7}$ [m^{-2}]

(b) Relay Link - $\lambda_R = 10^{-5}$ [m^{-2}]

Figure 6.15: CP of the complete link at time $t = 0$ [s] (dotted lines) and time $t = 100$ [s] (solid line), for different RNs' altitudes, with $\lambda_R = 10^{-7}$ [m^{-2}]. The dashed lines represents the CP of the direct link.

6.2.2 Average Spectral Efficiency

Relay Link Only

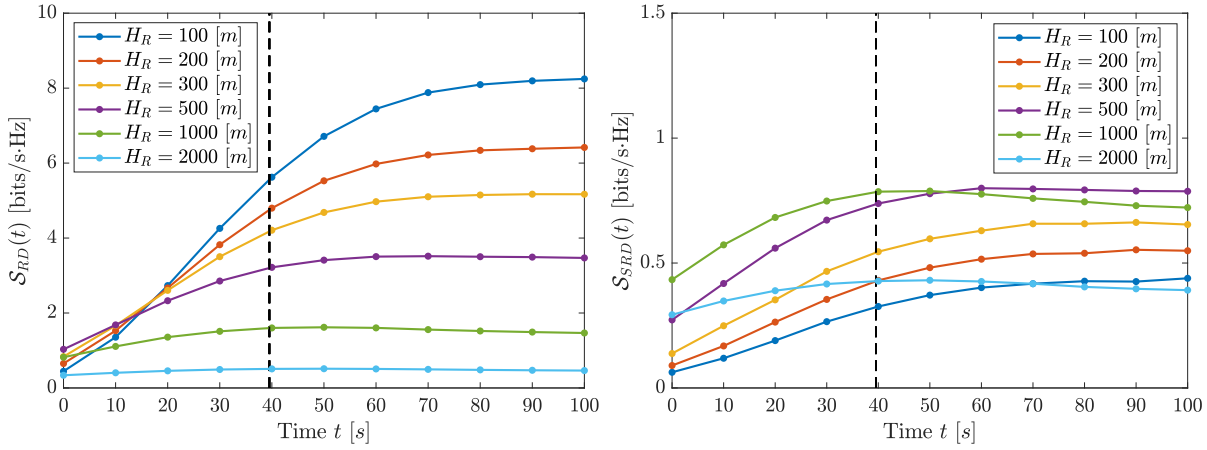

(a) Second Hop

(b) Relay Link

Figure 6.16: Evolution of the average SE of the second hop and relay link (solid lines) with time for different RNs' altitudes, with $\lambda_R = 10^{-7}$ [m^{-2}]. The dashed lines represent the expected travel time $\bar{T} = {}^{\mathbb{E}_{r_{RD}}[r_{RD}]}/_{v}$.

Figure 6.16 shows the evolution of the average SE of the first hop and relay link with time for different RNs' altitudes. For the second hop, as for the CP, the average SE is drastically improved thanks to the second mobility scheme, and especially at low altitudes. However, for the relay link, the improvement is limited by the performance of the first hop, therefore better results are obtained at higher altitudes. Although, as for the CP, at high altitudes, the best average SE is not reached at stationarity ($t \to \infty$), but close to the expected travel time $\bar{T} = {}^{\mathbb{E}_{r_{RD}}[r_{RD}]}/_{v}$.

Relay Link and Direct Link

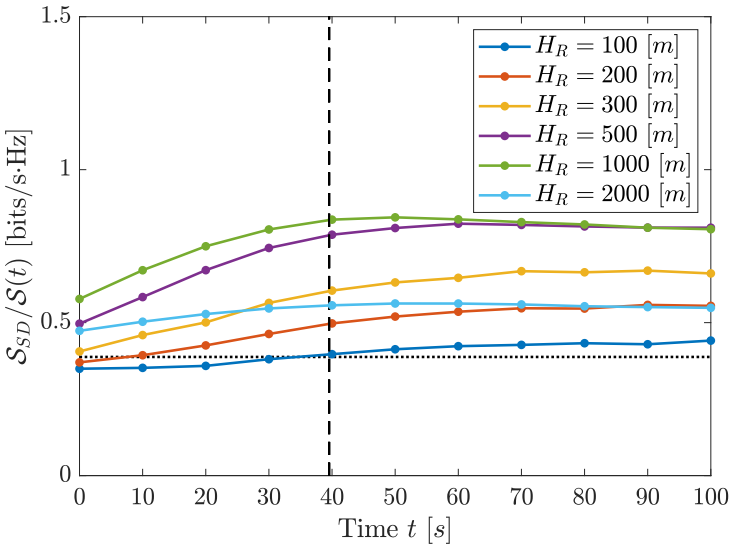

Figure 6.17: Second Hop

Figure 6.18: Evolution of the average SE of the complete link (solid lines) with time for different RNs' altitudes compared to the average SE of the direct link (dotted line), with $\lambda_R = 10^{-7}$ [m^{-2}]. The dashed line represents the expected travel time $\bar{T} = {}^{\mathbb{E}_{r_{RD}}[r_{RD}]}/_{v}$.

Figure 6.18 illustrates the evolution of the average SE of the complete link with time for different RNs' altitudes, compared to the average SE of the direct link. For a RNs' density of 10^{-7} [m^{-2}], the introduction of the second mobility scheme enables to hugely improve the average SE of the link, especially for RNs' altitudes close to the kilometer, since the second hop is the main bottleneck of the relay link.

6.2.3 Average Exposure

Figure 6.19 illustrates the evolution with time of the average exposure at the typical UE from the UAV RNs and TBSs for different RNs' densities and altitudes. The average exposure from the UAV RNs increases drastically with the time since the selected RN moves toward the typical UE and hovers above it. Additionally, the interfering RNs' density close to the typical UE also increases. However, the CP and average SE of the complete link can still be improved with a limited additional average exposure.

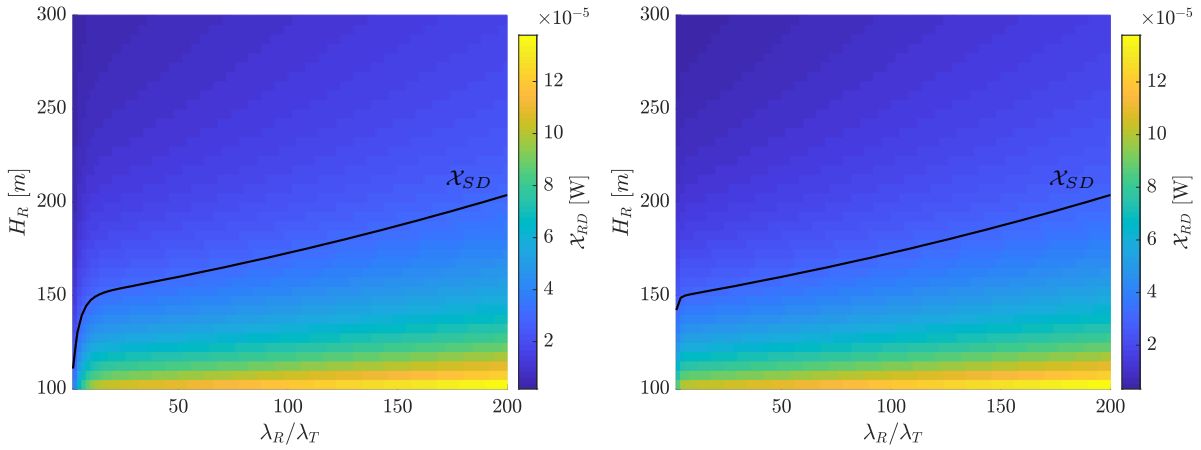

Figure 6.19: Average exposure at the typical UE for different RNs' densities and altitudes at time $t = \{30, 60\}$ $[s]$, with $v = 40$ $[m/s]$ and $\lambda_T = 5 \cdot 10^{-8}$ $[m^{-2}]$.

6.3 Summary

In summary, for a given network configuration and for the considered RNs' densities and altitudes, relay links can provide a good alternative to direct links while correct services cannot be provided to the UEs owing to severe obstruction. Additionally, when direct links are not neglected, with a joint optimisation of the RNs' density and altitude, the performance at the UEs can be enhanced thanks to relay links, with a limited additional average exposure.

The introduction of the second mobility scheme enables to further improve the performance at the typical UE when direct links are neglected or not, in particular for low RNs' densities. It enables to achieve a higher probability for the link to be in LoS (which tends to one when the selected RN hovers above the typical UE) and to reduce the attenuation of the second hop's link without affecting the performance of the first hop. With a joint optimisation of the RNs' density and altitude, the performance can be enhanced, still with a limited additional average exposure. Otherwise, the performance of the complete link can be worsened.

6.4 Stochastic Geometry vs Monte-Carlo Simulations

All the results detailed in this section are obtained thanks to a script written from scratch and executed in MATLAB R2017a, with basic knowledge in numerical integration. Therefore, the computation times which can be observed will vary from one script and one computer to another, but these values are still useful for a rough comparison of SG and MC simulations.

First, considering MC simulations, the computation time mainly depends on the RNs' density, the radius of the area in which the nodes are generated, and the number of iterations. It can also depend on the other parameters when the performance for a large set of values is evaluated, but this impact is neglected in this study. For the parameters

specified in Table 6.1, the MC simulations are executed approximatively in 60 seconds for a RNs' density of 10^{-7} $[m^{-2}]$, in 300 seconds for a RNs' density of 10^{-6} $[m^{-2}]$, and in 3000 seconds for a RNs' density of 10^{-5} $[m^{-2}]$.

However, the introduction of the mobility has a huge impact on the computation time: all the RNs of each network realisation must be displaced in a random direction at each time instant, and the number of iterations needs to be increased to keep the same accuracy. For instance, with 50000 iterations and one time instant, the MC simulations are executed approximatively in 300 seconds for a RNs' density of 10^{-7} $[m^{-2}]$ and in 1500 seconds for a RNs' density of 10^{-6} $[m^{-2}]$.

At the end of these simulations, an estimation of all the network statistics (probability of association, CDF of the power from the selected RN, CDF of the interfering power, ...) is available, and the performance metrics can be extracted from these statistics.

Contrariwise, with SG expressions, the computation time is nearly not affected by the network's parameters (except when the parameters are very low, where the numerical integrations can take a longer time depending on the integration rule). Moreover, it is not really impacted by the second mobility scheme. However, the noise power has a non negligible influence, because the functions to integrate in Proposition 4.3 and 5.3 oscillate when it is non zero. For the CP, the computation of one value (one given SINR threshold for the CP) for one specific link takes approximatively 15 seconds. The computation time is similar for the average SE. Finally, it takes less than 1 second for the average exposure.

Therefore, for the CP and the average SE, at low RNs' densities, MC simulations enable to obtain a complete description of the network faster than SG expressions with fixed UAVs. When mobility is introduced, the computation times of the two methods are more comparable, and SG expressions are faster to compute at high RNs' densities. Unfortunately, the shadowing must be neglected with SG owing to the high mathematical complexity of the analytic expressions.

However, the situation is different for the average exposure: SG clearly outperforms MC simulations even with shadowing!

Chapter 7

Conclusion

In this thesis, a general framework for the integration of UAV-based wireless communication networks has been developed using SG. For this purpose, models and metrics generally adopted in previous studies involving UAVs have been presented.

First, a simple scenario where the UAV RNs hover at a fixed position has been considered. For this scenario, analytical expressions have been developed to evaluate the CP and average exposure at a typical UE, with direct links either neglected or not. Additional expressions to estimate the average SE of each link and some clues to enhance the considered scenario have also been proposed.

Next, the modification of the performance when the UAV RNs are allowed to move following two mobility schemes has been analysed. The analytical expressions developed with fixed UAV RNs have been generalised to integrate these mobility schemes.

Finally, using MC simulations, the developed framework has been validated. Additionally, the developed mathematical expressions have been applied in order to evaluate the performance of a network with a given configuration. It has been shown that a joint design of the RNs' density and altitude improves the performance, and further enhancement can be achieved when mobility is introduced. Moreover, the mathematical complexity (computation time) of MC simulations has been compared to the numerical evaluation of SG expressions. Owing to their high mathematical complexity, MC simulations are still necessary when the shadowing is not neglected. Otherwise, SG enables to obtain a fast estimation of the average performance for a given network configuration.

In future studies, additional unsolved research issues need to be considered. First, for the framework which has been presented in this thesis:

- All the numerical results described in Chapter 6 neglect the **shadowing**, which introduce a lot of additional complexity in the SG expressions. Therefore, an elegant way to reduce the complexity without neglecting the shadowing needs to be developed. For this purpose, some clues have been proposed in Section 4.3. Additionally, its impact on the presented results should be quantified;
- The integration of the **maximum biased average power association rule** in the framework needs to be developed. For this purpose, Section 4.3 proposes SG expressions for the CP of the second hop with maximum biased average power association, but this expression should still be validated with special effort to reduce

the complexity. Besides, even if the nearest neighbour association rule could be considered as a worst case analysis, the precise impact of this association rule on the network performance has to be evaluated;

- A tractable **expression for the average SE** of the relay link should be derived. Furthermore, the development of a lower bound and the refinement of the presented upper bound are also open issues;

- Section 4.3 and 5.3 proposes SG expressions when the TBS which is the closest to the typical UE serves both the typical UE and the selected RN. However, a validation of this **correlated model** with reduction of its complexity is necessary. Additionally, the impact of this new selection rule on the presented results needs to be evaluated.

Next, the adaptation of this framework in order to optimise the network parameters is still a shelved interesting question. For instance, a worthwhile issue is the optimisation of the network parameters in order to achieve the best CP and/or to maximise the average SE of the typical UE given a maximum average exposure constraint.

Publications

The following paper has been written about UAV-based relay networks with fixed position:

François De Saint Moulin, Charles Wiame, Claude Oestges, Luc Vandendorpe, "Stochastic Geometry Modelling for UAV Relay Networks", Technical Document, *12th MC and Technical Meeting of the COST action CA15104 (IRACON)*, January 2020.

An additional paper will be submitted about the whole content of this master's thesis.

Bibliography

[1] A. Aragón-Zavala, J. L. Cuevas-Ruíz, and J. A. Delgado-Penín, "High-Altitude Platforms for Wireless Communications," pp. 1–241, July 2008.

[2] Y. Zeng, R. Zhang, and T. J. Lim, "Wireless communications with unmanned aerial vehicles: Opportunities and challenges," *IEEE Communications Magazine*, vol. 54, no. 5, pp. 36–42, 2016.

[3] M. Mozaffari, W. Saad, M. Bennis, Y. H. Nam, and M. Debbah, "A Tutorial on UAVs for Wireless Networks: Applications, Challenges, and Open Problems," *IEEE Communications Surveys and Tutorials*, vol. 21, no. 3, pp. 2334–2360, 2019.

[4] M. Di Renzo, "Intro to Stochastic Geometry & Point Processes," September 2016. http://www.eng.ox.ac.uk/sen/files/course2016/lec5.pdf.

[5] F. Baccelli and B. Blaszczyszyn, *Stochastic Geometry and Wireless Networks: Volume I - Theory*, vol. 1. 2009.

[6] C. Wiame, C. Oestges, and L. Vandendorpe, "Stochastic geometry-based analysis of wireless communication networks," Master's thesis, Université Catholique de Louvain, 2017.

[7] A. M. Hayajneh, S. A. R. Zaidi, D. C. McLernon, M. Di Renzo, and M. Ghogho, "Performance Analysis of UAV Enabled Disaster Recovery Networks: A Stochastic Geometric Framework Based on Cluster Processes," *IEEE Access*, vol. 6, pp. 26215–26230, 2018.

[8] M. Haenggi, "Mean interference in hard-core wireless networks," *IEEE Communications Letters*, vol. 15, no. 8, pp. 792–794, 2011.

[9] J. G. Andrews, A. K. Gupta, and H. S. Dhillon, "A Primer on Cellular Network Analysis Using Stochastic Geometry," pp. 1–46, 2016.

[10] R. Arshad, L. Lampe, H. Elsawy, and M. J. Hossain, "Integrating UAVs into Existing Wireless Networks: A Stochastic Geometry Approach," *2018 IEEE Globecom Workshops, GC Wkshps 2018 - Proceedings*, 2019.

[11] M. G. Khoshkholgh, K. Navaie, H. Yanikomeroglu, V. C. Leung, and K. G. Shin, "Coverage performance of aerial-terrestrial hetnets," *IEEE Vehicular Technology Conference*, pp. 1–5, April 2019.

[12] M. Rihan, M. M. Selim, C. Xu, and L. Huang, "D2D communication underlaying UAV on multiple bands in disaster area: Stochastic geometry analysis," *IEEE Access*, vol. 7, pp. 156646–156658, 2019.

[13] M. Mozaffari, W. Saad, M. Bennis, and M. Debbah, "Unmanned Aerial Vehicle with Underlaid Device-to-Device Communications: Performance and Tradeoffs," *IEEE Transactions on Wireless Communications*, vol. 15, no. 6, pp. 3949–3963, 2016.

[14] O. M. Bushnaq, A. Celik, H. Elsawy, M. S. Alouini, and T. Y. Al-Naffouri, "Aeronautical Data Aggregation and Field Estimation in IoT Networks: Hovering and Traveling Time Dilemma of UAVs," *IEEE Transactions on Wireless Communications*, vol. 18, no. 10, pp. 4620–4635, 2019.

[15] X. Zhou, S. Durrani, J. Guo, and H. Yanikomeroglu, "Underlay drone cell for temporary events: Impact of drone height and aerial channel environments," *IEEE Internet of Things Journal*, vol. 6, no. 2, pp. 1704–1718, 2019.

[16] S. Biswas, S. Vuppala, J. Xue, and T. Ratnarajah, "On the Performance of Relay Aided Millimeter Wave Networks," *IEEE Journal on Selected Topics in Signal Processing*, vol. 10, no. 3, pp. 576–588, 2016.

[17] V. V. Chetlur and H. S. Dhillon, "Downlink Coverage Analysis for a Finite 3-D Wireless Network of Unmanned Aerial Vehicles," *IEEE Transactions on Communications*, vol. 65, no. 10, pp. 4543–4558, 2017.

[18] T. Hou, Y. Liu, Z. Song, X. Sun, and Y. Chen, "Multiple Antenna Aided NOMA in UAV Networks: A Stochastic Geometry Approach," *IEEE Transactions on Communications*, vol. 67, no. 2, pp. 1031–1044, 2019.

[19] K. Belbase, Z. Zhang, H. Jiang, and C. Tellambura, "Coverage Analysis of Millimeter Wave Decode-and-Forward Networks with Best Relay Selection," *IEEE Access*, vol. 6, pp. 22670–22683, 2018.

[20] R. Ma, W. Yang, Y. Zhang, J. Liu, and H. Shi, "Secure mmWave Communication Using UAV-Enabled Relay and Cooperative Jammer," *IEEE Access*, vol. 7, pp. 119729–119741, 2019.

[21] W. Khawaja, I. Guvenc, D. W. Matolak, U.-C. Fiebig, and N. Schneckenburger, "A Survey of Air-to-Ground Propagation Channel Modeling for Unmanned Aerial Vehicles," *IEEE Communications Surveys & Tutorials*, vol. 21, no. 3, pp. 2361–2391, 2019.

[22] S. Sun, T. A. Thomas, T. S. Rappaport, H. Nguyen, I. Z. Kovacs, and I. Rodriguez, "Path loss, shadow fading, and line-of-sight probability models for 5G urban macrocellular scenarios," *2015 IEEE Globecom Workshops, GC Wkshps 2015 - Proceedings*, no. Ci, 2015.

[23] D. Ben Cheikh Battikh, *Outage probability formulas for cellular networks: contributions for MIMO, CoMP and time reversal features.* PhD thesis, Télécom ParisTech, 2012.

[24] "Comparing Rician and Nakagami Fading," 1999. http://www.wirelesscommunication.nl/reference/chaptr03/ricenaka/ricenaka.htm.

[25] X. Wang, H. Zhang, K. J. Kim, Y. Tian, and A. Nallanathan, "Performance Analysis of Cooperative Aerial Base Station-Assisted Networks with Non-Orthogonal Multiple Access," *IEEE Transactions on Wireless Communications*, vol. PP, no. c, pp. 1–1, 2019.

[26] 3GPP TR 36.873, "Study on 3D channel model for LTE (release 12)," March 2015. V12.1.0.

[27] M. K. Samimi, T. S. Rappaport, and G. R. Maccartney, "Probabilistic Omnidirectional Path Loss Models for Millimeter-Wave Outdoor Communications," *IEEE Wireless Communications Letters*, vol. 4, no. 4, pp. 357–360, 2015.

[28] I. Rodriguez, H. C. Nguyen, N. T. Jorgensen, T. B. Sorensen, J. Elling, M. B. Gentsch, and P. Mogensen, "Path loss validation for urban micro cell scenarios at 3.5 GHz compared to 1.9 GHz," *GLOBECOM - IEEE Global Telecommunications Conference*, pp. 3942–3947, 2013.

[29] A. Al-Hourani, S. Kandeepan, and S. Lardner, "Optimal LAP altitude for maximum coverage," *IEEE Wireless Communications Letters*, vol. 3, no. 6, pp. 569–572, 2014.

[30] B. Galkin, J. Kibilda, and L. A. DaSilva, "A Stochastic Model for UAV Networks Positioned Above Demand Hotspots in Urban Environments," *IEEE Transactions on Vehicular Technology*, vol. 68, no. 7, pp. 6985–6996, 2019.

[31] E. Hossain, M. Rasti, H. Tabassum, and A. Abdelnasser, "Evolution toward 5G multi-tier cellular wireless networks: An interference management perspective," *IEEE Wireless Communications*, vol. 21, no. 3, pp. 118–127, 2014.

[32] W. Lu and M. Di Renzo, "Stochastic Geometry Modeling and System-Level Analysis and Optimization of Relay-Aided Downlink Cellular Networks," *IEEE Transactions on Communications*, vol. 63, no. 11, pp. 4063–4085, 2015.

[33] J. N. Laneman, D. N. Tse, and G. W. Wornell, "Cooperative diversity in wireless networks: Efficient protocols and outage behavior," *IEEE Transactions on Information Theory*, vol. 50, no. 12, pp. 3062–3080, 2004.

[34] Z. Lin, X. Peng, F. Chin, and W. Feng, "Outage performance of relaying with directional antennas in the presence of co-channel interferences at relays," *IEEE Wireless Communications Letters*, vol. 1, no. 4, pp. 288–291, 2012.

[35] M. R. Souryal and B. R. Vojcic, "Performance of amplify-and-forward and decode-and-forward relaying in rayleigh fading with turbo codes," *ICASSP, IEEE International Conference on Acoustics, Speech and Signal Processing - Proceedings*, vol. 4, pp. 681–684, 2006.

[36] M. O. Hasna and M. S. Alouini, "Harmonic Mean and End-to-End Performance of Transmission Systems With Relays," *IEEE Transactions on Communications*, vol. 52, no. 1, pp. 130–135, 2004.

[37] A. Behnad, A. M. Rabiei, and N. C. Beaulieu, "Performance analysis of opportunistic relaying in a poisson field of amplify-and-forward relays," *IEEE Transactions on Communications*, vol. 61, no. 1, pp. 97–107, 2013.

[38] S. Atapattu, Y. Jing, H. Jiang, and C. Tellambura, "Relay selection and performance analysis in multiple-user networks," *IEEE Journal on Selected Areas in Communications*, vol. 31, no. 8, pp. 1517–1529, 2013.

[39] M. Di Renzo, A. Zappone, T. T. Lam, and M. Debbah, "System-Level Modeling and Optimization of the Energy Efficiency in Cellular Networks-A Stochastic Geometry Framework," *IEEE Transactions on Wireless Communications*, vol. 17, no. 4, pp. 2539–2556, 2018.

[40] T. Q. Quek, W. C. Cheung, and M. Kountouris, "Energy efficiency analysis of two-tier heterogeneous networks," *17th European Wireless Conference 2011, EW 2011*, vol. 1, no. 1, pp. 712–716, 2011.

[41] W. C. Cheung, T. Q. Quek, and M. Kountouris, "Throughput optimization, spectrum allocation, and access control in two-tier femtocell networks," *IEEE Journal on Selected Areas in Communications*, vol. 30, no. 3, pp. 561–574, 2012.

[42] Z. Zhang, Y. Li, K. Huang, S. Zhou, and J. Wang, "Energy efficiency analysis of cellular networks with cooperative relays via stochastic geometry," *China Communications*, vol. 12, no. 9, pp. 112–121, 2015.

[43] S. Enayati, H. Saeedi, H. Pishro-Nik, and H. Yanikomeroglu, "Moving Aerial Base Station Networks: A Stochastic Geometry Analysis and Design Perspective," *IEEE Transactions on Wireless Communications*, vol. 18, no. 6, pp. 2977–2988, 2019.

[44] A. M. Hayajneh, S. A. R. Zaidi, D. C. McLernon, and M. Ghogho, "Drone Empowered Small Cellular Disaster Recovery Networks for Resilient Smart Cities," *2016 IEEE International Conference on Sensing, Communication and Networking, SECON Workshops 2016*, 2016.

[45] C. S. Choi, F. Baccelli, and G. D. Veciana, "Modeling and analysis of data harvesting architecture based on unmanned aerial vehicles," *IEEE Transactions on Wireless Communications*, vol. 19, no. 3, pp. 1825–1838, 2020.

[46] S. Enayati, H. Saeedi, H. Pishro-Nik, and H. Yanikomeroglu, "Moving Aerial Base Station Networks: A Stochastic Geometry Analysis and Design Perspective," *IEEE Transactions on Wireless Communications*, vol. 18, no. 6, pp. 2977–2988, 2019.

[47] P. K. Sharma and D. I. Kim, "Random 3D Mobile UAV Networks: Mobility Modeling and Coverage Probability," *IEEE Transactions on Wireless Communications*, vol. 18, no. 5, pp. 2527–2538, 2019.

[48] M. Banagar and H. S. Dhillon, "3GPP-inspired Stochastic Geometry-based Mobility Model for a Drone Cellular Network," no. i, pp. 1–6, 2019.

[49] B. Blaszczyszyn, M. K. Karray, and H. P. Keeler, "Using Poisson processes to model lattice cellular networks," *Proceedings - IEEE INFOCOM*, pp. 773–781, 2013.

[50] B. Blaszczyszyn and H. P. Keeler, "Equivalence and comparison of heterogeneous cellular networks," *IEEE International Symposium on Personal, Indoor and Mobile Radio Communications, PIMRC*, pp. 153–157, 2013.

[51] H. P. Keeler, B. Blaszczyszyn, and M. K. Karray, "SINR-based k-coverage probability in cellular networks with arbitrary shadowing," *IEEE International Symposium on Information Theory - Proceedings*, pp. 1167–1171, 2013.

[52] Y. J. Chun, S. L. Cotton, H. S. Dhillon, F. J. Lopez-Martinez, J. F. Paris, and S. K. Yoo, "A comprehensive analysis of 5G heterogeneous cellular systems operating over κ-μ shadowed fading channels," *IEEE Transactions on Wireless Communications*, vol. 16, no. 11, pp. 6995–7010, 2017.

[53] M. D. Yacoub, "The κ-μ distribution and the η-μ distribution," *IEEE Antennas and Propagation Magazine*, vol. 49, no. 1, pp. 68–81, 2007.

[54] C. Galiotto, N. K. Pratas, N. Marchetti, and L. Doyle, "A stochastic geometry framework for LOS/NLOS propagation in dense small cell networks," *IEEE International Conference on Communications*, vol. 2015-Septe, pp. 2851–2856, 2015.

[55] K. A. Hamdi, "A useful lemma for capacity analysis of fading interference channels," *IEEE Transactions on Communications*, vol. 58, no. 2, pp. 411–416, 2010.

[56] M. Di Renzo, "System-Level Analysis of Cellular Networks," September 2016. http://www.eng.ox.ac.uk/sen/files/course2016/lec6.pdf.

Appendix A

Proofs

Lemmas

Proof of Lemma 4.1

Using the void probability of a PPP, the PDF of the distances between the typical UE and its closest TBS and the PDF of the distances between the typical UE and its closest UAV RN are respectively given by

$$f_{r_{SD}}(r) = -\frac{\mathrm{d}}{\mathrm{d}r}\mathbb{P}_{r_{SD}}\left(r_{SD} > r\right) = -\frac{\mathrm{d}}{\mathrm{d}r}V_{\mathbf{\Phi}_T}(\mathcal{B}\left(0,r\right)) = 2\pi\lambda_T\, r\, \exp\left(-\pi\lambda_T r^2\right), \tag{A.1}$$

$$f_{r_{RD}}(r) = -\frac{\mathrm{d}}{\mathrm{d}r}\mathbb{P}_{r_{RD}}\left(r_{RD} > r\right) = -\frac{\mathrm{d}}{\mathrm{d}r}V_{\mathbf{\Phi}_R}(\mathcal{B}\left(0,r\right)) = 2\pi\lambda_R\, r\, \exp\left(-\pi\lambda_R r^2\right). \tag{A.2}$$

Thanks to the stationarity property of an HPPP, the PDF of the distance between the selected RN and its closest TBS is equal to the PDF of the distance between the typical UE and its closest TBS.

■

Proof of Lemma 4.2

The proof focus only on the second hop, and the developments are identical for the first hop.

Knowing that

$$\theta_{RD} = \arctan\left(\frac{H_R}{r_{RD}}\right) \Leftrightarrow r_{RD} = \frac{H_R}{\tan\theta_{RD}}, \tag{A.3}$$

we have

$$f_{\theta_{RD}}(\theta_{RD}) = f_{r_{RD}}\left(r_{RD}(\theta_{RD})\right)\left|\frac{\mathrm{d}r_{RD}}{\mathrm{d}\theta_{RD}}\right| = 2\pi\lambda_R H_R^2\,\frac{\cos\theta_{RD}}{\sin^3\theta_{RD}}\exp\left(-\frac{\pi\lambda_R H_R^2}{\tan^2\theta_{RD}}\right). \tag{A.4}$$

■

Proof of Lemma 4.3

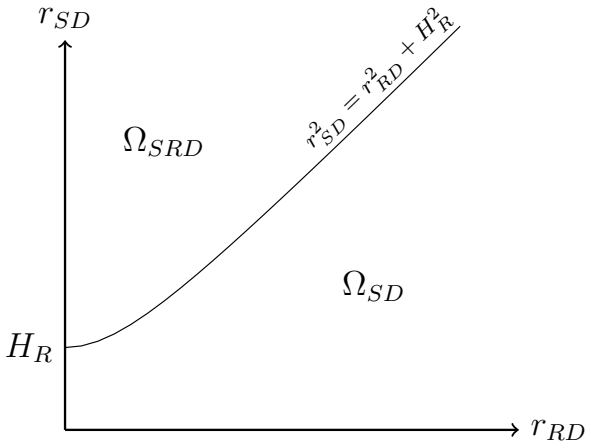

Figure A.1: Regions of association with nearest neighbour association rule. The typical UE selects the direct or the relay link if the couple (r_{SD}, r_{RD}) is respectively in Ω_{SD} or Ω_{SRD}.

Figure A.1 illustrates the regions for which the typical UE selects the direct or the relay link denoted respectively by Ω_{SD} and Ω_{SRD}.

Based on Equation (4.15), (4.17), since r_{SD} and r_{RD} are two independent RVs, the probability that typical UE selects the direct link can be developed as

$$\begin{aligned} p_{A,SD} &= \mathbb{P}_{r_{SD},r_{RD}}\left(r_{SD} \leq \sqrt{r_{RD}^2 + H_R^2}\right) \\ &= \int_{\Omega_{SD}} f_{r_{SD},r_{RD}}(r_{SD}, r_{RD}) \mathrm{d}r_{SD}\mathrm{d}r_{RD} \\ &= \int_0^{\infty} f_{r_{RD}}(r_{RD}) \int_0^{\sqrt{r_{RD}^2+H_R^2}} f_{r_{SD}}(r_{SD}) \mathrm{d}r_{SD}\mathrm{d}r_{RD} \\ &= 2\pi\lambda_R \int_0^{\infty} r_{RD} \exp\left(-\pi\lambda_R r_{RD}^2\right)\left(1 - \exp\left(-\pi\lambda_T(r_{RD}^2 + H_R^2)\right)\right) \mathrm{d}r_{RD} \\ &= 1 - \frac{\lambda_R}{\lambda_R + \lambda_T} \exp\left(-\pi\lambda_T H_R^2\right). \end{aligned} \tag{A.5}$$

Moreover, the probability that the typical UE selects the relay link is given by

$$p_{A,SRD} = 1 - p_{A,SRD} = \frac{\lambda_R}{\lambda_R + \lambda_T} \exp\left(-\pi\lambda_T H_R^2\right). \tag{A.6}$$

■

Proof of Lemma 4.4

Conditioned on r_{SD}, r_{SR} and r_{RD}, the direct link is in LoS with probability $p_{GL}(r_{SD})$, and each hop of the relay link is in LoS respectively with probability $p_{AL}(r_{SR})$ and $p_{AL}(r_{RD})$. Therefore, the proof is completed thanks to the law of total probability.

■

Proof of Lemma 4.5

Knowing that the PDF of the small-scale fading channel power gain is given by Equation (3.12), its LT is given by

$$\begin{aligned}\mathcal{L}_{|h|^2}(s) &= \int_0^\infty \frac{m^m}{\Gamma(m)} x^{m-1} \exp(-mx) \exp(-sx)\, \mathrm{d}x \\ &= \int_0^\infty \frac{m^m}{\Gamma(m)} \frac{u^{m-1}}{(m+s)^{m-1}} \exp(-u) \frac{1}{m+s} \mathrm{d}u \\ &= \left(\frac{m}{m+s}\right)^m. \end{aligned} \tag{A.7}$$

■

Proof of Lemma 4.6

Let us denote by ν^2 the power of the dominant path and $2\sigma^2$ the power of the scattered paths. The channel power gain can be expressed in cartesian coordinates as $|h|^2 = X^2 + Y^2$, where X and Y are two independent RVs which are normally distributed. By the properties of the normal distribution, ${}^{X^2}/_{\sigma^2}$ and ${}^{Y^2}/_{\sigma^2}$ follow a chi-square distribution with one degree of freedom, and therefore

$$X \sim \mathcal{N}(\nu\cos\theta, \sigma^2) \Rightarrow \mathcal{L}_{X^2}(s) = \exp\left(-\frac{\nu^2\cos^2\theta}{1+2\sigma^2 s} s\right)(1+2\sigma^2 s)^{-\frac{1}{2}} \tag{A.8}$$

$$Y \sim \mathcal{N}(\nu\sin\theta, \sigma^2) \Rightarrow \mathcal{L}_{Y^2}(s) = \exp\left(-\frac{\nu^2\sin^2\theta}{1+2\sigma^2 s} s\right)(1+2\sigma^2 s)^{-\frac{1}{2}}. \tag{A.9}$$

Finally, the proof is complete with $\mathcal{L}_{|h|^2}(s) = \mathcal{L}_{X^2}(s)\mathcal{L}_{Y^2}(s)$, knowing that the power is normalised ($\Omega = 1$) and using Equation (3.9).

■

Proof of Lemma 4.7

Since the link between each TBS in $\mathbf{\Phi}_T$ and the typical UE is in LoS or NLoS independently (there isn't any spatial correlation involved in the model), the PPs composed only of TBSs in LoS or NLoS denoted $\mathbf{\Phi}_{T,L}$ and $\mathbf{\Phi}_{T,N}$ are obtained by applying an independent thinning of $\mathbf{\Phi}_T$ with probabilities $p_{GL}(r)$ and $p_{GN}(r) = 1 - p_{GL}(r)$, for two nodes at a ground distance r. Therefore, they are distributed as two independent IHPPPs with densities $\lambda_{Tn}(r) = p_{Gn}(r)\lambda_T$. The same applies for the link between each RN in $\mathbf{\Phi}_R$ and the typical UE. Therefore, the PPs composed only of UAV RNs in LoS or NLoS denoted $\mathbf{\Phi}_{R,L}$ and $\mathbf{\Phi}_{R,N}$ are also distributed as two independent IHPPPs with densities $\lambda_{R,n}(r) = p_{An}(r)\lambda_R$.

Based on that, the PDFs of the distances between the typical UE and its closest TBS or closest RN in LoS and in NLoS, denoted $r_{SD,n}$ and $r_{RD,n}$, can be developed as

$$f_{r_{SD,n}}(r) = -\frac{\mathrm{d}}{\mathrm{d}r}\mathbb{P}_{r_{SD,n}}(r_{SD,n} > r) = -\frac{\mathrm{d}}{\mathrm{d}r} V_{\mathbf{\Phi}_{T,n}}(\mathcal{B}(0,r)), \tag{A.10}$$

$$f_{r_{RD,n}}(r) = -\frac{\mathrm{d}}{\mathrm{d}r}\mathbb{P}_{r_{RD,n}}(r_{RD,n} > r) = -\frac{\mathrm{d}}{\mathrm{d}r} V_{\mathbf{\Phi}_{R,n}}(\mathcal{B}(0,r)). \tag{A.11}$$

Knowing that the void probabilities of $\mathbf{\Phi}_{R,n}$ is given by

$$V_{\mathbf{\Phi}_{T,n}}(\mathcal{B}(0,r)) = \exp\left(-2\pi\lambda_T \int_0^r p_{Gn}(r')r'\mathrm{d}r'\right), \tag{A.12}$$

$$V_{\mathbf{\Phi}_{R,n}}(\mathcal{B}(0,r)) = \exp\left(-2\pi\lambda_R \int_0^r p_{An}(r')r'\mathrm{d}r'\right), \tag{A.13}$$

using the Leibniz's integration rule presented in Section 2.3, these PDFs are given by

$$\begin{aligned} f_{r_{SD,n}}(r) &= 2\pi\lambda_T \frac{\mathrm{d}}{\mathrm{d}r}\left(\int_0^r p_{Gn}(r')\mathrm{d}r'\right)\exp\left(-2\pi\lambda_T \int_0^r p_{Gn}(r')r'\mathrm{d}r'\right) \\ &= 2\pi\lambda_T\, p_{Gn}(r)\, r \exp\left(-2\pi\lambda_T \int_0^r p_{Gn}(r')r'\mathrm{d}r'\right), \end{aligned} \tag{A.14}$$

$$\begin{aligned} f_{r_{RD,n}}(r) &= 2\pi\lambda_R \frac{\mathrm{d}}{\mathrm{d}r}\left(\int_0^r p_{An}(r')\mathrm{d}r'\right)\exp\left(-2\pi\lambda_R \int_0^r p_{An}(r')r'\mathrm{d}r'\right) \\ &= 2\pi\lambda_R\, p_{An}(r)\, r \exp\left(-2\pi\lambda_R \int_0^r p_{An}(r')r'\mathrm{d}r'\right). \end{aligned} \tag{A.15}$$

Thanks to the stationarity property of an HPPP, the PDF of the distance between the selected RN and its closest TBS when the link is in LoS or NLoS is equal to the PDF of the distance between the typical UE and its closest TBS when the link is in LoS or NLoS. ■

Proof of Lemma 4.8

Using the law of cosines, we have

$$r_{SR}^2 = r_{RD}^2 + r_{SD}^2 - 2r_{RD}r_{SD}\cos\Theta \tag{A.16}$$

with $\Theta \sim \mathrm{Unif}([0,\pi])$.

Since the PDF of $Y = \cos\Theta$ is given by

$$f_Y(y) = \begin{cases} \dfrac{1}{\pi}\dfrac{1}{\sqrt{1-y^2}} & \text{if } y \in [-1,1] \\ 0 & \text{otherwise} \end{cases}, \tag{A.17}$$

the PDF of r_{SR}^2 conditioned on r_{RD} and r_{SD} is given by

$$f_{r_{SR}^2|r_{RD},r_{SD}}(x) = \begin{cases} \dfrac{1}{\pi}\dfrac{1}{\sqrt{4r_{SD}^2r_{RD}^2 - \left(x - r_{SD}^2 - r_{RD}^2\right)^2}} & \text{if } (r_{RD}-r_{SD})^2 \le x \le (r_{RD}+r_{SD})^2 \\ 0 & \text{otherwise} \end{cases}, \tag{A.18}$$

and therefore the PDF of r_{SR} conditioned on r_{RD} and r_{SD} is given by

$$f_{r_{SR}|r_{RD},r_{SD}}(r) = \begin{cases} \dfrac{1}{\pi}\dfrac{2r}{\sqrt{4r_{SD}^2r_{RD}^2 - \left(r^2 - r_{SD}^2 - r_{RD}^2\right)^2}} & \text{if } |r_{RD}-r_{SD}| \le r \le r_{RD}+r_{SD} \\ 0 & \text{otherwise} \end{cases}. \tag{A.19}$$

■

Proof of Lemma 4.9

The ergodic SE of the relay link can be developed as

$$\begin{aligned}
\mathcal{S}_{SRD} &= \frac{1}{2}\,\mathbb{E}_{\chi_{SRD}}\left[\log_2\left(1+\chi_{SRD}\right)\right] \\
&= \frac{1}{2}\,\mathbb{E}_{\chi_{SR},\chi_{RD}}\left[\log_2\left(1+\min\left(\chi_{SR},\chi_{RD}\right)\right)\right] \\
&\overset{(a)}{=} \frac{1}{2}\,\mathbb{E}_{\chi_{SR},\chi_{RD}}\left[\min\left(\log_2\left(1+\chi_{SR}\right),\log_2\left(1+\chi_{RD}\right)\right)\right] \\
&= \frac{1}{2}\int_0^\infty \mathbb{P}_{\chi_{SR},\chi_{RD}}\left(\min\left(\log_2\left(1+\chi_{SR}\right),\log_2\left(1+\chi_{RD}\right)\right)>\gamma\right)\mathrm{d}\gamma \\
&\overset{(b)}{=} \frac{1}{2}\int_0^\infty \mathbb{P}_{\chi_{SR}}\left(\log_2\left(1+\chi_{SR}\right)>\gamma\right)\mathbb{P}_{\chi_{RD}}\left(\log_2\left(1+\chi_{RD}\right)>\gamma\right)\mathrm{d}\gamma, \qquad \text{(A.20)}
\end{aligned}$$

where (a) is obtained since the logarithm function is strictly increasing, and (b) because the SINR of the two hops are independent of each other.

Since the CCDF of a RV is between 0 and 1,

$$\mathcal{S}_{SRD} \leq \underbrace{\frac{1}{2}\int_0^\infty \mathbb{P}_{\chi_{SR}}\left(\log_2\left(1+\chi_{SR}\right)>\gamma\right)\mathrm{d}\gamma}_{\mathcal{S}_{SR}} \qquad \text{(A.21)}$$

and

$$\mathcal{S}_{SRD} \leq \underbrace{\frac{1}{2}\int_0^\infty \mathbb{P}_{\chi_{RD}}\left(\log_2\left(1+\chi_{RD}\right)>\gamma\right)\mathrm{d}\gamma}_{\mathcal{S}_{RD}}. \qquad \text{(A.22)}$$

Therefore, if the ergodic SE of the relay link is lower or equal than the ergodic rate of each hop, it is also lower or equal to the minimum between the ergodic rate of each hop, and the proof is completed.

■

Proof of Lemma 5.1

Since the selected RN moves at a constant speed v in the direction of the typical UE, from the selected RN's perspective, the TBSs' PP is translated at a constant speed v in a fixed direction. Therefore, at time $t \geq 0$, the TBSs' PP remains an HPPP with density λ_T thanks to the stationary property. It implies that, at every time $t \geq 0$, $r_{SR}(t)$ is a RV equivalent to r_{SR}, with PDF given by Lemma 4.1, and also that the interfering TBSs PP' density remains the same.

■

Proof of Lemma 5.2

Figure A.2 illustrates the regions for which the typical UE selects the direct or the relay link at time $t \geq 0$ denoted respectively by $\Omega_{SD}(t)$ and $\Omega_{SRD}(t)$.

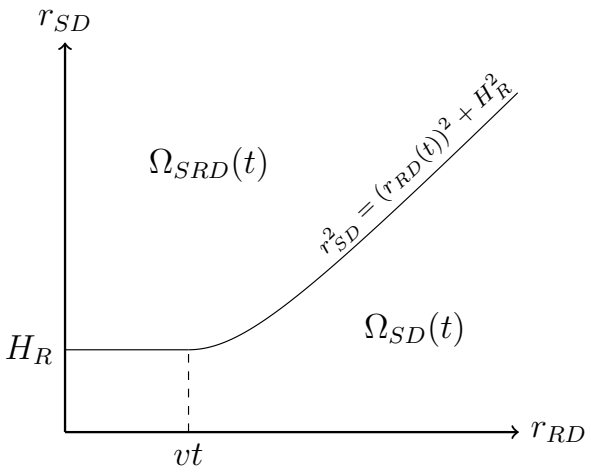

Figure A.2: Regions of association with nearest neighbour association rule for the second mobility scheme at time $t \geq 0$. The typical UE selects the direct or the relay link at time $t \geq 0$ if the couple (r_{SD}, r_{RD}) is respectively in $\Omega_{SD}(t)$ or $\Omega_{SRD}(t)$.

Based on Equation (4.15), (4.17), since r_{SD} and r_{RD} are two independent RVs, the probability typical UE selects the direct link can be developed as

$$\begin{aligned}
p_{A,SD} &= \mathbb{P}_{r_{SD},r_{RD}}\left(r_{SD} \leq \sqrt{(r_{RD}(t))^2 + H_R^2}\right) \\
&= \int_{\Omega_{SD}} f_{r_{SD},r_{RD}}(r_{SD}, r_{RD}) \mathrm{d}r_{SD}\mathrm{d}r_{RD} \\
&= \int_0^{vt} f_{r_{RD}}(r_{RD}) \int_0^{H_R} f_{r_{SD}}(r_{SD}) \mathrm{d}r_{SD}\mathrm{d}r_{RD} \\
&+ \int_{vt}^{\infty} f_{r_{RD}}(r_{RD}) \int_0^{\sqrt{(r_{RD}-vt)^2+H_R^2}} f_{r_{SD}}(r_{SD}) \mathrm{d}r_{SD}\mathrm{d}r_{RD} \\
&= \left(1 - \exp\left(-\pi\lambda_R v^2 t^2\right)\right)\left(1 - \exp\left(-\pi\lambda_T H_R^2\right)\right) \\
&+ 2\pi\lambda_R \int_{vt}^{\infty} r_{RD} \exp\left(-\pi\lambda_R r_{RD}^2\right)\left(1 - \exp\left(-\pi\lambda_T\left((r_{RD} - vt)^2 + H_R^2\right)\right)\right) \mathrm{d}r_{RD} \\
&= 1 - \exp\left(-\pi\lambda_T H_R^2\right)\left(1 - \exp\left(-\pi\lambda_R v^2 t^2\right)\right) + 2\pi\lambda_R \exp\left(-\pi\lambda_T(H_R^2 + v^2 t^2)\right)\mathcal{I}_{A,SD},
\end{aligned} \tag{A.23}$$

with

$$\mathcal{I}_{A,SD} = \int_{vt}^{\infty} r_{RD} \exp\left(-\pi(\lambda_R + \lambda_T) r_{RD}^2 + 2\pi\lambda_T vt\, r_{RD}\right) \mathrm{d}r_{RD}. \tag{A.24}$$

Moreover, the probability that the typical UE selects the relay link is given by

$$p_{A,SRD} = 1 - p_{A,SD}. \tag{A.25}$$

■

Proof of Lemma 5.3

Conditioned on r_{RD}, if $r_{RD} \leq vt$, the selected RN hovers above the typical UE and therefore, the link between these two is in LoS with probability 1 with the A2G LoS

probability model given by Equation 3.18. If $r_{RD} > vt$, the probability for this link to be in LoS or NLoS are respectively given by $p_{AL}(r_{RD} - vt)$ and $p_{AN}(r_{RD} - vt)$. Therefore, the proof is completed thanks to the law of total probability.

■

Proof of Lemma 5.4

When $r_{RD} \leq vt$, the selected RN hovers above the typical UE, and therefore the distance between the selected RN and the TBS is equal to the distance between the typical UE and the TBS.

When $r_{RD} > vt$, the proof is similar to the proof of Lemma 4.8, except that r_{RD} is replaced by $r_{RD} - vt$.

■

Proof of Lemma 5.5

The proof is similar to the proof of Lemma 4.6, except that ν, σ and K are replaced by $\nu(r)$, $\sigma(r)$ and $K(r)$.

■

Proof of Lemma 5.6

The proof is similar to the proof of Lemma 4.9, except that χ_{SRD} is replaced by $\chi_{SRD}(t)$.

■

Propositions

Proof of Proposition 4.1

With the nearest neighbour association rule, the CP of the complete link for a given SINR threshold β is given by

$$\begin{aligned}\mathcal{P}(\beta) &= \mathbb{P}_{\chi}\left(\chi \geq \beta\right) \\ &= \mathbb{E}_{r_{RD}, r_{SD}}\left[\mathbb{P}_{\chi|r_{RD}, r_{SD}}\left(\chi \geq \beta\right)\right].\end{aligned} \tag{A.26}$$

Conditioned on r_{RD} and r_{SD}, the SINR at the typical UE χ is given by

$$\chi = \begin{cases} \chi_{SRD} & \text{if} \quad r_{SD} > \sqrt{r_{RD}^2 + H_R^2} \\ \chi_{SD} & \text{if} \quad r_{SD} \leq \sqrt{r_{RD}^2 + H_R^2} \end{cases}. \tag{A.27}$$

The regions of association are illustrated by Figure A.1. The CP of the typical UE can be developed as

$$\begin{aligned}\mathcal{P}(\beta) = &\int_{\Omega_{SD}} \underbrace{\mathbb{P}_{\chi_{SD}|r_{RD}, r_{SD}}\left(\chi_{SD} \geq \beta\right)}_{\mathcal{P}_{SD|r_{RD}, r_{SD}}(\beta)} f_{r_{SD}, r_{RD}}(r_{SD}, r_{RD}) \mathrm{d}r_{SD} \mathrm{d}r_{RD} \\ &+ \int_{\Omega_{SRD}} \underbrace{\mathbb{P}_{\chi_{SRD}|r_{RD}, r_{SD}}\left(\chi_{SRD} \geq \beta\right)}_{\mathcal{P}_{SRD|r_{RD}, r_{SD}}(\beta)} f_{r_{SD}, r_{RD}}(r_{SD}, r_{RD}) \mathrm{d}r_{SD} \mathrm{d}r_{RD},\end{aligned} \tag{A.28}$$

where $\mathcal{P}_{SD|r_{RD},r_{SD}}(\beta)$ and $\mathcal{P}_{SRD|r_{RD},r_{SD}}(\beta)$ are respectively the CP of the direct link and relay link, both conditioned on r_{RD} and r_{SD}, and $f_{r_{SD},r_{RD}}(r_{SD},r_{RD})$ is the joint PDF of r_{SD} and r_{RD}. Since the direct link and the relay link are independent, we have

$$f_{r_{SD},r_{RD}}(r_{SD},r_{RD}) = f_{r_{SD}}(r_{SD}) f_{r_{RD}}(r_{RD}) \tag{A.29}$$

and

$$\mathcal{P}_{SD|r_{RD},r_{SD}}(\beta) \;\; = \mathcal{P}_{SD|r_{SD}}(\beta) \tag{A.30}$$

$$\mathcal{P}_{SRD|r_{RD},r_{SD}}(\beta) = \mathcal{P}_{SRD|r_{RD}}(\beta) = \mathcal{P}_{SR}(\beta)\mathcal{P}_{RD|r_{RD}}(\beta). \tag{A.31}$$

Furthermore, thanks to the independence between the two-hop of the relay link and using Equation (4.11),

$$\mathcal{P}_{SRD|r_{RD}}(\beta) = \mathbb{P}_{\chi_{SRD}|r_{RD},r_{SD}}\left(\chi_{SRD} \geq \beta\right) = \underbrace{\mathbb{P}_{\chi_{SR}}\left(\chi_{SR} \geq \beta\right)}_{\mathcal{P}_{SR}(\beta)} \underbrace{\mathbb{P}_{\chi_{RD}|r_{RD}}\left(\chi_{RD} \geq \beta\right)}_{\mathcal{P}_{RD|r_{RD}}(\beta)}. \tag{A.32}$$

Therefore,

$$\begin{aligned}
\mathcal{P}(\beta) = & \int_0^{H_R} \mathcal{P}_{SD|r_{SD}}(\beta) f_{r_{SD}}(r_{SD}) \int_0^{\infty} f_{r_{RD}}(r_{RD}) \mathrm{d}r_{RD} \mathrm{d}r_{SD} \\
& + \int_{H_R}^{\infty} \mathcal{P}_{SD|r_{SD}}(\beta) f_{r_{SD}}(r_{SD}) \int_{\sqrt{r_{SD}^2 - H_R^2}}^{\infty} f_{r_{RD}}(r_{RD}) \mathrm{d}r_{RD} \mathrm{d}r_{SD} \\
& + \int_0^{\infty} \mathcal{P}_{SRD|r_{RD}}(\beta) f_{r_{RD}}(r_{RD}) \int_{\sqrt{r_{RD}^2 + H_R^2}}^{\infty} f_{r_{SD}}(r_{SD}) \mathrm{d}r_{SD} \mathrm{d}r_{RD} \\
& \overset{(a)}{=} 2\pi\lambda_T \int_0^{H_R} \mathcal{P}_{SD|r_{SD}}(\beta)\, r_{SD} \exp\left(-\pi\lambda_T r_{SD}^2\right) \mathrm{d}r_{SD} \\
& + 2\pi\lambda_T \exp\left(\pi\lambda_R H_R^2\right) \int_{H_R}^{\infty} \mathcal{P}_{SD|r_{SD}}(\beta)\, r_{SD} \exp\left(-\pi(\lambda_R + \lambda_T) r_{SD}^2\right) \mathrm{d}r_{SD} \\
& + 2\pi\lambda_R \exp\left(-\pi\lambda_T H_R^2\right) \mathcal{P}_{SR}(\beta) \int_0^{\infty} \mathcal{P}_{RD|r_{RD}}(\beta)\, r_{RD} \exp\left(-\pi(\lambda_R + \lambda_T) r_{RD}^2\right) \mathrm{d}r_{RD},
\end{aligned} \tag{A.33}$$

where (a) is obtained thanks to Lemma 4.1.

■

Proof of Proposition 4.2

The proof focus only on the second hop, and the developments are identical for the two others links.

With Nakagami-m fading, the small-scale fading channel power gain follows a Gamma distribution given by Equation (3.12). Therefore, its CCDF is given by

$$\mathbb{P}\left(|h_{RD,n}|^2 \geq x\right) = \frac{\gamma\left(m_{An}, m_{An}x\right)}{\Gamma(m_{An})} = \exp\left(-m_{An}x\right) \sum_{i=0}^{m_{An}-1} \frac{(m_{An}x)^i}{i!}, \tag{A.34}$$

where γ is the lower incomplete gamma function.

Therefore, the CP of the second hop if the link is in LoS or NLoS, and conditioned in respect to r_{RD} can be developed as

$$\begin{aligned}
\mathcal{P}_{RD|n,r_{RD}}(\beta) &= \mathbb{P}_{|h_{RD,n}|^2,S_{RD,n},I_{RD}|r_{RD}}\left(\frac{C_{RD,n}(r_{RD}^2+H_R^2)^{-\frac{\alpha_{An}}{2}}|h_{RD,n}|^2 S_{RD,n}}{I_{RD}+\sigma^2}\geq\beta\right)\\
&= \mathbb{E}_{S_{RD,n},I_{RD}}\left[\mathbb{P}_{|h_{RD,n}|^2|r_{RD},S_{RD,n},I_{RD}}\left(|h_{RD,n}|^2\geq\beta\frac{I_{RD}+\sigma^2}{C_{RD,n}(r_{RD}^2+H_R^2)^{-\frac{\alpha_{An}}{2}}S_{RD,n}}\right)\right]\\
&= \mathbb{E}_{S_{RD,n},I_{RD}}\left[\exp\left(-\frac{m_{An}\beta}{C_{RD,n}}\frac{I_{RD}+\sigma^2}{(r_{RD}^2+H_R^2)^{-\frac{\alpha_{An}}{2}}S_{RD,n}}\right)\right.\\
&\qquad\left.\cdot\sum_{i=0}^{m_n-1}\frac{1}{i!}\left(\frac{m_{An}\beta}{C_{RD,n}}\frac{I_{RD}+\sigma^2}{(r_{RD}^2+H_R^2)^{-\frac{\alpha_{An}}{2}}S_{RD,n}}\right)^i\right].
\end{aligned}\tag{A.35}$$

If we define

$$D_{SD,n}=\frac{C_{RD,n}(r_{RD}^2+H_R^2)^{-\frac{\alpha_{An}}{2}}S_{RD,n}}{m_{An}\beta},\tag{A.36}$$

it becomes

$$\begin{aligned}
\mathcal{P}_{RD|n,r_{RD}}(\beta) &= \mathbb{E}_{S_{RD,n},I_{RD}}\left[\exp\left(-\frac{I_{RD}+\sigma^2}{D_{RD,n}}\right)\sum_{i=0}^{m_{An}-1}\frac{1}{i!}\left(\frac{I_{RD}+\sigma^2}{D_{RD,n}}\right)^i\right]\\
&\overset{(a)}{=} \mathbb{E}_{S_{RD,n},I_{RD}}\left[\exp\left(-\frac{I_{RD}+\sigma^2}{D_{RD,n}}\right)\sum_{i=0}^{m_{An}-1}\sum_{k=0}^{i}\frac{1}{i!D_{RD,n}^i}\binom{i}{k}I_{RD}^k(\sigma^2)^{i-k}\right]\\
&= \mathbb{E}_{S_{RD,n}}\left[\exp\left(-\frac{\sigma^2}{D_{RD,n}}\right)\sum_{i=0}^{m_{An}-1}\sum_{k=0}^{i}\frac{1}{i!D_{RD,n}^i}\binom{i}{k}(\sigma^2)^{i-k}\mathbb{E}_{I_{RD}}\left[I_{RD}^k\exp\left(-\frac{I_{RD}}{D_{RD,n}}\right)\right]\right]\\
&\overset{(b)}{=} \mathbb{E}_{S_{RD,n}}\left[\exp\left(-\frac{\sigma^2}{D_{RD,n}}\right)\sum_{i=0}^{m_{An}-1}\sum_{k=0}^{i}\frac{(-1)^k}{i!D_{RD,n}^i}\binom{i}{k}(\sigma^2)^{i-k}\frac{\partial^k\mathcal{L}_{I_{RD}|r_{RD}}}{\partial s^k}\Big|_{s=\frac{1}{D_{RD,n}}}\right],
\end{aligned}\tag{A.37}$$

where (a) is obtained thanks to the binomial theorem, presented in Section 2.3, and (b) is obtained thanks to derivatives of the LT of a RV:

$$\frac{\partial^k\mathcal{L}_X(s)}{\partial s^k}=\int_{-\infty}^{\infty}f_X(x)\frac{\partial^k}{\partial s^k}\exp(-sx)\,\mathrm{d}x=\mathbb{E}_X\left[(-X)^k\exp(-sX)\right].\tag{A.38}$$

■

Proof of Proposition 4.3

The proof focus only on the second hop, and the developments are identical for the two others links.

The CP of the second hop for a LoS or NLoS link, and conditioned in respect to r_{RD}

can be developed as

$$\mathcal{P}_{RD|n,r_{RD}}(\beta) = \mathbb{P}_{|h_{RD,n}|^2,S_{RD,n},I_{RD}|r_{RD}}\left(\frac{C_{RD,n}(r_{RD}^2+H_R^2)^{-\frac{\alpha_{An}}{2}}|h_{RD,n}|^2 S_{RD,n}}{I_{RD}+\sigma^2}\geq\beta\right)$$
$$= \mathbb{E}_{S_{RD,n}}\left[\mathbb{P}_{|h_{RD,n}|^2,I|r_{RD},S_{RD,n}}\left(\underbrace{C_{RD,n}(r_{RD}^2+H_R^2)^{-\frac{\alpha_{An}}{2}}|h_{RD,n}|^2 S_{RD,n}-\beta I_{RD}}_{Z_{RD}}\right)\geq\beta\sigma^2\right]$$
$$= \frac{1}{2}+\frac{1}{\pi}\mathbb{E}_{S_{RD,n}}\left[\int_0^\infty\frac{1}{\tau}\mathrm{Im}\left[\phi_{Z_{RD}|r_{RD}}(\tau)\exp\left(-j\tau\beta\sigma^2\right)\right]\mathrm{d}\tau\right]. \quad (A.39)$$

Since Z_{RD} is a linear combination of $|h_{RD,n}|^2$ and I_{RD} which are two independent RVs, knowing that $\phi_{aX}(\tau)=\phi_X(a\tau)$ for any RV X and $a\in\mathbb{R}$, the characteristic function of Z_{RD} conditioned on r_{RD} can be expressed as

$$\phi_{Z_{RD}|r_{RD}}(\tau) = \phi_{|h_{RD,n}|^2}(\tau C_{RD,n}(r_{RD}^2+H_R^2)^{-\frac{\alpha_{An}}{2}}|h_{RD,n}|^2 S_{RD,n})\phi_{I_{RD}}(-\tau\beta). \quad (A.40)$$

Finally, using the relation $\phi_X(\tau)=\mathcal{L}_X(-j\tau)$ for any RV X, the proof is completed. ■

Proof of Proposition 4.4

The proof focus only on the second hop, and the developments are identical for the two others links.

By definition of the aggregate interference given by Equation (4.10), the LT of I_{RD} conditioned on r_{RD} can be developed as

$$\mathcal{L}_{I_{RD}|r_{RD}}(s) = \mathbb{E}_{-|r_{RD}}\left[\exp\left(-s\sum_{n=\{L,N\}}\sum_{\phi_j\in\mathbf{\Phi}_{RDI,n}}c_{RD,n}(\|\boldsymbol{\phi}_j\|^2+H_R^2)^{-\frac{\alpha_{An}}{2}}|h_{RD,n,j}|^2 S_{RD,n,j}\right)\right]$$
$$\overset{(a)}{=}\prod_{n=\{L,N\}}\mathbb{E}_{-|r_{RD}}\left[\prod_{\phi_j\in\mathbf{\Phi}_{RDI,n}}\exp\left(-s\,|h_{RD,n,j}|^2\underbrace{c_{RD,n}(\|\boldsymbol{\phi}_j\|^2+H_R^2)^{-\frac{\alpha_{An}}{2}}S_{RD,n,j}}_{g(\|\boldsymbol{\phi}_j\|,S_{RD,n,j})}\right)\right]$$
$$\overset{(b)}{=}\prod_{n=\{L,N\}}\mathbb{E}_{\mathbf{\Phi}_{RDI,n}|r_{RD}}\left[\prod_{\phi_j\in\mathbf{\Phi}_{RDI,n}}\mathbb{E}_{|h_{RD,n,j}|^2,S_{RD,n,j}}\left[\exp\left(-s\,|h_{RD,n,j}|^2 g(\|\boldsymbol{\phi}_j\|,S_{RD,n,j})\right)\right]\right]$$
$$\overset{(c)}{=}\prod_{n=\{L,N\}}\exp\left(-2\pi\lambda_R\int_{r_{RD}}^\infty\left(1-\mathbb{E}_{\tilde{S}_{RD,n}}\left[\mathcal{L}_{|\tilde{h}_{RD,n}|^2}\left(s\,g(r,\tilde{S}_{RD,n})\right)\right]\right)p_{An}(r)r\mathrm{d}r\right)$$
$$= \exp\left(-2\pi\lambda_R\,\mathbb{E}_{\tilde{S}_{RD,L},\tilde{S}_{RD,N}}\left[\int_{r_{RD}}^\infty\left(1-\sum_{n=\{L,N\}}p_{An}(r)\mathcal{L}_{|\tilde{h}_{RD,n}|^2}\left(s\,g(r,\tilde{S}_{RD,n})\right)\right)r\mathrm{d}r\right]\right). \quad (A.41)$$

where (a), and (b) are obtained because $\mathbf{\Phi}_{RI,L}$ and $\mathbf{\Phi}_{RI,N}$ are generated with an independent thinning of $\mathbf{\Phi}_{RI}$, and all the links are supposed to be independent. The PGFL of a PPP in polar coordinates given by Equation (2.16) is used to obtain (c). The two RVs $|\tilde{h}_{RD,n}|^2$ and $\tilde{S}_{RD,n}$ are equivalent to the small-scale fading channel power gain and the shadowing of the interferers' links.

■

Proof of Proposition 4.5

With the maximum biased average power association rule, the CP of the second hop at a given SINR threshold β is given by

$$\begin{aligned}\mathcal{P}_{RD}(\beta) &= \mathbb{P}_{\chi_{RD}}\left(\chi_{RD} \geq \beta\right) \\ &= \mathbb{E}_{S_{RD,L},S_{RD,N},r_{RD,L},r_{RD,N}}\left[\mathbb{P}_{\chi_{RD}|S_{RD,L},S_{RD,N},r_{RD,L},r_{RD,N}}\left(\chi_{RD} \geq \beta\right)\right],\end{aligned} \tag{A.42}$$

where $r_{RD,L}$ and $r_{RD,N}$ are respectively the distances between the typical UE and the closest RN in LoS and NLoS.

Conditioned on $r_{RD,L}$ and $r_{RD,N}$, the SINR of the second hop is given by

$$\chi_{RD} = \begin{cases} \chi_{RD,L} \text{ if } C_{RD,L}\left(r_{RD,L}^2 + H_R^2\right)^{-\frac{\alpha_{AL}}{2}} S_{RD,L} \geq C_{RD,N}\left(r_{RD,N}^2 + H_R^2\right)^{-\frac{\alpha_{AN}}{2}} S_{RD,N} \\ \chi_{RD,N} \text{ if } C_{RD,L}\left(r_{RD,L}^2 + H_R^2\right)^{-\frac{\alpha_{AL}}{2}} S_{RD,L} < C_{RD,N}\left(r_{RD,N}^2 + H_R^2\right)^{-\frac{\alpha_{AN}}{2}} S_{RD,N} \end{cases}. \tag{A.43}$$

The conditions to be associated with a RN in LoS or NLoS can be respectively rewritten as

$$r_{RD,N}^2 \geq \underbrace{\left(\frac{C_{RD,N}S_{RD,N}}{C_{RD,L}S_{RD,L}}\right)^{\frac{2}{\alpha_{AN}}}\left(r_{RD,L}^2 + H_R^2\right)^{\frac{\alpha_{AL}}{\alpha_{AN}}} - H_R^2}_{g_{RD,N}(r_{RD,L})}, \tag{A.44}$$

$$r_{RD,L}^2 > \underbrace{\left(\frac{C_{RD,L}S_{RD,L}}{C_{RD,N}S_{RD,N}}\right)^{\frac{2}{\alpha_{AL}}}\left(r_{RD,N}^2 + H_R^2\right)^{\frac{\alpha_{AN}}{\alpha_{AL}}} - H_R^2}_{g_{RD,L}(r_{RD,N})}. \tag{A.45}$$

These conditions are respectively fulfilled whatever the value of $r_{RD,N}$ or $r_{RD,L}$ if

$$r_{RD,L}^2 \leq \left(\frac{C_{RD,L}S_{RD,L}}{C_{RD,N}S_{RD,N}}H_R^{\alpha_{AN}}\right)^{\frac{2}{\alpha_{AL}}} - H_R^2, \tag{A.46}$$

and

$$r_{RD,N}^2 < \left(\frac{C_{RD,N}S_{RD,N}}{C_{RD,L}S_{RD,L}}H_R^{\alpha_{AL}}\right)^{\frac{2}{\alpha_{AN}}} - H_R^2. \tag{A.47}$$

Therefore, if we define

$$d_{RD,L} = \left(\max\left\{\left(\frac{C_{RD,L}S_{RD,L}}{C_{RD,N}S_{RD,N}}H_R^{\alpha_{AN}}\right)^{\frac{2}{\alpha_{AL}}} - H_R^2, 0\right\}\right)^{\frac{1}{2}}, \tag{A.48}$$

$$d_{RD,N} = \left(\max\left\{\left(\frac{C_{RD,N}S_{RD,N}}{C_{RD,L}S_{RD,L}}H_R^{\alpha_{AL}}\right)^{\frac{2}{\alpha_{AN}}} - H_R^2, 0\right\}\right)^{\frac{1}{2}}, \tag{A.49}$$

depending on the shadowing, two specific cases are distinguished: either $d_{RD,L} > 0$ and $d_{RD,N} = 0$, or $d_{RD,L} = 0$ and $d_{RD,N} > 0$. Figure A.3 illustrates the regions of association of the typical UE.

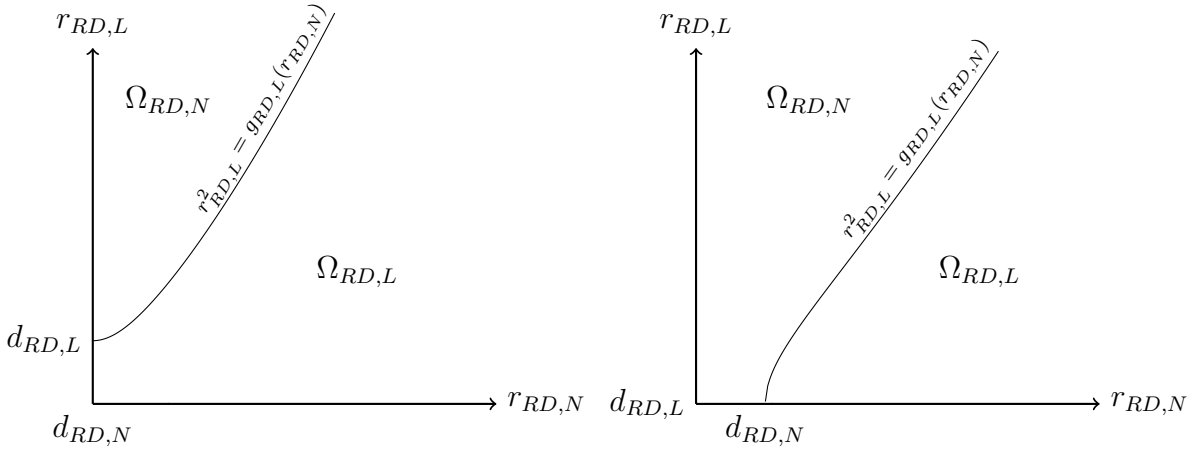

(a) $d_{RD,L} > 0$, $d_{RD,N} = 0$. (b) $d_{RD,L} = 0$, $d_{RD,N} > 0$.

Figure A.3: Regions of association with the maximum biased average power association rule. The typical UE selects a RN in LoS or NLoS if the couple $(r_{RD,L}, r_{RD,N})$ is respectively in $\Omega_{RD,L}$ or $\Omega_{RD,N}$.

The CP can be developed as

$$\mathcal{P}_{RD}(\beta) = \mathbb{E}_{S_{RD,L},S_{RD,N}}\left[\int_{\Omega_{RD,L}} \underbrace{\mathbb{P}_{\chi_{RD,L}|S_{RD,L},r_{RD,L}}\left(\chi_{RD,L} \geq \beta\right)}_{\mathcal{P}_{RD,L|S_{RD,L},r_{RD,L}}(\beta)} \mathrm{d}r_{RD,L}\mathrm{d}r_{RD,N} + \int_{\Omega_{RD,N}} \underbrace{\mathbb{P}_{\chi_{RD,N}|S_{RD,N},r_{RD,N}}\left(\chi_{RD,N} \geq \beta\right)}_{\mathcal{P}_{RD,N|S_{RD,N},r_{RD,N}}(\beta)} \mathrm{d}r_{RD,L}\mathrm{d}r_{RD,N}\right]. \tag{A.50}$$

In the first case ($d_{RD,L} > 0$ and $d_{RD,N} = 0$),

$$\begin{aligned}
\mathcal{P}_{RD}(\beta) &= \mathbb{E}_{S_{RD,L},S_{RD,N}}\left[\int_0^{d_{RD,L}} \mathcal{P}_{RD,L|S_{RD,L},r_{RD,L}}(\beta) f_{r_{RD,L}}(r_{RD,L})\mathrm{d}r_{RD,L}\right. \\
&+ \int_{d_{RD,L}}^{\infty} \mathcal{P}_{RD,L|S_{RD,L},r_{RD,L}}(\beta) f_{r_{RD,L}}(r_{RD,L}) \int_{\sqrt{g_{RD,N}(r_{RD,L})}}^{\infty} f_{r_{RD,N}}(r_{RD,N})\mathrm{d}r_{RD,N}\mathrm{d}r_{RD,L} \\
&\left.+ \int_0^{\infty} \mathcal{P}_{RD,N|S_{RD,N},r_{RD,N}}(\beta) f_{r_{RD,N}}(r_{RD,N}) \int_{\sqrt{g_{RD,L}(r_{RD,N})}}^{\infty} f_{r_{RD,L}}(r_{RD,L})\mathrm{d}r_{RD,L}\mathrm{d}r_{RD,N}\right] \\
&= \mathbb{E}_{S_{RD,L},S_{RD,N}}\left[\int_0^{d_{RD,L}} \mathcal{P}_{RD,L|S_{RD,L},r_{RD,L}}(\beta) f_{r_{RD,L}}(r_{RD,L})\mathrm{d}r_{RD,L}\right. \\
&+ \int_{d_{RD,L}}^{\infty} \mathcal{P}_{RD,L|S_{RD,L},r_{RD,L}}(\beta) f_{r_{RD,L}}(r_{RD,L}) \exp\left(-2\pi\lambda_R \int_0^{\sqrt{g_{RD,N}(r_{RD,L})}} p_{AN}(r) r\mathrm{d}r\right)\mathrm{d}r_{RD,L} \\
&\left.+ \int_0^{\infty} \mathcal{P}_{RD,N|S_{RD,N},r_{RD,N}}(\beta) f_{r_{RD,N}}(r_{RD,N}) \exp\left(-2\pi\lambda_R \int_0^{\sqrt{g_{RD,L}(r_{RD,N})}} p_{AL}(r) r\mathrm{d}r\right)\mathrm{d}r_{RD,N}\right].
\end{aligned} \tag{A.51}$$

In the second case ($d_{RD,L} > 0$ and $d_{RD,N} = 0$),

$$\begin{aligned}
\mathcal{P}_{RD}(\beta) &= \mathbb{E}_{S_{RD,L},S_{RD,N}}\Bigg[\int_0^{d_{RD,N}} \mathcal{P}_{RD,N|S_{RD,N},r_{RD,N}}(\beta) f_{r_{RD,N}}(r_{RD,N})\mathrm{d}r_{RD,N} \\
&+ \int_{d_{RD,N}}^{\infty} \mathcal{P}_{RD,N|S_{RD,N},r_{RD,N}}(\beta) f_{r_{RD,N}}(r_{RD,N}) \int_{\sqrt{g_{RD,L}(r_{RD,N})}}^{\infty} f_{r_{RD,L}}(r_{RD,L})\mathrm{d}r_{RD,L}\mathrm{d}r_{RD,N} \\
&+ \int_0^{\infty} \mathcal{P}_{RD,L|S_{RD,L},r_{RD,L}}(\beta) f_{r_{RD,L}}(r_{RD,L}) \int_{\sqrt{g_{RD,N}(r_{RD,L})}}^{\infty} f_{r_{RD,N}}(r_{RD,N})\mathrm{d}r_{RD,N}\mathrm{d}r_{RD,L}\Bigg] \\
&= \mathbb{E}_{S_{RD,L},S_{RD,N}}\Bigg[\int_0^{d_{RD,N}} \mathcal{P}_{RD,N|S_{RD,N},r_{RD,N}}(\beta) f_{r_{RD,N}}(r_{RD,N})\mathrm{d}r_{RD,N} \\
&+ \int_{d_{RD,N}}^{\infty} \mathcal{P}_{RD,N|S_{RD,N},r_{RD,N}}(\beta) f_{r_{RD,N}}(r_{RD,N}) \exp\left(-2\pi\lambda_R \int_0^{\sqrt{g_{RD,L}(r_{RD,N})}} p_{AL}(r) r\mathrm{d}r\right)\mathrm{d}r_{RD,N} \\
&+ \int_0^{\infty} \mathcal{P}_{RD,L|S_{RD,L},r_{RD,L}}(\beta) f_{r_{RD,L}}(r_{RD,L}) \exp\left(-2\pi\lambda_R \int_0^{\sqrt{g_{RD,N}(r_{RD,L})}} p_{AN}(r) r\mathrm{d}r\right)\mathrm{d}r_{RD,L}\Bigg].
\end{aligned} \tag{A.52}$$

■

Proof of Proposition 4.6

The LoS and NLoS RNs PPs are respectively denoted by $\mathbf{\Phi}_{R,L}$ and $\mathbf{\Phi}_{R,N}$. Since the link of each point of $\mathbf{\Phi}_R$ is in LoS or NLoS independently (there isn't any spatial correlation involved in the model), these two PPs are obtained by applying an independent thinning of $\mathbf{\Phi}_R$ with probabilities $p_{AL}(r)$ and $p_{AN}(r) = 1 - p_{AL}(r)$, for two nodes at a ground distance r. Therefore, they are distributed as two independent IHPPPs with densities $\lambda_{R,n}(r) = p_{An}(r)\lambda_R$.

Assuming that the realisations of the shadowing are known, let us define a transformation g by

$$g : \mathbb{R}^2 \to \mathbb{R}^2 : \boldsymbol{\phi}_i \to \boldsymbol{\phi}'_i = \frac{\boldsymbol{\phi}_i}{\|\boldsymbol{\phi}_i\|}\left(\left(\frac{C_{RD,L}S_{RD,L}}{C_{RD,N}S_{RD,N}}\right)^{\frac{2}{\alpha_{AL}}}\left(\|\boldsymbol{\phi}_i\|^2 + H_R^2\right)^{\frac{\alpha_{AN}}{\alpha_{AL}}} - H_R^2\right)^{\frac{1}{2}}. \tag{A.53}$$

This mapping is defined such that a RN in NLoS located at a distance r from the typical UE transmits the same average power than a RN in LoS located at a distance r' from the typical UE:

$$C_{RD,N}(r^2 + H_R^2)^{-\frac{\alpha_{AN}}{2}} S_{RD,N} = C_{RD,L}(r'^2 + H_R^2)^{-\frac{\alpha_{AL}}{2}} S_{RD,L}. \tag{A.54}$$

Even if this transformation is always defined, it is not the case of the inverse mapping

$$g^{-1} : \mathbb{R}^2 \to \mathbb{R}^2 : \boldsymbol{\phi}'_i \to \boldsymbol{\phi}_i = \frac{\boldsymbol{\phi}'_i}{\|\boldsymbol{\phi}'_i\|}\left(\left(\frac{C_{RD,N}S_{RD,N}}{C_{RD,L}S_{RD,L}}\right)^{\frac{2}{\alpha_{AN}}}\left(\|\boldsymbol{\phi}'_i\|^2 + H_R^2\right)^{\frac{\alpha_{AL}}{\alpha_{AN}}} - H_R^2\right)^{\frac{1}{2}}, \tag{A.55}$$

which is defined only when

$$\|\boldsymbol{\phi}'_i\|^2 \geq \left(\frac{C_{RD,L}S_{RD,L}}{C_{RD,N}S_{RD,N}}H_R^{\alpha_{AN}}\right)^{\frac{2}{\alpha_{AL}}} - H_R^2. \tag{A.56}$$

Using the transformation g on $\boldsymbol{\Phi}_{R,N}$ to generate the IHPPP $\boldsymbol{\Phi}'_{R,L}$, a new PPP $\boldsymbol{\Phi}'_R = \boldsymbol{\Phi}_{R,L} \cup \boldsymbol{\Phi}'_{R,L}$ is defined by superposition, composed only of RNs in LoS. Using the maximum biased average power association rule, the selected RN is the closest RN in $\boldsymbol{\Phi}'_R$ since all the RN in $\boldsymbol{\Phi}'_R$ are in LoS. With that equivalent PP, the CP of the second hop is given by

$$\mathcal{P}_{RD}(\beta) = \int_0^\infty \mathcal{P}_{RD,L|r'_{RD}}(\beta) f_{r'_{RD}}(r'_{RD}) \mathrm{d}r'_{RD}. \tag{A.57}$$

If we define

$$\tilde{g}^{-1} : \mathbb{R} \to \mathbb{R} : r' \to r = \left(\left(\frac{C_{RD,N}S_{RD,N}}{C_{RD,L}S_{RD,L}}\right)^{\frac{2}{\alpha_{AN}}} \left(r'^2 + H_R^2\right)^{\frac{\alpha_{AL}}{\alpha_{AN}}} - H_R^2\right)^{\frac{1}{2}} \tag{A.58}$$

and

$$d_{min} = \left(\max\left\{\left(\frac{C_{RD,L}S_{RD,L}}{C_{RD,N}S_{RD,N}}H_R^{\alpha_{AN}}\right)^{\frac{2}{\alpha_{AL}}} - H_R^2, 0\right\}\right)^{\frac{1}{2}}, \tag{A.59}$$

the PDF of r'_{RD} is given by

$$\begin{aligned} f_{r'_{RD}}(r) &= -\frac{\mathrm{d}}{\mathrm{d}r}\mathbb{P}_{r'_{RD}}\left(r'_{RD} > r\right) \\ &= -\frac{\mathrm{d}}{\mathrm{d}r}V_{\boldsymbol{\Phi}'_R}(\mathcal{B}(0,r)) \\ &\overset{(a)}{=} -\frac{\mathrm{d}}{\mathrm{d}r}\left(V_{\boldsymbol{\Phi}_{R,L}}(\mathcal{B}(0,r))V_{\boldsymbol{\Phi}'_{R,L}}(\mathcal{B}(0,r))\right) \\ &= -\frac{\mathrm{d}}{\mathrm{d}r}V_{\boldsymbol{\Phi}_{R,L}}(\mathcal{B}(0,r))V_{\boldsymbol{\Phi}'_{R,L}}(\mathcal{B}(0,r)) - V_{\boldsymbol{\Phi}_{R,L}}(\mathcal{B}(0,r))\frac{\mathrm{d}}{\mathrm{d}r}V_{\boldsymbol{\Phi}'_{R,L}}(\mathcal{B}(0,r)), \end{aligned} \tag{A.60}$$

where (a) is obtained thanks to the independence between $\boldsymbol{\Phi}_{R,L}$ and $\boldsymbol{\Phi}'_{R,L}$.

The void probabilities of $\boldsymbol{\Phi}_{R,L}$ and $\boldsymbol{\Phi}'_{R,L}$ are given by

$$V_{\boldsymbol{\Phi}_{R,L}}(\mathcal{B}(0,r)) = \exp\left(-2\pi\lambda_R \int_0^r p_{AL}(r')r'\mathrm{d}r'\right) \tag{A.61}$$

$$V_{\boldsymbol{\Phi}'_{R,L}}(\mathcal{B}(0,r)) = V_{\boldsymbol{\Phi}_{R,N}}\left(\mathcal{B}\left(0,\tilde{g}^{-1}(r)\right)\right) = \begin{cases} \exp\left(-2\pi\lambda_R \int_0^{\tilde{g}^{-1}(r)} p_{AN}(r')r'\mathrm{d}r'\right) & \text{if } r > d_{min} \\ 1 & \text{otherwise} \end{cases} \tag{A.62}$$

Using the Leibniz's integration rule presented in Section 2.3, the derivative of these void probabilities are obtained following the development of Equation (A.15):

$$\frac{\mathrm{d}}{\mathrm{d}r}V_{\boldsymbol{\Phi}_{R,L}}(\mathcal{B}(0,r)) = -2\pi\lambda_R\, p_{AL}(r)\, r \exp\left(-2\pi\lambda_R \int_0^r p_{AL}(r')r'\mathrm{d}r'\right), \tag{A.63}$$

$$\frac{\mathrm{d}}{\mathrm{d}r}V_{\boldsymbol{\Phi}'_{R,L}}(\mathcal{B}(0,r)) = -2\pi\lambda_R\, p_{AN}(r)\, r \exp\left(-2\pi\lambda_R \int_0^{\tilde{g}^{-1}(r)} p_{AN}(r')r'\mathrm{d}r'\right) u(r - d_{min}). \tag{A.64}$$

Finally the PDF of r'_{RD} is given by

$$f_{r'_{RD}}(r'_{RD}) = 2\pi\lambda_R\, r'_{RD} \exp\left(-2\pi\lambda_R \int_0^{r'_{RD}} p_{R,L}(r) r \mathrm{d}r\right) \tilde{f}_{r'_{RD}}(r'_{RD}) \tag{A.65}$$

with

$$\tilde{f}_{r'_{RD}}(r) = \begin{cases} \exp\left(-2\pi\lambda_R \int_0^r p_{AN}(r') r' \mathrm{d}r'\right) \left(p_{AL}(r) + p_{AN}(r) \dfrac{\mathrm{d}}{\mathrm{d}r} \tilde{g}^{-1}(r)\right) & \text{if } r > d_{min} \\ p_{R,L}(r) & \text{otherwise} \end{cases}. \tag{A.66}$$

The derivative of $\tilde{g}^{-1}(r)$ when $r > d_{min}$ is given by

$$\frac{\mathrm{d}}{\mathrm{d}r} \tilde{g}_3^{-1}(r) = \frac{\left(\frac{C_{RD,L} S_{RD,L}}{C_{RD,N} S_{RD,N}}\right)^{\frac{2}{\alpha_{AN}}} \frac{\alpha_{AL}}{\alpha_{AN}} \left(r^2 + H_R^2\right)^{\frac{\alpha_{AL}}{\alpha_{AN}} - 1} r}{\left(\left(\frac{C_{RD,L} S_{RD,L}}{C_{RD,N} S_{RD,N}}\right)^{\frac{2}{\alpha_{AN}}} \left(r^2 + H_R^2\right)^{\frac{\alpha_{AL}}{\alpha_{AN}}} - H_R^2\right)^{\frac{1}{2}}}. \tag{A.67}$$

■

Proof of Proposition 4.7

Following the proof of Proposition 4.1, we have now

$$\begin{aligned} \mathcal{P}_{SRD|r_{SD},r_{RD}}(\beta) &= \mathbb{P}_{\chi_{SRD}|r_{SD},r_{RD}}\left(\chi_{SRD} \geq \beta\right) \\ &= \underbrace{\mathbb{P}_{\chi_{SR}|r_{SD},r_{RD}}\left(\chi_{SR} \geq \beta\right)}_{\mathcal{P}_{SR|r_{SD},r_{RD}}(\beta)} \underbrace{\mathbb{P}_{\chi_{RD}|r_{RD}}\left(\chi_{RD} \geq \beta\right)}_{\mathcal{P}_{RD|r_{RD}}(\beta)}. \end{aligned} \tag{A.68}$$

Additionally, we have

$$\mathcal{P}_{SR|r_{SD},r_{RD}}(\beta) = \int_{|r_{SD}-r_{RD}|}^{r_{SD}+r_{RD}} \mathcal{P}_{SR|r_{SR}}(\beta) f_{r_{SR}|r_{SD},r_{RD}}(r_{SR}) \mathrm{d}r_{SR}. \tag{A.69}$$

Therefore,

$$\begin{aligned} \mathcal{P}(\beta) &= \int_0^{H_R} \mathcal{P}_{SD|r_{SD}}(\beta) f_{r_{SD}}(r_{SD}) \int_0^{\infty} f_{r_{RD}}(r_{RD}) \mathrm{d}r_{RD} \mathrm{d}r_{SD} \\ &+ \int_{H_R}^{\infty} \mathcal{P}_{SD|r_{SD}}(\beta) f_{r_{SD}}(r_{SD}) \int_{\sqrt{r_{SD}^2 - H_R^2}}^{\infty} f_{r_{RD}}(r_{RD}) \mathrm{d}r_{RD} \mathrm{d}r_{SD} \\ &+ \int_0^{\infty} \int_{\sqrt{r_{RD}^2 + H_R^2}}^{\infty} \mathcal{P}_{SRD|r_{RD}}(\beta) f_{r_{RD}}(r_{RD}) f_{r_{SD}}(r_{SD}) \mathrm{d}r_{SD} \mathrm{d}r_{RD} \\ &\overset{(a)}{=} 2\pi\lambda_T \int_0^{H_R} \mathcal{P}_{SD|r_{SD}}(\beta)\, r_{SD} \exp\left(-\pi\lambda_T r_{SD}^2\right) \mathrm{d}r_{SD} \\ &+ 2\pi\lambda_T \exp\left(\pi\lambda_R H_R^2\right) \int_{H_R}^{\infty} \mathcal{P}_{SD|r_{SD}}(\beta)\, r_{SD} \exp\left(-\pi(\lambda_R + \lambda_T) r_{SD}^2\right) \mathrm{d}r_{SD} \\ &+ \int_0^{\infty} \int_{\sqrt{r_{RD}^2 + H_R^2}}^{\infty} \int_{|r_{RD}-r_{SD}|}^{r_{RD}+r_{SD}} \mathcal{P}_{SR|r_{SR}}(\beta) \mathcal{P}_{SD|r_{SD}}(\beta) \tilde{f}_{r_{SD},r_{SR},r_{RD}}(r_{SD}, r_{SR}, r_{RD}) \mathrm{d}r_{SR} \mathrm{d}r_{SD} \mathrm{d}r_{SD}, \end{aligned} \tag{A.70}$$

where (a) is obtained thanks to Lemma 4.1 and Lemma 4.8, and with

$$\tilde{f}_{r_{SD},r_{SR},r_{RD}}(r_{SD},r_{SR},r_{RD}) = \frac{8\pi\lambda_R\lambda_T\, r_{SR}r_{RD}r_{SD}\exp\left(-\pi(\lambda_R r_{RD}^2+\lambda_T r_{SD}^2)\right)}{\sqrt{4r_{SD}^2r_{RD}^2-\left(r^2-r_{SD}^2-r_{RD}^2\right)^2}}. \quad \text{(A.71)}$$

■

Proof of Proposition 4.8

The proof focus only on the average exposure from the RNs, and the developments are identical for the average exposure from the TBSs.

The RNs' average exposure can be developed as

$$\mathcal{X}_{c,RD} = \mathbb{E}_{U_{RD},I_{RD}}\left[U_{RD}+I_{RD}\right] = \mathbb{E}_{r_{RD}}\left[\mathbb{E}_{U_{RD}|r_{RD}}\left[U_{RD}\right]+\mathbb{E}_{I_{RD}|r_{RD}}\left[I_{RD}\right]\right], \quad \text{(A.72)}$$

where U_{RD} is defined as

$$U_{RD} = \begin{cases} U_{RD,L} = C_{RD,L}\left(r_{RD}^2+H_R^2\right)^{-\frac{\alpha_{AL}}{2}}|h_{RD,L}|^2S_{RD,L} & \sim p_{AL}(r_{RD}), \\ U_{RD,N} = C_{RD,N}\left(r_{RD}^2+H_R^2\right)^{-\frac{\alpha_{AN}}{2}}|h_{RD,N}|^2S_{RD,N} & \sim p_{AN}(r_{RD}). \end{cases} \quad \text{(A.73)}$$

Therefore,

$$\begin{aligned} \mathbb{E}_{U_{RD}|r_{RD}}\left[U_{RD}\right] &= \mathbb{E}_{U_{RD,L},U_{RD,N}|r_{RD}}\left[\sum_{n=\{L,N\}} p_{An}(r_{RD})U_{RD,n}\right] \\ &\overset{(a)}{=} \sum_{n=\{L,N\}} p_{An}(r_{RD})\,\mathbb{E}_{|h_{RD,n}|^2,S_{RD,n}|r_{RD}}\left[C_{RD,n}\left(r_{RD}^2+H_R^2\right)^{-\frac{\alpha_{An}}{2}}|h_{RD,n}|^2S_{RD,n}\right] \\ &\overset{(b)}{=} \sum_{n=\{L,N\}} C_{RD,n}\exp\left(\frac{\ln^2 10}{200}\sigma_{S_n}^2\right)p_{An}(r_{RD})\left(r_{RD}^2+H_R^2\right)^{-\frac{\alpha_{An}}{2}}, \end{aligned} \quad \text{(A.74)}$$

where (a) is obtained since the fading RVs in LoS or NLoS are independent, and (b) is obtained because the small-scale fading channel power gain has a normalised power ($\Omega_{An}=1$). If we define $X_{RD,n} = 10\log_{10}S_{RD,n} \sim \mathcal{N}(0,\sigma_{An}^2)$, thanks to the LT of a normally distributed RV,

$$\mathbb{E}_S\left[S\right] = \mathbb{E}_X\left[10^{\frac{X_{RD,n}}{10}}\right] = \mathbb{E}_X\left[\exp\left(\frac{\ln 10}{10}X_{RD,n}\right)\right] = \exp\left(\frac{\ln^2 10}{200}\sigma_{S_{An}}^2\right). \quad \text{(A.75)}$$

We also have

$$\begin{aligned} \mathbb{E}_{I_{RD}|r_{RD}}\left[I_{RD}\right] &= \mathbb{E}_{-|r_{RD}}\left[\sum_{n=\{L,N\}}\sum_{\phi_j\in\mathbf{\Phi}_{RDI,n}} c_{RD,n}\left(\|\boldsymbol{\phi}_j\|^2+H_R^2\right)^{-\frac{\alpha_{An}}{2}}|h_{RD,n,j}|^2S_{RD,n,j}\right] \\ &\overset{(a)}{=} \sum_{n=\{L,N\}}\exp\left(\frac{\ln^2 10}{200}\sigma_{S_{An}}^2\right)\mathbb{E}_{\mathbf{\Phi}_{RDI,n}|r_{RD}}\left[\sum_{\phi_j\in\mathbf{\Phi}_{RDI,n}} c_{RD,n}\left(\|\boldsymbol{\phi}_j\|^2+H_R^2\right)^{-\frac{\alpha_{An}}{2}}\right] \\ &\overset{(b)}{=} \sum_{n=\{L,N\}} c_{RD,n}\exp\left(\frac{\ln^2 10}{200}\sigma_{S_{An}}^2\right)2\pi\lambda_R\int_{r_{RD}}^{\infty}\left(r^2+H_R^2\right)^{-\frac{\alpha_{An}}{2}}p_{An}(r)r\mathrm{d}r, \end{aligned} \quad \text{(A.76)}$$

where (a) is obtained since the fading parameters and the RNs PPs composed only of RNs with links in LoS or NLoS are independent, the small-scale fading channel power gains have normalised powers ($\Omega_{An} = 1$), and thanks to the expectation of the shadowing given in the previous Equation. (b) is obtained using the Campbell's theorem for a PPP in polar coordinates, given by Equation (2.11).

With the nearest neighbour association rule, the PDF or r_{RD} is given by Lemma 4.1. ■

Proof of Proposition 4.9

The proof is similar to the proof of Proposition 4.8, except that there is only interfering nodes, with the interfering PPs being $\mathbf{\Phi}_R$ and $\mathbf{\Phi}_T$ instead of $\mathbf{\Phi}_{RDI}$ and $\mathbf{\Phi}_{SDI}$. ■

Proof of Proposition 4.10

The proof focus only on the second hop, and the developments are identical for the two other links.

Using the lemma presented in [55], the ergodic SE of the second hop is given by

$$\begin{aligned}
\mathcal{S}_{RD} &= \frac{1}{2}\,\mathbb{E}_{\chi_{RD}}\left[\log_2\left(1+\chi_{RD}\right)\right] \\
&= \frac{1}{2}\,\mathbb{E}_{r_{RD}}\left[\sum_{n\in\{L,N\}} p_{An}(r_{RD})\,\mathbb{E}_{\chi_{RD,n}|r_{RD}}\left[\log_2\left(1+\chi_{RD,n}\right)\right]\right] \\
&= \frac{1}{2}\,\mathbb{E}_{r_{RD}}\left[\sum_{n\in\{L,N\}} p_{An}(r_{RD})\,\mathbb{E}_{U_{RD,n},I_{RD}|r_{RD}}\left[\log_2\left(1+\frac{U_{RD,n}}{I_{RD}+\sigma^2}\right)\right]\right] \\
&= \frac{1}{2\ln 2}\,\mathbb{E}_{r_{RD}}\left[\sum_{n\in\{L,N\}} p_{An}(r_{RD})\int_0^\infty \mathcal{L}_{I_{RD}|r_{RD}}(s)\left(1-\mathcal{L}_{U_{RD,n}|r_{RD}(s)}\right)\frac{\exp\left(-s\sigma^2\right)}{s}\mathrm{d}s\right].
\end{aligned} \tag{A.77}$$

where $\mathcal{L}_{I_{RD}|r_{RD}}$ and $\mathcal{L}_{U_{RD,n}|r_{RD}}$ are respectively the LT of the LT of the aggregate interference of the second hop and the LT of the power from the selected RN in LoS or NLoS, both conditioned on r_{RD}. The factor $1/2$ which appears in these expressions is a consequence of the DF protocol executed in two steps. The primer is given by Proposition 4.4, and the latter can be developed as

$$\begin{aligned}
\mathcal{L}_{U_{RD,n}|r_{RD}}(s) &= \mathbb{E}_{U_{RD,n}|r_{RD}}\left[\exp\left(-s\,U_{RD,n}\right)\right] \\
&= \mathbb{E}_{|h_{RD,n}|^2,S_{RD,n}|r_{RD}}\left[\exp\left(-s\,C_{RD,n}\left(r_{RD}^2+H_R^2\right)^{-\frac{\alpha_{An}}{2}}|h_{RD,n}|^2 S_{RD,n}\right)\right] \\
&= \mathbb{E}_{S_{RD,n}}\left[\mathcal{L}_{|h_{RD,n}|^2}\left(s\,C_{RD,n}\left(r_{RD}^2+H_R^2\right)^{-\frac{\alpha_{An}}{2}} S_{RD,n}\right)\right].
\end{aligned} \tag{A.78}$$

■

Proof of Proposition 5.1

If a UAV RN starts from the position $\boldsymbol{x} = (x, y)$ and moves at a constant speed v in a random direction $\Theta \sim \text{Unif}([0, 2\pi])$, its position $\boldsymbol{x}' = (x', y')$ at time $t \geq 0$ is given by

$$\boldsymbol{x}' = \boldsymbol{x} + \begin{pmatrix} vt\cos\Theta \\ vt\sin\Theta \end{pmatrix}. \tag{A.79}$$

The joint PDF of $\boldsymbol{x'} - \boldsymbol{x}$ is given by

$$f_{\boldsymbol{x'}-\boldsymbol{x}}(\Delta x, \Delta y) = \frac{\delta\left(\sqrt{(\Delta x)^2 + (\Delta y)^2} - vt\right)}{2\pi vt}, \tag{A.80}$$

and therefore, the PDF of the displacement vector from $\boldsymbol{x}$ to $\boldsymbol{x}'$ conditioned on $\boldsymbol{x}$ is given by

$$f_{\boldsymbol{x}'|\boldsymbol{x}}(x', y') = f_{\boldsymbol{x}'-\boldsymbol{x}}(x' - x, y' - y) = \frac{1}{2\pi vt}\delta\left(\sqrt{(x' - x)^2 + (y' - y)^2} - vt\right). \tag{A.81}$$

Using the displacement theorem in cartesian coordinates given by Equation (2.19), the resulting PP is a PPP with density

$$\lambda'(x', y') = \lambda_R \int_{\mathbb{R}^2} f_{\boldsymbol{x}'|\boldsymbol{x}}(x', y')\, \mathrm{d}\boldsymbol{x} = \lambda_R. \tag{A.82}$$

■

Proof of Proposition 5.2

With the second mobility scheme and the nearest neighbour association rule, the CP of the typical UE at time $t \geq 0$ for a given SINR threshold β is given by

$$\begin{aligned} \mathcal{P}(\beta, t) &= \mathbb{P}_{\chi(t)}\left(\chi(t) \geq \beta\right) \\ &= \mathbb{E}_{r_{RD}, r_{SD}}\left[\mathbb{P}_{\chi(t)|r_{RD}, r_{SD}}\left(\chi(t) \geq \beta\right)\right], \end{aligned} \tag{A.83}$$

where r_{RD} is the initial distance between the typical UE and the selected RN.

Conditioned on r_{RD} and r_{SD}, at time $t \geq 0$, the SINR at the typical UE $\chi(t)$ is given by

$$\chi(t) = \begin{cases} \chi_{SRD}(t) \text{ if } r_{SD} > \sqrt{(r_{RD}(t))^2 + H_R^2} \\ \chi_{SD} \qquad \text{if } r_{SD} \leq \sqrt{(r_{RD}(t))^2 + H_R^2} \end{cases}. \tag{A.84}$$

The regions of association are illustrated in Figure A.2. The CP of the complete link at time $t \geq 0$ can be developed as

$$\begin{aligned} \mathcal{P}(\beta, t) = &\int_{\Omega_{SD}(t)} \underbrace{\mathbb{P}_{\chi_{SD}|r_{RD}, r_{SD}}\left(\chi_{SD} \geq \beta\right)}_{\mathcal{P}_{SD|r_{RD}, r_{SD}}(\beta)} f_{r_{SD}, r_{RD}}(r_{SD}, r_{RD}) \mathrm{d}r_{SD}\mathrm{d}r_{RD} \\ &+ \int_{\Omega_{SRD}(t)} \underbrace{\mathbb{P}_{\chi_{SRD}|r_{RD}, r_{SD}}\left(\chi_{SRD}(t) \geq \beta\right)}_{\mathcal{P}_{SRD|r_{RD}, r_{SD}}(\beta, t)} f_{r_{SD}, r_{RD}}(r_{SD}, r_{RD}) \mathrm{d}r_{SD}\mathrm{d}r_{RD}, \end{aligned} \tag{A.85}$$

where $\mathcal{P}_{SD|r_{RD},r_{SD}}(\beta)$ and $\mathcal{P}_{SRD|r_{RD},r_{SD}}(\beta,t)$ are respectively the CP of the direct link and relay link at time $t \geq 0$, both conditioned on r_{RD} and r_{SD}, and $f_{r_{SD},r_{RD}}(r_{SD},r_{RD})$ is the joint PDF of r_{SD} and r_{RD}.

Since the direct link and the relay link are independent, we have

$$f_{r_{SD},r_{RD}}(r_{SD},r_{RD}) = f_{r_{SD}}(r_{SD})f_{r_{RD}}(r_{RD}) \tag{A.86}$$

and

$$\mathcal{P}_{SD|r_{RD},r_{SD}}(\beta) \quad = \mathcal{P}_{SD|r_{SD}}(\beta) \tag{A.87}$$
$$\mathcal{P}_{SRD|r_{SD},r_{RD}}(\beta,t) = \mathcal{P}_{SRD|r_{RD}}(\beta,t). \tag{A.88}$$

Furthermore, thanks to the independence between the two-hop of the relay link, using Equation (4.11) and Lemma 5.1, when $r_{RD} \leq vt$, we have

$$\begin{aligned}\mathcal{P}^{(a)}_{SRD|r_{RD}}(\beta,t) &= \mathbb{P}_{\chi_{SRD}(t)|r_{SD},r_{RD},r_{RD}\leq vt}\left(\chi_{SRD}(t) \geq \beta\right) \\ &= \underbrace{\mathbb{P}_{\chi_{SR}}\left(\chi_{SR} \geq \beta\right)}_{\mathcal{P}_{SR}(\beta)} \underbrace{\mathbb{P}_{\chi_{RD}(t)|r_{RD},r_{RD}\leq vt}\left(\chi_{RD}(t) \geq \beta\right)}_{\mathcal{P}^{(a)}_{RD|r_{RD}}(\beta,t)},\end{aligned} \tag{A.89}$$

and similarly, when $r_{RD} > vt$, we have

$$\begin{aligned}\mathcal{P}^{(b)}_{SRD|r_{RD}}(\beta,t) &= \mathbb{P}_{\chi_{SRD}(t)|r_{SD},r_{RD},r_{RD}> vt}\left(\chi_{SRD}(t) \geq \beta\right) \\ &= \underbrace{\mathbb{P}_{\chi_{SR}}\left(\chi_{SR} \geq \beta\right)}_{\mathcal{P}_{SR}(\beta)} \underbrace{\mathbb{P}_{\chi_{RD}(t)|r_{RD},r_{RD}> vt}\left(\chi_{RD}(t) \geq \beta\right)}_{\mathcal{P}^{(b)}_{RD|r_{RD}}(\beta,t)},\end{aligned} \tag{A.90}$$

Therefore,

$$\begin{aligned}\mathcal{P}(\beta,t) &= \int_0^{H_R} \mathcal{P}_{SD|r_{SD}}(\beta)f_{r_{SD}}(r_{SD}) \int_0^{\infty} f_{r_{RD}}(r_{RD})\mathrm{d}r_{RD}\mathrm{d}r_{SD} \\ &+ \int_{H_R}^{\infty} \mathcal{P}_{SD|r_{SD}}(\beta)f_{r_{SD}}(r_{SD}) \int_{\sqrt{r_{SD}^2-H_R^2}+vt}^{\infty} f_{r_{RD}}(r_{RD})\mathrm{d}r_{RD}\mathrm{d}r_{SD} \\ &+ \int_0^{vt} \mathcal{P}^{(a)}_{SRD|r_{RD}}(\beta,t)f_{r_{RD}}(r_{RD}) \int_{H_R}^{\infty} f_{r_{SD}}(r_{SD})\mathrm{d}r_{SD}\mathrm{d}r_{RD} \\ &+ \int_{vt}^{\infty} \mathcal{P}^{(b)}_{SRD|r_{RD}}(\beta,t)f_{r_{RD}}(r_{RD}) \int_{\sqrt{(r_{RD}-vt)^2+H_R^2}}^{\infty} f_{r_{SD}}(r_{SD})\mathrm{d}r_{SD}\mathrm{d}r_{RD} \\ &\overset{(a)}{=} \int_0^{H_R} \mathcal{P}_{SD|r_{SD}}(\beta)f_{r_{SD}}(r_{SD})\mathrm{d}r_{SD} \\ &+ \int_{H_R}^{\infty} \mathcal{P}_{SD|r_{SD}}(\beta)\tilde{f}_{r_{SD}}(r_{SD})\mathrm{d}r_{SD} \\ &+ \mathcal{P}_{SR}(\beta) \int_0^{vt} \mathcal{P}^{(a)}_{RD|r_{RD}}(\beta,t)\tilde{f}^{(a)}_{r_{RD}}(r_{RD})\mathrm{d}r_{RD} \\ &+ \mathcal{P}_{SR}(\beta) \int_{vt}^{\infty} \mathcal{P}^{(b)}_{RD|r_{RD}}(\beta,t)\tilde{f}^{(b)}_{r_{RD}}(r_{RD})\mathrm{d}r_{RD},\end{aligned} \tag{A.91}$$

where (a) is obtained thanks to Lemma 4.1, and with

$$\tilde{f}_{r_{SD}}(r_{SD}) = f_{r_{SD}}(r_{SD}) \exp\left(-\pi\lambda_R\left(v^2t^2 - H_R^2\right)\right) \exp\left(-\pi\lambda_R\left(r_{SD}^2 + 2vt\sqrt{r_{SD}^2 - H_R^2}\right)\right), \tag{A.92}$$

$$\tilde{f}^{(a)}_{r_{RD}}(r_{RD}) = f_{r_{RD}}(r_{RD}) \exp\left(-\pi\lambda_T H_R^2\right), \tag{A.93}$$

$$\tilde{f}^{(b)}_{r_{RD}}(r_{RD}) = f_{r_{RD}(r_{RD})} \exp\left(-\pi\lambda_T\left(H_R^2 + v^2t^2\right)\right) \exp\left(-\pi\lambda_T(r_{RD}^2 - 2r_{RD}vt)\right). \tag{A.94}$$

The superscript (a) and (b) indicates respectively that $r_{RD} \leq vt$ and $r_{RD} > vt$.

■

Proof of Proposition 5.3

The proof is similar to the proof of Proposition 4.3, Except that the χ_{RD} is replaced by $\chi_{RD}(t)$.

■

Proof of Proposition 5.4

The proof is similar with the proof of Proposition 4.4, except that I_{RD} is replaced by $I_{RD}(t)$. The integrals have been splitted to isolate each part of the density given by Equation (5.10). The expression of $\mathcal{L}^{(a)}_{I_{RD}(t)|r_{RD}}$ is further simplified thanks to the property $\arccos(x) = \pi - \arccos(-x)$.

■

Proof of Proposition 5.5

Following the proof of Proposition 4.1, when $r_{RD} \leq vt$, we have

$$\begin{aligned}\mathcal{P}^{(a)}_{SRD|r_{SD},r_{RD}}(\beta,t) &= \mathbb{P}_{\chi_{SRD}(t)|r_{SD},r_{RD},r_{RD}\leq vt}\left(\chi_{SRD}(t) \geq \beta\right) \\ &= \underbrace{\mathbb{P}_{\chi_{SR}|r_{SD},r_{RD},r_{RD}\leq vt}\left(\chi_{SR} \geq \beta\right)}_{\mathcal{P}^{(a)}_{SR|r_{SD},r_{RD}}(\beta)} \underbrace{\mathbb{P}_{\chi_{RD}(t)|r_{RD},r_{RD}\leq vt}\left(\chi_{RD}(t) \geq \beta\right)}_{\mathcal{P}^{(a)}_{RD|r_{RD}}(\beta,t)},\end{aligned} \tag{A.95}$$

and when $r_{RD} > vt$, we have

$$\begin{aligned}\mathcal{P}^{(b)}_{SRD|r_{SD},r_{RD}}(\beta,t) &= \mathbb{P}_{\chi_{SRD}(t)|r_{SD},r_{RD},r_{RD}>vt}\left(\chi_{SRD}(t) \geq \beta\right) \\ &= \underbrace{\mathbb{P}_{\chi_{SR}|r_{SD},r_{RD},r_{RD}>vt}\left(\chi_{SR} \geq \beta\right)}_{\mathcal{P}^{(b)}_{SR|r_{SD},r_{RD}}(\beta)} \underbrace{\mathbb{P}_{\chi_{RD}(t)|r_{RD},r_{RD}>vt}\left(\chi_{RD}(t) \geq \beta\right)}_{\mathcal{P}^{(b)}_{RD|r_{RD}}(\beta,t)}.\end{aligned} \tag{A.96}$$

Additionally, we have

$$\mathcal{P}^{(a)}_{SR|r_{SD},r_{RD}}(\beta) = \int_0^\infty \mathcal{P}_{SR|r_{SR}}(\beta) f^{(a)}_{r_{SR}|r_{SD},r_{RD}}(r_{SR})\mathrm{d}r_{SR}, \tag{A.97}$$

and

$$\mathcal{P}^{(b)}_{SR|r_{SD},r_{RD}}(\beta) = \int_{|r_{SD}-r_{RD}+vt|}^{r_{SD}+r_{RD}-vt} \mathcal{P}_{SR|r_{SR}}(\beta) f^{(b)}_{r_{SR}|r_{SD},r_{RD}}(r_{SR})\mathrm{d}r_{SR}. \tag{A.98}$$

Therefore,

$$\begin{aligned}
\mathcal{P}(\beta,t) &= \int_0^{H_R} \mathcal{P}_{SD|r_{SD}}(\beta) f_{r_{SD}}(r_{SD}) \int_0^{\infty} f_{r_{RD}}(r_{RD}) \mathrm{d}r_{RD} \mathrm{d}r_{SD} \\
&+ \int_{H_R}^{\infty} \mathcal{P}_{SD|r_{SD}}(\beta) f_{r_{SD}}(r_{SD}) \int_{\sqrt{r_{SD}^2 - H_R^2}+vt}^{\infty} f_{r_{RD}}(r_{RD}) \mathrm{d}r_{RD} \mathrm{d}r_{SD} \\
&+ \int_0^{vt} \int_{H_R}^{\infty} \mathcal{P}^{(a)}_{SRD|r_{SD},r_{RD}}(\beta,t) f_{r_{SD},r_{RD}}(r_{SD},r_{RD}) \mathrm{d}r_{SD} \mathrm{d}r_{RD} \\
&+ \int_{vt}^{\infty} \int_{\sqrt{(r_{RD}-vt)^2+H_R^2}}^{\infty} \mathcal{P}^{(b)}_{SRD|r_{SD},r_{RD}}(\beta,t) f_{r_{SD},r_{RD}}(r_{SD},r_{RD}) \mathrm{d}r_{SD} \mathrm{d}r_{RD} \\
&\overset{(a)}{=} \int_0^{H_R} \mathcal{P}_{SD|r_{SD}}(\beta) f_{r_{SD}}(r_{SD}) \mathrm{d}r_{SD} \\
&+ \int_{H_R}^{\infty} \mathcal{P}_{SD|r_{SD}}(\beta) \tilde{f}_{r_{SD}}(r_{SD}) \mathrm{d}r_{SD} \\
&+ \int_0^{vt} \int_{H_R}^{\infty} \mathcal{P}_{SR|r_{SR}}(\beta)\big|_{r_{SR}=r_{SD}} \mathcal{P}^{(a)}_{RD|r_{RD}}(\beta,t) f_{r_{SD},r_{RD}}(r_{SD},r_{RD}) \mathrm{d}r_{SD} \mathrm{d}r_{RD}
\end{aligned}$$

$$\begin{aligned}
&+ \int_{vt}^{\infty} \int_{\sqrt{(r_{RD}-vt)^2+H_R^2}}^{\infty} \int_{|r_{SD}-r_{RD}+vt|}^{r_{SD}+r_{RD}-vt} \mathcal{P}_{SR|r_{SR}}(\beta) \mathcal{P}^{(b)}_{RD|r_{RD}}(\beta,t) \\
&\qquad \cdot \tilde{f}^{(b)}_{r_{SD},r_{SR},r_{RD}}(r_{SD},r_{SR},r_{RD}) \mathrm{d}r_{SR} \mathrm{d}r_{SD} \mathrm{d}r_{RD}, \quad \text{(A.99)}
\end{aligned}$$

where (a) is obtained thanks to Lemma 4.1, and with

$$\tilde{f}_{r_{SD}}(r_{SD}) = f_{r_{SD}}(r_{SD}) \exp\left(-\pi\lambda_R \left(v^2t^2 - H_R^2\right)\right) \exp\left(-\pi\lambda_R \left(r_{SD}^2 + 2vt\sqrt{r_{SD}^2 - H_R^2}\right)\right), \quad \text{(A.100)}$$

$$f_{r_{SD},r_{RD}}(r_{SD},r_{RD}) = 4\pi^2\lambda_R\lambda_T \, r_{SD} r_{RD} \exp\left(-\pi(\lambda_R r_{RD}^2 + \lambda_T r_{SD}^2)\right), \quad \text{(A.101)}$$

$$\tilde{f}^{(b)}_{r_{SD},r_{SR},r_{RD}}(r_{SD},r_{SR},r_{RD}) = \frac{8\pi\lambda_R\lambda_T \, r_{SR} r_{RD} r_{SD} \exp\left(-\pi(\lambda_R r_{RD}^2 + \lambda_T r_{SD}^2)\right)}{\sqrt{4r_{SD}^2(r_{RD}-vt)^2 - \left(r^2 - r_{SD}^2 - (r_{RD}-vt)^2\right)^2}}. \quad \text{(A.102)}$$

■

Proof of Proposition 5.6

The proof is similar to the proof of Proposition 4.8, except that U_{RD} and I_{RD} are replaced by $U_{RD}(t)$ and $I_{RD}(t)$. The integrals have been splitted to isolate each part of the density given by Equation (5.10). The expression of $\mathcal{X}^{(a)}_{c,RD|r_{RD}}$ is further simplified thanks to the property $\arccos(x) = \pi - \arccos(-x)$.

■

Proof of Proposition 5.7

The proof is similar to the proof of Proposition 4.10, except that U_{RD} and I_{RD} are replaced by $U_{RD}(t)$ and $I_{RD}(t)$.

■

UNIVERSITÉ CATHOLIQUE DE LOUVAIN
École polytechnique de Louvain
Rue Archimède, 1 bte L6.11.01, 1348 Louvain-la-Neuve, Belgique | **www.uclouvain.be/epl**